Techno Economic Analysis Of A Plasma Gasification Biomass To Liquids Plant.

By Sylvain A. Motycka

B.S. in Electrical and Electronics, June 2002, University of Dundee, Scotland

M.S. in Energetic and Environment, June 2005, University of Orléans, France

M.S. in Plasma Physics, Optics and Electronics, June 2005, Ecole Polytechnique de l'Université d'Orléans, France

A Dissertation submitted to

The Faculty of
School of Engineering and Applied Sciences
Of the George Washington University
In partial fulfillment of the requirements
Of the degree of Doctor of Philosophy.

August 31st, 2013

Dissertation directed by

Michael R. Duffey
Associate Professor of Engineering Management

The School of Engineering and Applied Sciences of The George Washington University certifies that Sylvain Andre Luc Motycka has passed the Final Examination for the degree of Doctor of Philosophy as of April 10th 2013. This is the final and approved form of the dissertation.

Techno economic analysis of a plasma gasification biomass to liquids plant

Sylvain A. Motycka

Dissertation Research Committee:

Michael R. Duffey, Associate Professor of Engineering Management, Dissertation Director.

Greg L. Shaw, Associate Professor of Engineering Management and Systems Engineering, Committee Chair.

Charles A. Garris, Professor of Engineering, Committee member.

Royce A. Francis, Assistant Professor of Engineering Management and Systems Engineering, Committee member.

© Copyright 2013 by Sylvain A. Motycka
All rights reserved.

Acknowledgements

I would like to express my gratitude to Solena who financed my PhD program.

I am very thankful to Professor Michael Duffey for his trust throughout the program; I thank him for his guidance.

Lastly, I thank Sofia for her unconditional support, encouragement and patience.

Abstract

Techno Economic Analysis Of A Plasma Gasification Biomass To Liquids Plant.

Price volatility for jet fuel makes it difficult for airlines to predict their fuel-related operating expenses beyond a few months. This is due to both crude oil price uncertainty and the widening “cracking premium” from crude oil into downstream kerosene and diesel products.

In this research, we analyze an alternative production method for synthetic paraffinic kerosene (SPK) with potential for predictable production costs and little to no raw material price volatility. An integrated plasma gasification biomass-to-liquids plant was analyzed to determine the product cost of its Fischer-Tropsch (FT) products. It is shown that, assuming zero cost for waste refuse derived fuel feedstock, the resulting products, i.e. FT diesel and kerosene, would be cost-competitive with similar products obtained from a petroleum process.

First, a chemical process model was developed to study the performance of the plasma gasification subsystem. A biomass to liquids process model, which integrates downstream stages with the plasma gasification process model, is then developed using

a cobalt-based catalyst Fischer-Tropsch system. Finally, a discounted cash flow model is developed to analyze the liquid fuels product cost.

A case study was performed to process 78 tonnes per hour of refuse derived fuel into mainly diesel and jet. Results show that the atmospheric pressure plasma gasification provides sufficient operating conditions flexibility to maximize carbon monoxide and hydrogen production. Overall plant conversion efficiency greater than 49% was achieved and the corresponding plant throughput is 2,200 barrels per day of F-T liquids based on a once-through Fischer-Tropsch configuration with no supplemental natural gas to improve the efficiency. Lastly, implications and further research to assess commercial viability are discussed.

Table of Contents

Acknowledgements iv

Abstract v

Table of contents vii

List of figures x

List of tables xii

List of acronyms xiv

1 Introduction 1

1.1 Statement of the problem 1

1.2 Background 2

1.3 Purpose of the study 5

1.4 Significance 5

1.5 Scope and limitations 6

1.6 Research goal 7

1.7 Organization of the document 7

2 Methodology 9

2.1 Introduction 9

2.2 Process model 9

2.3 Techno-economic model 32

3 Plasma gasification process model 38

3.1 Introduction 38

3.2 Mathematical formulation in bed zones 38

3.3 Model description 42

3.4 Results and discussions 45

3.5 Conclusion 61

4 Biomass to Liquid and Power process model 64

4.1 Introduction 64

4.2 Feedstock characterization 64

4.3 Plasma gasification island 68

4.4 Syngas cooling, cleaning and conditioning 69

4.5 Fischer-Tropsch and FT-products hydrocracking 82

4.6 Power Generation 90

4.7 Balance of the plant 92

4.8 Results and discussion 92

4.9 Conclusion 101

5 Techno-economic model 102

5.1 Introduction 102

5.2 Methodology 103

5.3 Product value analysis 106

5.4 Conclusion 116

6 Conclusion 118

7 Works Cited 121

Appendix A 137

Appendix B 141

Appendix C 144

Appendix D 153

Appendix E 155

List of Figures

Figure 2-1: MSW Generation vs. Recovery per capita per day 10

Figure 2-2: Feedstock attributes 11

Figure 2-3: Synopsis of MSW to feedstock (1/2) 12

Figure 2-4: Synopsis of MSW to feedstock (2/2) 13

Figure 2-5: Fixed-bed gasifier 15

Figure 2-6: Circulating fluidized bed gasifier 16

Figure 2-7: Entrained flow gasifier 17

Figure 2-8: Degree of polymerization - FT product distribution 24

Figure 2-9: Biomass to Liquid - BTL - process 28

Figure 2-10: Structure of the atmospheric pressure plasma gasification BTL model 33

Figure 3-1: Schematic of the bed zones 39

Figure 3-2: Cold Gas Efficiency of a given feedstock under different gasification operating conditions 47

Figure 3-3: Syngas volumetric composition of the selected cases 48

Figure 3-4: Syngas composition of selected cases (vol. % basis) 51

Figure 3-5: syngas composition for selected cases (Wt. % basis) 52

Figure 3-6: Syngas composition (vol. %) of a waste plasma gasification process 54

Figure 3-7: syngas composition (vol. and wt. %) of a waste plasma gasification process 56

Figure 3-8: CO contour at plasma power 2.5 MW (left) and 7.0 MW (right) 60

Figure 3-9: H_2 contour response at plasma power 2.5 MW (left) and 7.0 MW (right) 60

Figure 3-10: Syngas temperature contour response for plasma power 2.5 MW (left) and 7.0 MW (right)..... 60

Figure 4-1: Conceptual diagram of a heat exchanger..... 70

Figure 4-2: Aqueous solubility of syngas components at 1 bar (Van Ree, et al. 1995) 73

Figure 4-3: Block flow diagram of the conditioning island 82

Figure 4-4: Anderson-Flury-Schultz distribution for 2 alpha values 84

Figure 4-5: Schematic of the FT synthesis concept..... 84

Figure 4-6: Hydrocracking process flow diagram (Meyers 2004)..... 86

Figure 4-7: Determination of the FT system throughput 94

Figure 4-8: Energy efficiency for the process configurations selected..... 97

Figure 4-9: Tornado graph of plant energy efficiency for BTL base case 99

Figure 4-10: Spider graph of the plant energy efficiency for BTL base case 99

Figure 5-1: Liquid fuels spot price comparison. Data derived from (US EIA 2013) (US EIA 2013) 104

Figure 5-2: Jet crack price vs. WTI. Data from (Airlines for America 2013)..... 104

Figure 5-3: Project's IRR resulting from the Monte-Carlo simulation 114

Figure 5-4: Tornado chart resulting from the Monte Carlo simulation..... 115

List of Tables

Table 2-1: Gaseous molecule's stoichiometry and thermodynamic data 31

Table 2-2: Feedstock sub-module's I/Os 34

Table 2-3: Plasma gasification sub-module's I/Os 35

Table 2-4: Process engineering sub-module's I/Os 36

Table 2-5: O&M module's input variables 37

Table 2-6: Engineering economics' input variables 37

Table 3-1: Raw MSW composition for base case scenario 45

Table 3-2: Raw MSW elemental and proximate compositions and the related LHV 46

Table 3-3: RDF composition (in wt. %) & LHV considered for the gasification base case scenario 47

Table 3-4: Cold gas efficiencies and (H2+CO)/(H2O+CO2) ratio for selected cases 50

Table 3-5: Summary of the Design o Expriment for the Gasification Process 57

Table 3-6: List of responses of the design of experiments 58

Table 4-1: Material discarded in the municipal solid waste stream, 1960 to 2009 67

Table 4-2: Chemical absorption process performance summary (National Renewable Energy Laboratory 2009) 76

Table 4-3: Physical absorption process performance summary (National Renewable Energy Laboratory 2009) 77

Table 4-4: Microchannel FT technology operating and performance parameters 85

Table 4-5: Hydrocracking facility typical operating parameters 87

Table 4-6: Wax hydrocracking yields from (Shah, et al. 1988) 88

Table 4-7: FT and hydrocracking process parameters and product yields 89

Table 4-8: FT fuels LHV 90

Table 4-9: Operating and performance parameters of the BTL process 93

Table 4-10: Plant energy efficiency vs. CO vol. rate target at FT inlet 94

Table 4-11: Base case process model operating parameters 96

Table 4-12: FT fuel production rate (barrels/day) 97

Table 4-13: Input parameters for process sensibility analysis 98

Table 5-1: Plant total capital cost methodology 105

Table 5-2: Reference process units' capital costs 107

Table 5-3: Plasma Gasification Biomass to Liquid Total Capital Costs estimation 108

Table 5-4: Financial assumptions 109

Table 5-5: Variable operating costs per process unit 110

Table 5-6: Comparison of assumptions and results with Tijmensen study 111

Table 5-7: Input parameters for Monte-Carlo simulation 112

List of Acronyms

A_S	Interfacial area per unit volume of bed
CH_4	Methane
CO	Carbon Monoxide
CO_2	Carbon Dioxide
COS	Carbonyl Sulfide
C_p	Specific heat at constant pressure
C_{P_G}	Heat capacity of gas
$C_{P_{feedstock}}$	Specific heat of feedstock
C_{P_S}	Heat capacity of solid
δ	Void fraction
D	Coefficient of molecular diffusion
E	Turbulent eddy diffusion
f_{fc}	Fraction of fixed carbon in feedstock's proximate analysis.

f_{vol}	Fraction of volatile matter in feedstock's proximate analysis.
$\dot{G}$	Gas mass flow in the gasification bed
G	Volumetric flow rate of gas
$H_{C,comb}$	Carbon enthalpy in the combustion zone
$H_{C,devol}$	Carbon enthalpy in the devolatilization zone
$H_{C,gasif}$	Carbon enthalpy in the gasification zone
H_j	Heat of reaction per mole of j
h_v	Heat transfer coefficient based on unit volume
H_2	Hydrogen
H_2O	Water
H_2S	Hydrogen Sulfide
HCl	Hydrogen Chloride
HCN	Hydrogen Cyanide
k_C	Mass transfer coefficient
HHV	Higher Heating Value
HHV_c	Higher Heating Value of graphite

HHV_{vol}	Higher Heating Value of volatile matter fraction
K_G	Effective gas conductivity
K_S	Packed bed thermal conductivity
LHV	Lower Heating Value
$\dot{m}_{C,unconv}$	Mass flow rate of unconverted carbon
MSW	Municipal Solid Waste
N_2	Nitrogen
NH_3	Ammonia
Qa	Heat power absorbed by cold fluid
Qe	Heat power emitted from hot fluid
ρ_G	Gas density
ρ_S	Solid density
Re	Reynold's number
R_j	Rate of reaction of specie j
RDF	Refuse-Derived Fuel
Sc	Schmidt number of the gas

T_{comb}	Solids input temperature of the combustion zone
T_G	Gas temperature
T_S	Solid temperature
$\dot{U}$	Solid mass flow in the gasification bed

Chapter 1

1 INTRODUCTION

1.1 Statement of the problem

This study aims at developing a methodology to analyze the economics of a biomass to liquids (BTL) plant that integrates plasma gasification with FT synthesis. BTL is an alternative to the traditional petroleum refineries that produce liquid hydrocarbon fuels from crude oil. BTL also stands as an alternative to coal to liquids (CTL) and gas to liquids (GTL) plants that produce liquid hydrocarbon fuels from respectively coal and natural gas. Both petroleum refining and CTL processes are well-established and facilities have been operating at commercial scale with production rates greater than several hundred thousand barrels per day. GTL facilities are at the early stages of their commercialization with production rates greater than tens of thousands barrels per day.

BTL is a new concept – not yet proven at commercial stage - based on using a feedstock composed 100% of biomass products with a hydrocarbon liquids target production in the range of thousands of barrels per day. As such, BTL could not compete with the oil industry but could, on the other hand, be used as an alternative drop-in fuel to blend with the regular petroleum-derived liquid fuel pool. Considering the early stages of this process, BTL fuel production faces several barriers of distinct types such as business, economic and engineering. Publicly available models have studied the economic feasibility of BTL systems and the corresponding studies assumed a low temperature

biomass gasification system. These types of systems are well-known to be unreliable because of the presence of tar in syngas which is a harmful compound difficult to handle and remove. Furthermore, gasification is very often designed as a pressurized system, which could face practical and operational issues when attempting to process ligno-cellulosic feedstock such as biomass.

Lastly, traditional refinery and CTL plants are designed for dedicated production of specific types and quantities of liquid fuels. Similarly, this study will investigate the production costs and plant efficiency for manufacturing liquid hydrocarbon fuels production such as diesel and/or jet kerosene from biomass. Lastly, existing BTL models' algorithms assume static inputs and could potentially hide the effect of some factors thus limiting the results of an economic study.

1.2 Background

Governments have been investing massively in the energy sector in an attempt to reduce their dependency on foreign oil and accelerate domestic drop-in biofuels development. In addition to deteriorating climate and the local environment, governments and transportation sectors face increasing oil prices and persistent oil dependency. A response to such challenges would be to independently manufacture a less expensive and sustainable clean fuels.

The airline industry was responsible for emitting 650 million tonnes of CO_2 in 2010 which represents 2% of anthropogenic carbon emissions (Air Transport Action Group (ATAG) 2012). The European Union (EU) already set targets for aviation and maritime

emissions. The International Air Transport Association (IATA) set its own climate protection goals of reaching 50% reduction in net CO_2 emission by 2050 relative to 2005 levels (International Air Transportation Association (IATA) 2009). Booz & Company predicts that annual aviation CO_2 emissions will continuously increase more than three-fold by 2050 if current practices are unchanged and despite assumed efficiency improvements (Booz & Company 2011). The airline industry assumes improvement of 1.5% per year in fleet fuel efficiency and these improvements will be possible through 2030 with the further development of today's technologies. A number of improvements on frames and engines are under development to improve aerodynamics, weight and fuel efficiency. The use of advanced materials can dramatically reduce aircraft weight; for example, the Boeing 787 has been shown to reduce fuel use by up to 8%. Aviation infrastructures – such as air traffic management and airports – as well as aircraft operations are other sources of potential improvements.

For global industrial applications, biofuels account for about 2% of transport fuel consumption (Booz & Company 2011). Currently, transportation alternative fuel is dominated by first-generation biofuels which are derived from edible crops. Bioethanol is produced by a combination of fermentation and distillation processes but it is more corrosive than gasoline and has a lower energy density. Biodiesel is produced by an esterification process known as fatty acid methyl ester ("FAME"). The combination of first generation biofuel's competition with food crops, use of arable lands and related water management issues led to the development of second generation biofuels (Shell 2007).

Second generation biofuels are manufactured from agricultural and forest residue, non-food crop feedstock and organic fraction of solid waste. Collectively, these types of feedstock are referred as ligno-cellulosic feedstock. When such feedstock has to be grown on arable land, several concerns remain over land use although higher energy yields could be obtained and poorer quality land could be used than if feedstock grown for 1st generation biofuels were produced on the same land (Agence Internationale de l'Energie 2008). Furthermore, supply chain and logistics of feedstock grown for 2nd generation biofuels shall be carefully analyzed prior to implementing a plant to reduce the project investment risks.

The production of 2nd generation biofuels can be achieved via two very different processes, although not limited to:

1. Bio-chemical. Micro-organisms convert cellulose and hemicellulose components into sugars prior to their fermentation.
2. Thermo-chemical. Gasification is used to convert carbon and hydrogen contained in feedstock into a gas of synthesis, primarily composed of carbon monoxide and hydrogen, which is subsequently synthesized into long hydrocarbon chains such as synthetic paraffinic kerosene and diesel.

This study will focus on processing the organic fraction of municipal solid waste into a thermo-chemical pathway to manufacture synthetic paraffinic kerosene and diesel.

1.3 Purpose of the study

The purpose of this study is to develop a techno-economic model for a biomass to liquid plant that integrates (i) an innovative plasma gasification system represented by a kinetic model specially developed with (ii) a FT system represented by a thermodynamic model.

The techno-economic model will enable the study of the project economics assuming the plant will process waste whose total input energy corresponds to about 350 MW. In addition, the impact of the gasification process conditions on the gas of synthesis composition and volume will be assessed by means of a plasma gasification model. A biomass to liquid process model, integrated with the plasma gasification process model, will then be developed to determine the plant efficiency and FT liquid fuels production rate. Lastly, an economic study will determine the corresponding production costs and a risk analysis will define the related uncertainty and the most influential parameters. This model could be used as a decision-making tool for investors and/or project developers who could use it to mitigate risks and identify the plant operating design that makes the most economical sense.

1.4 Significance

Biomass gasification systems have been operating for decades and they have been associated primarily with steam production for either power generation or combined heat and power (CHP) systems. One of the recurrent operational issues that these facilities faced is the massive production of tar when biomass is subjected to combustion. To overcome this issue, tar cracking systems have been developed and

they are currently operating at a pilot scale. Current BTL cost estimation models assumed a pressurized biomass gasification system integrated with a tar cracking unit at commercial scales. However, pressurized gasification systems are designed to process very stable feedstock, both from composition and physical standpoints. As such, any variation in either feedstock composition or size would have an immediate negative impact on gasification process efficiency and syngas composition and characteristics, with subsequent drawbacks for liquids production and plant profitability. Because of these gasification process' limitations, BTL projects seem restricted mainly to those that process feedstock with highly reliable composition, such as pre-treated wood. To model uncertainty, the corresponding cost models typically assume only price of pre-treated feedstock and price of FT-products as stochastic input variables. In this research, further stochastic input variables shall be taken into consideration when analyzing risks and production costs of a BTL project, such as the gasification process conditions, systems' operating conditions, and biomass to liquid process configuration.

1.5 Scope and limitations

The main purpose of this study is to model the production costs of an atmospheric pressure plasma gasification biomass to liquid plant. A "gas to liquids" plant process model shall be established and it will be based upon results found in the literature. As such, assuming a pre-defined feedstock mass rate and composition, the study will evaluate the production costs' fluctuations based upon variation of the systems' process conditions and configurations. The impact of the feedstock mass rate and composition fluctuations on the FT liquid fuels production rate will not be studied in this work.

1.6 Research goal

The major goal of this research is to develop a holistic system model for an atmospheric pressure plasma gasification biomass to liquids plant to calculate and analyze the liquid hydrocarbons' production costs under uncertainty.

The research will try to answer the following questions:

1. Considering a specific feedstock, could the syngas composition be modified for a specific syngas application by adjusting the plasma gasification island's operating conditions?
2. What is the BTL plant's process configuration that leads to optimum biomass to liquid conversion efficiency?
3. Considering a pre-set feedstock composition and mass rate, what are the corresponding FT liquid fuels production rates?
4. What are the related production costs?
5. How cost-competitive are the products resulting from the atmospheric pressure plasma gasification biomass to liquid process versus (i) other biofuels produced otherwise and (ii) crude oil-derived?

1.7 Organization of the document

In the second chapter, the methodology to perform the techno-economic study is described. In particular, a literature review for the state of the art corresponding to each major system of the process is first provided. The methodology to develop the plasma gasification and the BTL process model is then described, along with the related energy

and mass balance. Finally, a section dealing with the method to develop the economic model is developed.

The third chapter deals with the plasma gasification model. The principles of (i) gasification thermodynamics and (ii) kinetics of atmospheric pressure plasma gasification are detailed and a plasma gasification process model is subsequently developed and described. This model is used to analyze the impact of the process conditions on syngas characterization. Results are summarized and discussed.

The fourth chapter deals with designing the biomass to liquids process and sizing the related systems. Feedstock characterization is first detailed and then integrated with the plasma gasification process model developed in chapter 3. The process scheme to cool, clean and condition the syngas prior to being fed into the FT synthesis system is developed. Finally, the FT system, along with the hydrocracking and the power generation systems are designed and sized. A process flow diagram and the related energy and mass balance are developed and used to determine the plant's energy efficiency. Results are summarized and discussed.

The fifth and last chapter deals with the plant economic model. A discounted cash flow model is developed to calculate the plant's production rates and a Monte-Carlo simulation is performed to quantify the uncertainty of these production costs and to identify the most influential stochastic parameters.

Chapter 2

2 METHODOLOGY

2.1 Introduction

The methodology described in this chapter ultimately leads to a system design that is subsequently used to create a discounted cash flow model. This model is used to analyze the production costs of an atmospheric pressure plasma gasification biomass to liquids plant.

This chapter introduces the methodology that was followed to develop both the process model and the economic model.

2.2 Process model

2.2.1 Feedstock composition

Although this model enables the user to set a specific feedstock composition, including elemental and proximate characteristics, the base case scenario assumes municipal solid waste (MSW) as primary feedstock. The most up-to-date data generated by the United States Environmental Protection Agency and available online were retrieved to this end (US EPA 2011). According to USEPA, and as shown on Figure 2-1, about 34% of the MSW was recycled in 2010 while only 16% was recycled in 1990. It is further assumed that the non-recycled materials are doomed to be discarded in landfills. Considering that the amount of waste recovered has increased over the past several decades, this model will let the user to set the amount of MSW available and the corresponding percentage that

is recycled. In this model, the non-recycled fraction of MSW is therefore considered as primary feedstock.

Data in pounds per person per day	1990	2000	2010
MSW generation	4.57	4.72	4.43
Total materials recovered	0.73	1.35	1.51
Percentage of material recovered	16%	29%	34%
Population (millions)	250	281	309

Figure 2-1: MSW Generation vs. Recovery per capita per day

Not only to quantify the fraction of waste recovered, this model further qualifies the types of materials that compose MSW, and their corresponding amount. Therefore, typical MSW in the United States includes paper and cardboard, glass, metals, plastics, rubber and leather, textiles, wood, food and yard trimmings in respective quantities as described in the USEPA's report mentioned above.

The model so far combines the types of materials that enter the facility along with their respective quantities. However, in order to properly develop the plasma gasification process, it is necessary to determine more accurately the feedstock's composition upon entering the gasification island. To this end, available data bases were consulted to retrieve the elemental composition, proximate analysis and heating content for each

type of material that constitute the primary feedstock. These attributes are summarized in Figure 2-2.

Categories	Attributes
Ultimate Analysis	Carbon, Hydrogen, Oxygen, Sulfur, Chlorine and Nitrogen.
Proximate Analysis	Inert, Moisture, volatile matter and fixed carbon.
Misc.	Lower Heating Value

Figure 2-2: Feedstock attributes

In the event where several compositions were sampled for a same material, statistical means were calculated for each attribute and these statistics were subsequently considered as the primary attributes in the feedstock characterization.

At this point, all the necessary information is available to accurately characterize the feedstock to be processed in the gasification island. This synopsis is summarized in the Figure 2-3 and Figure 2-4 below.

It is important to keep in mind that this MSW recycling facility has been computerized with the intention to characterize the feedstock that is delivered to the plasma biomass gasification to liquid plant. It is not the intention to design the plant with such a MSW recycling facility.

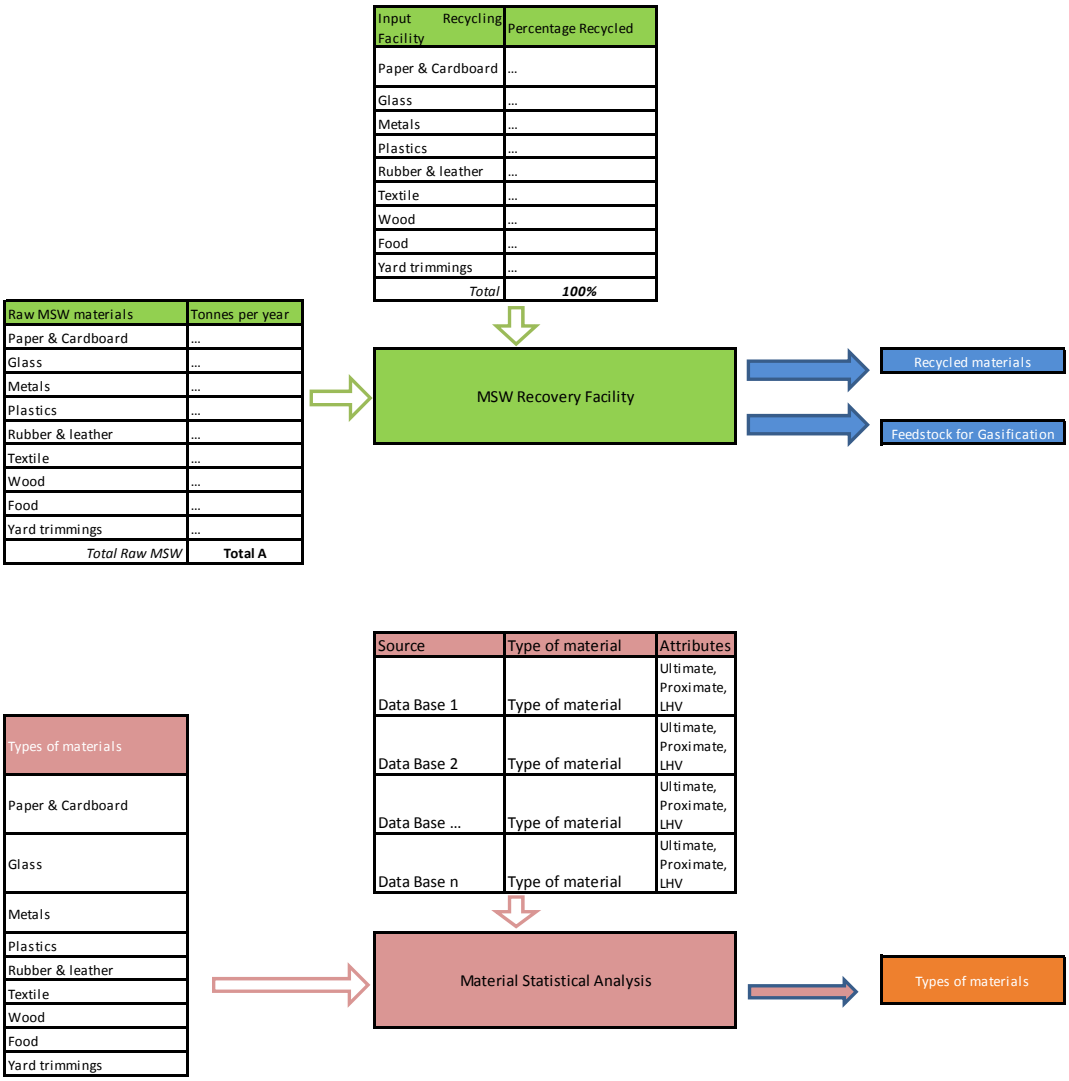

Figure 2-3: Synopsis of MSW to feedstock (1/2)

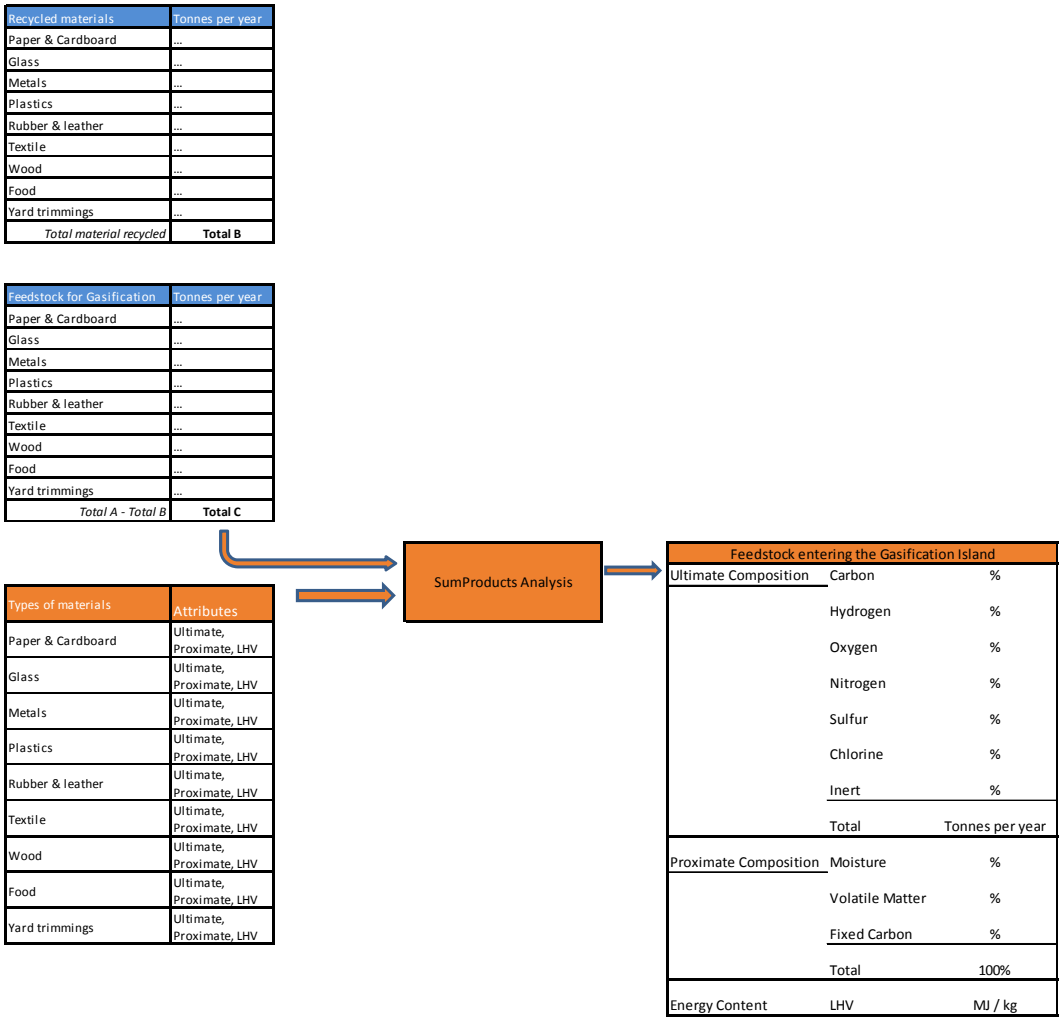

Figure 2-4: Synopsis of MSW to feedstock (2/2)

2.2.2 Gasification

At this point, the feedstock is ready to be processed. The first stage is to depolymerize the feedstock, i.e. to break its chemical bonds, and reform the resulting atoms into a gas of synthesis, also known as syngas. This process is known as gasification.

A generic definition for gasification is the conversion of a carbonaceous fuel into a gaseous product with a useable heating value. The main chemical reactions that occur during a gasification process are those listed below (Higman and Burgt 2003):

Combustion reactions

$C + {}^{1}/_{2}\, O_2 = CO$ - 111 MJ/kmol

$CO + {}^{1}/_{2}\, O_2 = CO_2$ - 283 MJ/kmol

$H_2 + {}^{1}/_{2}\, O_2 = H_2O$ - 242 MJ/kmol

Boudouard reaction

$C + CO_2 \leftrightarrow 2\, CO$ + 172 MJ/kmol

Water Gas reaction

$C + H_2O \leftrightarrow CO + H_2$ + 131 MJ/kmol

Methanization reaction

$C + 2\, H_2 \leftrightarrow CH_4$ - 75 MJ/kmol

There are many different types of gasification processes currently operating and they could be characterized into two types: fixed beds and fluidized beds.

A **fixed bed gasifier** is depicted on Figure 2-5: a fixed bed of feedstock moves slowly downwards because of gravity. As it moves downwards, it faces hot oxidant gases that move upwards, creating a counter-current effect. This type of gasifier traditionally processes lump coal and excessive amounts of fine particles can block the way of the up-flowing syngas.

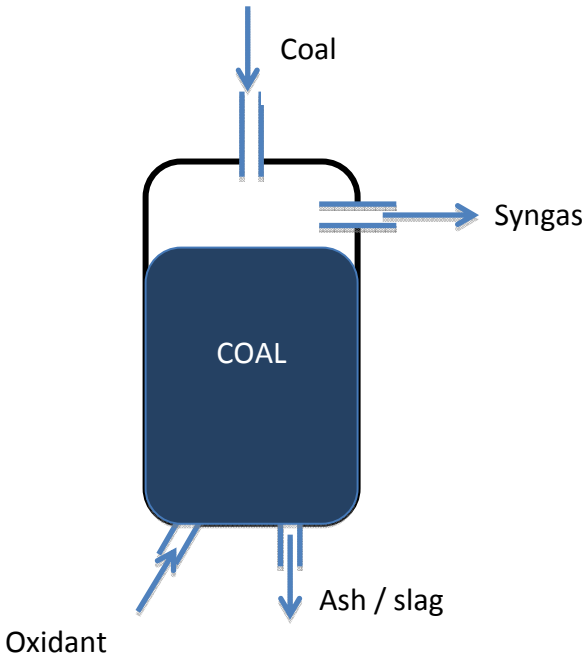

Figure 2-5: Fixed-bed gasifier

A **fluidized bed gasifier** is depicted on Figure 2-6.

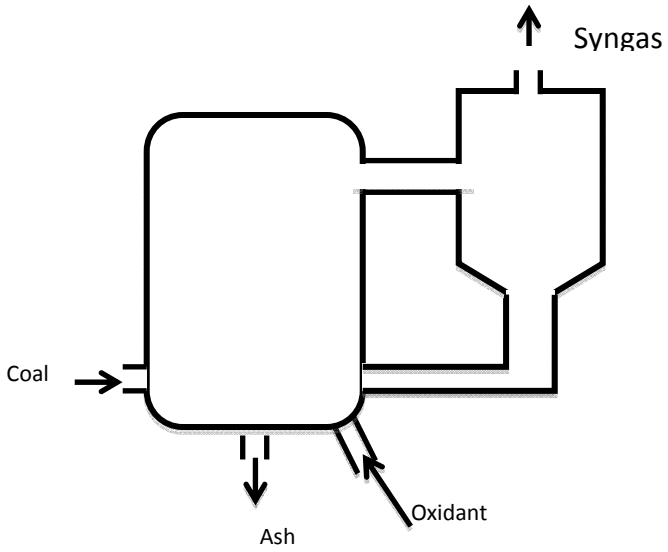

Figure 2-6: Circulating fluidized bed gasifier

In a fluidized bed gasifier, the gas velocity is sufficiently high that all solid particles are carried with the gas. If the ash content of the fuel softens, then individual particles might agglomerate and form larger particles that would fall to the bottom of the bed, which would lead to major removal problems. Therefore, it is mandatory that fluidized bed gasifiers operate at a temperature below the softening point of the ash, i.e. around 1000 deg. C for coal and around 900 deg. C for biomass. Another issue is related to fuel size. Fluidized bed gasifiers require that it does not exceed a 10 mm in cross section in order to maintain a fluidized bed.

Lastly, an **entrained flow gasifier** is depicted on Figure 2-7. This type of gasifier has the ability to process any kind of coal and to produce a methane-free, tar-free syngas. Fuel size is even more restricted than in a fluidized bed gasifier as the size shall not exceed 100 μm. Entrained bed gasifiers usually operate at high pressure (20 – 70 bar) and at temperatures above 1400 deg. C.

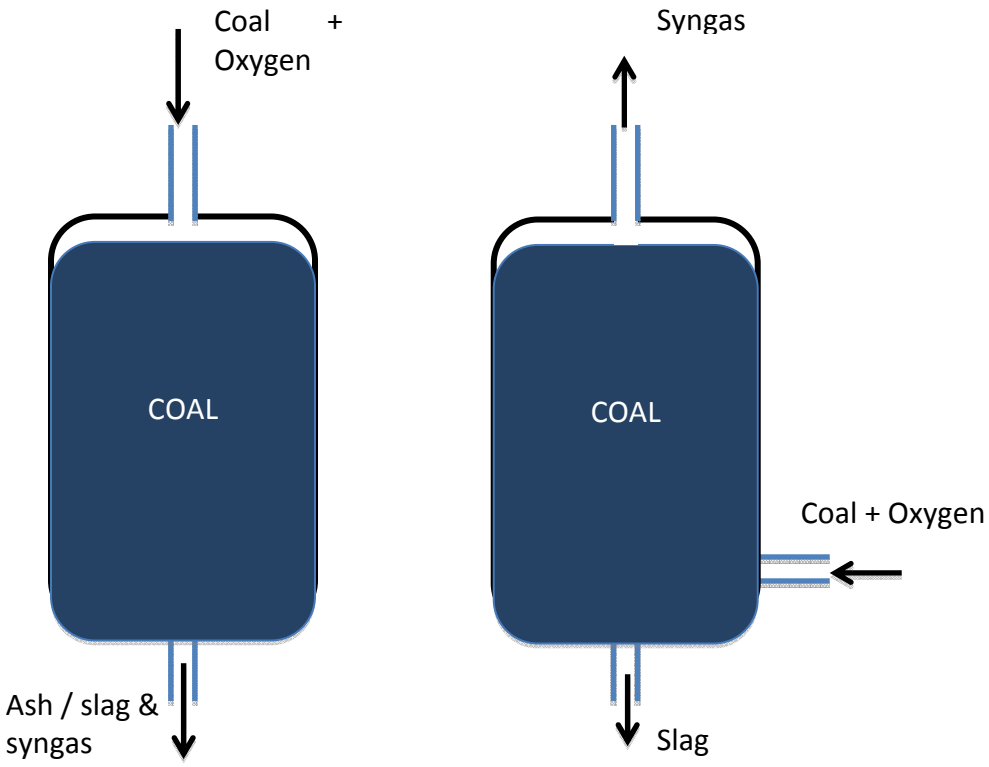

Figure 2-7: Entrained flow gasifier

Depending upon the nature of feedstock processed and gasification operating conditions, variations in syngas composition occur. When dealing with biomass and waste derived feedstock, most syngas contain tar and impurities e.g. hydrogen sulfide and hydrogen chloride. Although sulfur and chlorine were already contained in the feedstock material, tar is derived from the gasification operating conditions. Tar is considered as "the organics, produced under thermal of partial-oxidation regimes – or gasification – of any organic material and are generally assumed to be largely aromatic" (Milne 1998). The most important issue in regard to the presence of tar in syngas is its condensability (condensation temperatures range from 200°C to 600°C). Most of the syngas applications require its use below tar's condensation temperature, leading to tar

deposition on pipes and heat exchanger systems. This could damage systems located downstream of the gasifier such as gas turbines and engines (Klein n.d.). Subsequently, the presence of tar inevitably lowers the overall plant efficiency because of (i) the carbon contained in tar molecules and thus the related energy and (ii) increased probability of unplanned plant shutdowns to clean the fouled systems. Extensive literature is available on tar presence in syngas from biomass gasification as well as on catalytic systems for tar removal. However, despite the numerous systems developed to crack tars, they remain an enduring challenge for the biomass gasification industry (Rabou 2009). Although tars are produced whether with a moving bed, fluid bed, entrained flow or a fixed bed biomass gasification process, their distribution depends upon the operating conditions chosen and ranges from 1% to 15% of the product syngas in most of the cases (Monteiro Nunes 2007) (Ponzio 2006) (Kinoshita 2004). However, it was demonstrated that tar is no longer present in the syngas when the temperature is above 1100°C (Milne 1998) (Gupta 2007).

Biomass gasification is the conversion of a solid biomass into a gaseous product, known as syngas, under an oxygen-deprived environment to avoid the biomass complete oxidation. Therefore, it is necessary to control the amount and quality of oxidant fed into the gasifier. Usually, air, steam, oxygen or combinations thereof are used as gasifying agents. The use of air is certainly the cheapest way considering its abundance and free access. However, air being composed at 78% of nitrogen and 21% of oxygen, large amount of N_2 are introduced into gasification reactors and end up in the product syngas as nitrogen-based compound, including N_2, HCN, NH_3. Under this configuration,

syngas from air-blown gasifiers contains ca. 40% N_2, which is considered as inert for FT process and power production (Van Steen 2008). This leads to additional costs for the syngas cleaning systems especially considering that a larger amount of syngas is produced with an air-blown gasifier rather than with an oxygen-based gasifier. This is the reason why enriched air or pure oxygen – based gasifiers are preferred. Experimental results indicate that compared to biomass air gasification, biomass oxygen/steam gasification nearly doubles the heating value of the syngas (Lv 2007) to more than 11MJ/Nm^3.

Effects of temperature and oxidant on gasification have been analyzed. The purpose of this section is to analyze the influence of pressure over syngas composition. Experiments have demonstrated that primary and secondary aromatic tar concentrations decline when increasing the temperature or the pressure (Wolfesberger 2009). However, syngas composition is modified as pressure varies. For example, assuming a gasification temperature of 1000°C, the effect on the syngas composition of increasing gasification pressure from 1 to 30 atmosphere will drop CO and H2 from 60% and 40% to less than 40% and 30% respectively. Methane, CH4, will increase from 0% to 10% under the same conditions (Higman and Burgt 2003).

Depending on the feedstock and on the syngas application, a pressurized or an atmospheric pressure gasifier will be preferred. However, for a biomass to liquid project, the use of an atmospheric pressure biomass gasifier seems more interesting because of (i) its higher carbon conversion into CO and (ii) methane avoidance which is

considered neutral when processed in a FT system. Furthermore, the use of an oxygen/steam gasifier produces a more energetic syngas that is more suitable for power and chemical applications. Nitrogen present in the syngas comes from nitrogen contained in the biomass and from the amount of air blown into the gasifier if air is used as the oxidant agent. Avoiding a large amount of syngas throughput reduces *de facto* high capital expenditures corresponding to large-scale gasifiers and high operating expenditures because of large volumes of syngas to clean. If an atmospheric pressure, oxygen/steam gasification system seems the best option to gasify biomass and produce FT liquid fuels, the presence of tar remains a constraint.

Plasma technology seems to be an efficient way to overcome this if the plasma torch is integrated within the gasification vessel. Experiments showed that under this configuration, syngas is mainly composed of CO and H2 (Van Oost 2008) (Byun 2011) (Rutberg 2011). Plasma gasification technology has been demonstrated as one of the most effective and environmentally friendly methods for solid waste treatment and energy utilization. Studies focused on the thermodynamic analysis of plasma gasification technology and equilibrium models that incorporate thermodynamic data, energy and exergy analysis were developed in order to predict the performances of the plasma gasification process (Mountouris 2006). Syngas composition results were in total accordance with the literature. Despite the presence of approx. 40% of nitrogen in the produced syngas because of an air blown plasma gasification process, a methodology was developed to simulate a complex plasma gasification process. As demonstrated (Van Oost 2008), plasma technology provides a promising way to ensure the total

absence of tar in the syngas produced by an atmospheric pressure oxygen-blown plasma gasifier.

So far, this section highlighted a new way to produce a clean syngas by means of atmospheric pressure enriched-air-blown plasma gasifier. The expected resulting syngas is primarily composed of carbon monoxide and hydrogen with small volumes of nitrogen, carbon dioxide and other inert gases. It is also characterized by the absence of methane and longer hydrocarbon chains.

A subsequent section will be dedicated to develop a kinetic model of an atmospheric pressure plasma gasification process. Data resulting from this kinetic model will be benchmarked against similar systems found in the literature.

2.2.3 Fischer-Tropsch

An atmospheric pressure biomass gasification facility produces a syngas with a carbon monoxide to hydrogen molar ratio in the range of 1:1 whereas the FT reaction requires a ratio that ranges between 1:1 and 2:1 depending upon the type of catalyst used and the related operating conditions. The most commonly used catalysts are either cobalt-based or iron-based.

Cobalt-based catalysts do not have significant CO shift activity and the related conversion reaction is given below:

$$\mathbf{2}\ H_2 + CO \rightarrow\ H_2O +\ (-CH_2-)$$

Where (- CH_2 -) is a paraffinic hydrocarbon chain.

Iron-based catalysts do have CO shift activity and the related conversion reaction is given below:

$$\frac{3}{2}\ H_2 + \frac{3}{2} CO + \frac{1}{2}\ H_2O \rightarrow\ 2\ H_2 + 1\ CO +\ 0.5\ CO_2$$

$$2\ H_2 + 1\ CO \rightarrow\ H_2O +\ (-\ CH_2\ -)$$

Therefore, the type of catalyst does not influence the amount of H_2 and CO required to produce a given amount of (- CH_2 -).

The FT process is initiated by the adsorption of carbon monoxide on the catalyst surface and the hydrocarbon chain grows with more CO being adsorbed. In addition to the hydrocarbon chains, water is also produced along with CO_2 in the case of an iron-based catalyst FT system. Finally, regardless of the type of catalyst used, the FT process is highly exothermic and the corresponding heat of reaction is given below (Steynberg and Dry 2004):

$$\Delta H_{FT}^{0} =\ -165\ kJ.mol^{-1}$$

High heat transfer efficiency is sought to ensure that the mixture constituted of syngas and catalyst within the reactor is at the optimum operating temperature, therefore leading to high CO conversion yields.

Amongst other performance metrics, a FT process is characterized by its liquid selectivity that represents the chance that a hydrocarbon chain grows with another – CH_2 – chain instead of terminating. A high liquid selectivity is considered for any

hydrocarbon chains that contain five or more carbon atoms (S_{C5+}). Consequently, to reach high S_{C5+} yields, carbon chains in the C1 to C4 range shall decrease as much as possible, although it can be efficiently used in a gas turbine for power generation (Tijmensen, et al. 2002).

FT synthesis occurs on metallic catalysts yielding to long chain organic product compounds. These compounds are mainly aliphatic straight-chain hydrocarbons (C_xH_y). The product distribution obtained from FT synthesis includes light hydrocarbons (CH_4), ethene (C_2H_4) and ethane (C_2H_6), liquefied petroleum gas (C_3–C_4, propane and butane), gasoline (C_5–C_{12}), diesel fuel (C_{13}–C_{22}), and light and waxes (C_{23}–C_{33}) (Demirbas 2007). The Anderson-Schultz-Flory equation describes the distribution of these hydrocarbon products:

$$\log\left(\frac{W_n}{n}\right) = n\log\alpha + \log\frac{(1-\alpha)^2}{\alpha}$$

where Wn is the weight fraction of product with carbon number n, and α is the chain growth probability (Green and Perry 2007). The Anderson-Schultz-Flory distribution is then given on Figure 2-8 (Cao, et al. 2003).

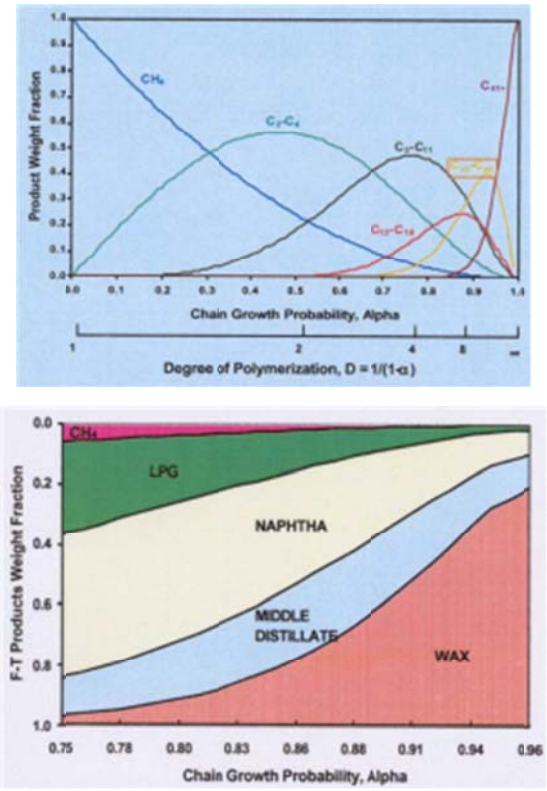

Figure 2-8: Degree of polymerization - FT product distribution

Since 1926 and the gasoline synthesis by Fischer and Tropsch, both iron and cobalt have been the predominant metals used in catalyst for industrial applications.

2.2.4 Biomass to Liquids: thermochemical process

BTL demonstration facilities have been successfully operating at small scale. Typically, a BTL facility comprises a biomass gasification step, syngas cleaning, syngas compression, carbon dioxide removal, and FT synthesize. Many studies and works have assumed woody biomass as feedstock. In an operational study, 13 kg of eucalyptus wood chip was gasified to produce almost 2 liters of hydrocarbon liquids (Hanaoka, et al. 2007). The study focused on validating a bench scale facility to produce FT liquids that were

subsequently upgraded into diesel, kerosene, gasoline and wax. The systems used were an air/oxygen-enriched air downdraft fixed bed gasifier and a cobalt-based catalyst in a FT slurry bed reactor. The authors emphasized the issues faced with tarry products and high nitrogen concentration (~40% vol.) in the syngas as well as with the issues faced with H_2: CO ratio adjustment. In regard to syngas cleaning, the authors mentioned that a dry syngas cleaning process using activated carbon was preferred over a wet syngas cleaning process for carbonyl sulfide compounds (COS) to achieve sulfur concentration lower than 5 parts per billion. The study further mentioned that the H_2: CO ratio obtained in the experiments was closer to one while a ratio close to two is recommended for cobalt-based FT reactors. Consequently, a water gas shift reaction to promote hydrogen formation is needed. In this step, although it decreases the process' carbon efficiency because of the CO_2 production, steam reacts with carbon monoxide to produce hydrogen ($CO + H_2O \rightarrow CO_2 + H_2$).

Inert gaseous compounds are considered as neutral for the FT synthesis. However, depending upon their concentration, they might considerably increase the volume of syngas to be processed in the FT reactor, thus increasing the capital cost of the FT Island. A BTL plant could therefore include an acid gas scrubbing unit to remove CO_2 prior to feeding the syngas in the FT reactor. In a BTL process, carbon contained in feedstock is partially recombined into CO_2 either at the gasification stage or at the water gas shift stage in a cobalt-based catalyst FT reactor case. We have seen that more nitrogen and carbon dioxide could reduce the FT-liquid selectivity of hydrocarbon chains. In addition, considering the higher concentration of CO_2 in this syngas than in

combustion processes' flue gas, it is expected to capture CO_2 at relatively low additional costs (Tijmensen, et al. 2002). Lastly, it is anticipated that the CO_2 captured on the plant could be stored and sold to local gas supplier companies, thus generating a potential additional source of revenues.

Other works (Larson and Jin, Biomass conversion to Fischer-Tropsch liquids: preliminary energy balances 1999) explored a process to convert biomass into FT liquids. The analysis was based on using an indirectly heated gasifier primarily because the resulting syngas would not be diluted by nitrogen since no air was blown in the process. Further, FT's α index was assumed to be 0.95, which seems optimistic considering the related literature review in section 2.2 above. Based upon these assumptions, Larson and Jin's results predict an overall high heating value efficiency ranging from 43.7% under a "Once-Through" concept to 49.4% under a "Full Recycle" concept whereas a "Full Recycle" configuration refers to a process where the syngas is processed through the FT system and any residual tail-gas is reformed into additional syngas which is fed back to the FT system and whereas a "Once-Through" configuration refers to a process where the residual tail-gas is not reformed into additional syngas to be fed back to the FT system. This difference is explained by the fact that FT's process efficiency is greater than any electricity generation system's. Larson and Jin further investigated the impact of using other gasification technologies. A combination of atmospheric and pressurized reactors, using indirect heat, air blown or oxygen blown gasifiers was used for this analysis and results show that best efficiency is achieved if an oxygen blown gasifier is used (HHV = 51.5%). However, the corresponding analysis did not include economical

aspects and further investigation should be performed to analyze the economical viability of an oxygen gasification process.

In their work, (Tijmensen, et al. 2002) aimed at identifying the most promising system configurations. They explored pressurized and atmospheric gasification pressure, as well as a cobalt catalyst for the FT unit. They explored the processes of using FT-tail gas to drive a gas turbine or recycle it in a reformer to produce additional syngas and enhance the FT liquids production. Although the study analyses several process configurations, a high temperature gasification system was missing in their design of experiments. The authors concluded that efficiencies of nearly 50% were achievable using once-through configurations.

Although there is no commercial biofuels production via gasification currently operating, there has been a continuous interest and increasing efforts in the development of BTL plants. While individual technologies within the Biomass-to-Liquids process (e.g. gasification, syngas cleaning, FT) have been proven independently, the main challenges remain in process integration (Faaij, Modern biomass conversion technologies 2006) at a commercial scale. Further, technological concepts might offer lower production costs and higher overall efficiencies, particularly if biofuels production is combined with power generation (Faaij, Modern biomass conversion technologies 2006).

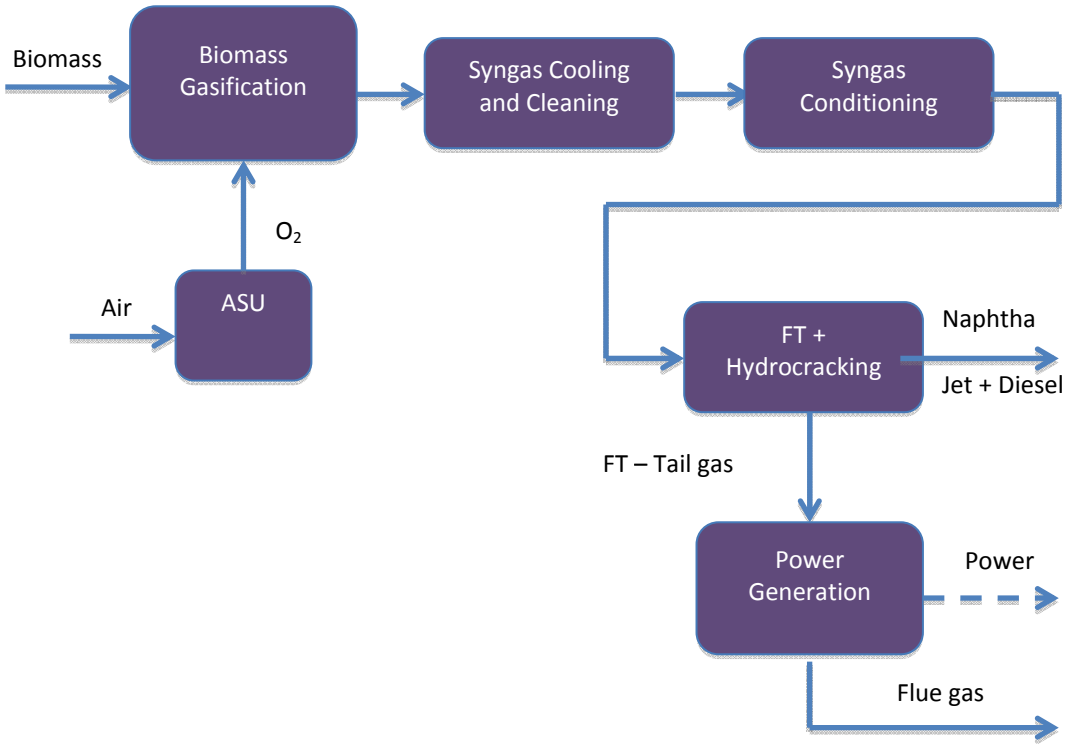

Figure 2-9: Biomass to Liquid - BTL - process

The once-through configuration shown on Figure 2-9 depicts a typical biomass gasification BTL plants process. Syngas cleaning is a critical module that not only cools down the syngas temperature, but it also recovers syngas' sensible energy. Chlorine and sulfur gaseous compounds are removed from the syngas, along with any residual water.

Syngas conditioning is another important module that allows adjustment of the H2:CO ratio to match with the FT's system. A CO2 sequestration unit could be taken into consideration in this module to decrease the volume of syngas routed to the FT reactor. The FT tail-gas is used as a fuel to drive a gas turbine in a power generation module.

Depending upon plant's parasitic loads and the amount of electricity generated, some of this power could be exported to a local grid and contribute to plant revenues.

2.2.5 Heat and material balance

Throughout every step in the process developed herein, the model shall determine the mass and energy balance for every solid, liquid and gaseous stream.

2.2.5.1 Standard

This document will follow the *Système International d'Unité* (SI) standard. As such, mass units are expressed in kilogram [kg] and energy units are expressed in Joule [J].

2.2.5.2 Mass balance

The mass balance for every system must match the following formula:

$$\sum_{i=1}^{a} \dot{m}_{sol_in} + \sum_{j=1}^{b} \dot{m}_{liq_in} + \sum_{k=1}^{c} \dot{m}_{gas_in} = \sum_{l=1}^{d} \dot{m}_{sol_out} + \sum_{m=1}^{e} \dot{m}_{liq_out} + \sum_{n=1}^{f} \dot{m}_{gas_out}$$

Where $\dot{m}_{sol_in}$ is the mass flow rate of a solid stream at the inlet of the system;

Where $\dot{m}_{liq_in}$ is the mass flow rate of a liquid stream at the inlet of the system;

Where $\dot{m}_{gas_in}$ is the mass flow rate of a gaseous stream at the inlet of the system;

Where $\dot{m}_{sol_out}$ is the mass flow rate of a solid stream at the outlet of the system;

Where $\dot{m}_{liq_in}$is the mass flow rate of a liquid stream at the outlet of the system;

Where $\dot{m}_{gas_in}$is the mass flow rate of a gaseous stream at the outlet of the system;

Where i is the number of solid streams at the inlet of the system, j is the number of liquid streams at the inlet of the system and k is the number of gaseous streams at the inlet of the system, and where a, b and c are positive integers.

Where l is the number of solid streams at the outlet of the system, m is the number of liquid streams at the outlet of the system and n is the number of gaseous streams at the outlet of the system, and where d, e and f are positive integers.

2.2.5.3 Energy balance

The energy balance for every system must match the following formula:

$$\sum_{i=1}^{a} \varepsilon_{sol_in} + \sum_{j=1}^{b} \varepsilon_{liq_in} + \sum_{k=1}^{c} \varepsilon_{gas_in} = \sum_{l=1}^{d} \varepsilon_{sol_out} + \sum_{m=1}^{e} \varepsilon_{liq_out} + \sum_{n=1}^{f} \varepsilon_{gas_out}$$

Where ε_{sol_in} is the mass flow rate of a solid stream at the inlet of the system;

Where ε_{liq_in} is the mass flow rate of a liquid stream at the inlet of the system;

Where ε_{gas_in} is the mass flow rate of a gaseous stream at the inlet of the system;

Where ε_{sol_out} is the mass flow rate of a solid stream at the outlet of the system;

Where $\varepsilon_{liq_in}$is the mass flow rate of a liquid stream at the outlet of the system;

Where ε_{gas_out} is the mass flow rate of a gaseous stream at the outlet of the system;

Where i is the number of solid streams at the inlet of the system, j is the number of liquid streams at the inlet of the system and k is the number of gaseous streams at the inlet of the system, and where a, b and c are positive integers.

Where l is the number of solid streams at the outlet of the system, m is the number of liquid streams at the outlet of the system and n is the number of gaseous streams at the outlet of the system, and where d, e and f are positive integers.

Thermodynamic data that relate to water and steam are drawn from "SteamTab Companion", verison 2.0, which is an application developed by ChemicaLogic, a corporation based in Burlington, MA.

When it relates to gaseous streams, fundamentals of stoichiometry and thermodynamics are observed, as shown in Table 2-1 below.

Table 2-1: Gaseous molecule's stoichiometry and thermodynamic data

Fuel Species	Molec Weight	Stoichiometric Reaction	LHV Btu/lbm
CO	28.011	$CO + \frac{1}{2} O_2 \rightarrow CO_2$	4,346
H2	2.016	$H_2 + \frac{1}{2} O_2 \rightarrow H_2O$	51,593
CH4	16.043	$CH_4 + 2 O_2 \rightarrow CO_2 + 2 H_2O$	21,515
C2H2	26.038	$C_2H_2 + 2\frac{1}{2} O_2 \rightarrow 2 CO_2 + H_2O$	20,734
C2H4	28.054	$C_2H_4 + 3 O_2 \rightarrow 2 CO_2 + 2 H_2O$	20,276
C2H6	30.070	$C_2H_6 + 3\frac{1}{2} O_2 \rightarrow 2 CO_2 + 3 H_2O$	20,431
C3H8	44.097	$C_3H_8 + 5 O_2 \rightarrow 3 CO_2 + 4 H_2O$	19,944
C4H10	58.124	$C_4H_{10} + 6\frac{1}{2} O_2 \rightarrow 4 CO_2 + 5 H_2O$	19,679
C5H12	72.151	$C_5H_{12} + 8 O_2 \rightarrow 5 CO_2 + 6 H_2O$	19,513
C6H14	86.178	$C_6H_{14} + 9\frac{1}{2} O_2 \rightarrow 6 CO_2 + 7 H_2O$	19,130
C8H18	114.232	$C_8H_{18} + 12\frac{1}{2} O_2 \rightarrow 8 CO_2 + 9 H_2O$	19,029
NH3	17.031	$NH_3 + \frac{3}{4} O_2 \rightarrow H_2O + \frac{1}{2} N_2$	8,001
H2S	34.080	$H_2S + 1\frac{1}{2} O_2 \rightarrow H_2O + SO_2$	6,537
COS	60.075	$COS + 1\frac{1}{2} O_2 \rightarrow CO_2 + SO_2$	3,912

The lower heating values of these fuel species are derived from (Moran and Shapiro 1995). From Table 2-1, the chemical energy contained in a gaseous stream can be derived as described:

$$Energy_{gaseous_stream} = \sum_{m=1}^{a} \prod GasSpecie_RelMass \times GasSpecie_LHVm$$

Where $Energy_{gaseous_stream}$ is the energy contained in the gaseous stream.

Where $GasSpecie_RelMass$ is the mass fraction of a specific gas molecule relative to the overall gaseous stream mass and where:

$$\sum_{m=1}^{a} GasSpecie_RelMass = 100\%$$

Where m is the number of gas species in the gaseous stream and a is a positive integer.

Where $GasSpecie_LHVm$ is the mass lower heating value of a specific gaseous molecule.

In order to comply with the SI standard, the function *CONVERT* will be used in Microsoft Excel to convert the energy expressed in BTU into Watt-hours.

2.3 Techno-economic model

The objective is to develop a discounted cash flow model that analyzes the production costs of an atmospheric pressure plasma gasification BTL plant. This model will integrate the stochastic behavior of several model components. To accomplish this objective, a process model along with a discounted cash flow model will be designed using Microsoft Excel software. The stochastic analysis will be performed using Palisade's @Risk software.

The model will be composed of 5 independent sub-models for feedstock, plasma gasification, process engineering, operation & maintenance and engineering economics.

Its structure is depicted on Figure 2-10.

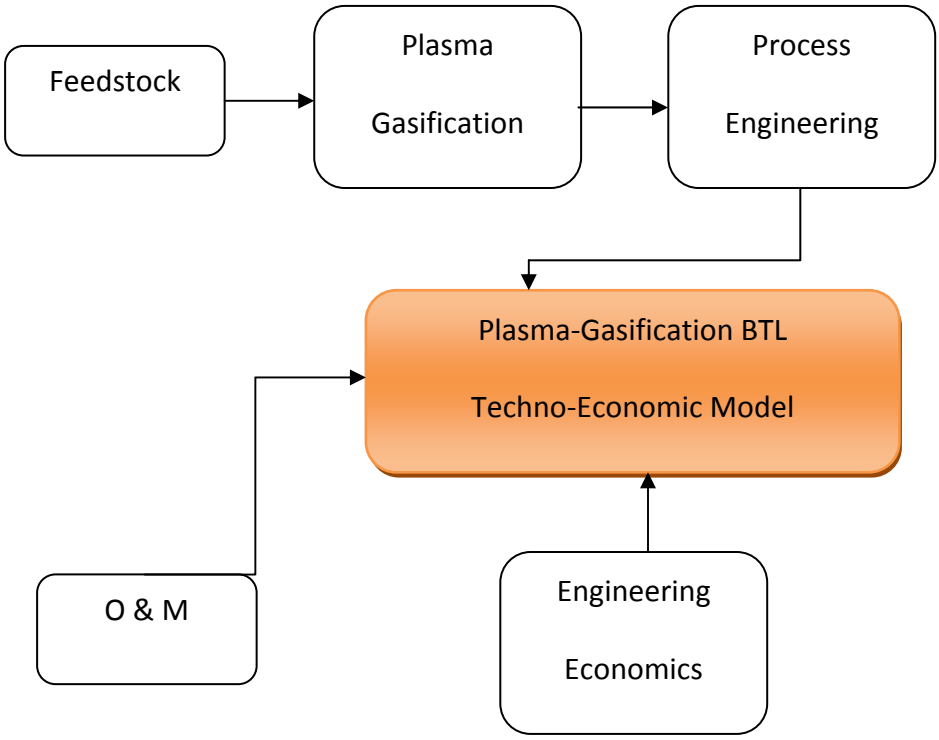

Figure 2-10: Structure of the atmospheric pressure plasma gasification BTL model

Although the model assumes that a solid refuse-derived fuel is supplied to the facility, it is critical to understand the composition of the material that is processed into the gasification system. Therefore, the feedstock sub-model will assume some types of waste, commonly used and known in the specialized literature, along with their

respective quantity and moisture content. The respective compositions will be derived from specialized literature, including elemental composition, proximate composition and lower heating content.

Inputs and outputs of this feedstock sub-module are listed in Table 2-2.

Table 2-2: Feedstock sub-module's I/Os

Feedstock	**Input** • Type of feedstock and respective quantity: wood, plastic, textile, paper, cardboard, glass, metal, etc. • Elemental composition (carbon, hydrogen, oxygen, sulfur, chlorine) • Proximate composition: Moisture, Volatile, Fixed carbon, Inert. • Low Heating content. **Output** • Feedstock elemental and proximate composition's probability density function. • Feedstock's Low Heating content.

The plasma gasification module will determine the syngas characteristics depending upon the feedstock characteristics and the process conditions.

Inputs and outputs of this plasma gasification sub-module are listed in Table 2-3.

Table 2-3: Plasma gasification sub-module's I/Os

Plasma gasification	**Input** • Output from "Feedstock" sub-module. • Catalyst and Oxidant compositions and rates. • Plasma power. • Plasma gas composition and rate. **Output** • Syngas composition (CO, H_2, CO_2, H_2O, N_2, HCl, H_2S, COS, NH_3, HCN). • Syngas temperature, rate. • Heat and mass balance.

The Process engineering module will suggest a given plant process configuration similar to the one shown on Figure 2-9 and will detail the systems contained in each of the 6 blocks – Air Separation Unit, biomass gasification, syngas cooling and cleaning, syngas conditioning, FT and hydrocracking and power generation. The module's input and output variables are shown on Table 2-4.

Table 2-4: Process engineering sub-module's I/Os

Process engineering	**Input** • Output from "Plasma gasification" sub-module. • Target amount of carbon monoxide at FT inlet. • Quantity of carbon dioxide to remove from syngas. • H_2: CO molecular ratio at FT inlet. • FT module's variables (CO conversion, alpha level) • Amount of hydrogen to supply to the hydrocracking system. • Selection of biofuels to produce (diesel, jet fuel, naphtha) and corresponding yields. • Minimum acceptable heating content of gaseous fuel entering the gas turbine. • Gas turbine heat rate. • Steam turbine heat rate. **Output** • Biofuels' production rates. • Power generation produced. • Plant efficiency.

Operation & maintenance's input variables are shown on Table 2-5.

Table 2-5: O&M module's input variables

Operation & Maintenance	• Overhead / Labor / General • Consumables (catalyst, chemicals) • Routine maintenance

Engineering economics input variables are shown on Table 2-6.

Table 2-6: Engineering economics' input variables

Engineering economics	• Systems direct capital costs – Inside battery limit • Systems direct capital costs – Outside battery limit • Indirect capital costs • Investment spent during 1st year of construction • MARR and general inflation rate • Marginal tax rate • Escalation rate • Consumables costs • Plant availability during 1st year of operation • Plant availability at full capacity • Study period • Interest rate for sinking fund • Depreciation

Chapter 3

3 PLASMA GASIFICATION PROCESS MODEL

3.1 Introduction

The development of a plasma gasification model is critical to provide accurate inputs to the techno-economic analysis.

The objective of this chapter is to develop a kinetic model of a plasma gasification process operating at atmospheric pressure to eventually predict its steady-state performances. The main hypothesis is that a kinetic model is more accurate than an equilibrium model for biomass gasification because of its complex matrix.

This section explores the bed zones of a fixed-bed counter-current plasma gasification process operating at atmospheric pressure. Once built, the model is used to predict the syngas characterization for a pre-set feedstock composition and mass rate. Finally, the results obtained are summarized and discussed.

3.2 Mathematical formulation in bed zones

The general conservation equations for energy and mass are (Sarofim, et al. 1973):

Energy balance of gas phase:

$$K_g \frac{\partial^2 T_g}{\partial z^2} - \dot{G} C_{p_g} \frac{\partial T_g}{\partial z} + h_v \left(T_s - T_g\right) = \delta \rho_g C_{p_g} \frac{\partial T_g}{\partial t}$$

Mass balance of gas phase:

$$D^E \frac{\partial^2 C_j^b}{\partial z^2} - \frac{\dot{G}}{\rho_g}\frac{\partial C_j^b}{\partial z} + k_c A_s\left(C_j^i - C_j^b\right) = \frac{\delta \partial C_j^b}{\partial t}$$

Energy balance of solid phase:

$$K_s^E \frac{\partial^2 T_s}{\partial z^2} - \dot{U} C_{p_s}\frac{\partial T_s}{\partial z} + h_v\left(T_s - T_g\right) + \sum_j R_j^* \Delta H_j = (1-\delta)\rho_s C_{p_s}\frac{\partial T_s}{\partial t}$$

Mass balance of gas phase:

$$-\sum R_j^* = (1-\delta)\frac{\partial \rho_s}{\partial t}$$

Considering the complex composition of a gasification fixed bed, these general equations will be applied to four separate zones that constitute the bed as shown on Figure 3-1 (Shadle, Berry and Syamlal 2010).

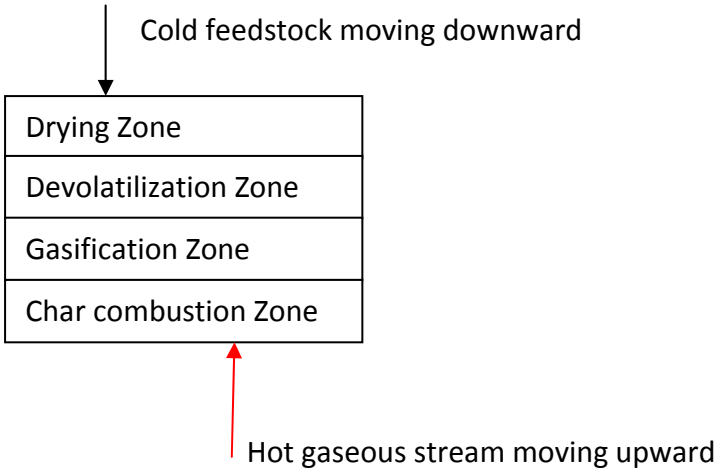

Figure 3-1: Schematic of the bed zones

Char combustion zone

The char combustion zone is defined as the zone where all oxidant is consumed unless sufficient carbon is not present. Heat transfer in this zone is given by Hobbs (Hobbs 1990) as:

$$Q_w = \frac{A_w\left(T_g - T_\infty\right)}{\frac{1}{h_w} + R_w}$$

The gas temperature in this zone is actually derived from the energy balance:

$$\dot{m}_{g_{out}} H_{g_{out}} = \dot{m}_{g_{in}} H_{g_{in}} - \left(\dot{m}_{C_{out}} H_{C_{comb}} - \dot{m}_{C_{in}} H_{C_{gasif}}\right) - \dot{m}_{ash} C_{P_{ash}}\left(T_{comb} - T_{gasif}\right) - Q_w$$

The overall reaction constant of this zone is given by the following equation (Hobbs 1990):

$$k_{ov} = \frac{A_v}{\frac{1}{k_{reac}} + \frac{1}{k_{mass_trans}}}$$

Where Av is the particle surface area per unit volume and the parameter for k_{reac} is given by:

$$k_{reac} = 2.3\, T_{comb} e^{11{,}100/T_{comb}}$$

The mass transfer coefficient is given by the following equation (Hobbs 1990):

$$k_{mass_trans} = 2.06\, \frac{G}{\delta \rho_G} Re^{-0.575} Sc^{-2/3}$$

Gasification zone

In this gasification zone, heat transfer and gas temperature are determined the same way than in the combustion zone.

The gas enthalpy can be found from the heat balance:

$$\dot{m}_{g_{out}} H_{g_{out}} = \dot{m}_{g_{in}} H_{g_{in}} - \left(\dot{m}_{C_{unconv}} H_{C_{gasif}} - \dot{m}_{C_{in}} H_{C_{devol}}\right) - \dot{m}_{ash} C_{P_{ash}} \left(T_{gasif} - T_{devol}\right) - Q_w$$

In this zone, the mass transfer coefficient k_{mass_trans} is calculated the same way it was in the combustion zone.

Devolatilization zone

In this zone, the feedstock enters the gas phase according to the volatile fraction specified in the feedstock proximate analysis.

The energy balance in this zone depends on the enthalpy of the volatiles which can be derived from:

$$HHV_{feedstock} = f_{fc}.HHV_c + f_{vol}.HHV_{vol}$$

Where $HHV_{feedstock}$ is the higher heating value of the feedstock, and HHV_c is the higher heating value of graphite which is 32,750 kJ/kg. From the definition of heating value, the heat of formation of volatiles can be derived as:

$$H_{vol}^f = \frac{\dot{m}_{prod} H_{prod}^f}{\dot{m}_{vol}} HHV_{vol}$$

Where H_f is the heat of formation and where the subscript "prod" refers to the hypothetical products of complete combustion of the volatiles. The enthalpy of the volatiles in solid forms is given as:

$$H_{vol} = H_{vol}^f + C_{P_{feedstock}} T$$

Where $C_{P_{feedstock}}$ is the specific heat of the solid feedstock.

The gas temperature can now be derived from the heat balance in a similar manner to the other zones.

$$\dot{m}_{g_{out}} H_{g_{out}} = \dot{m}_{g_{in}} H_{g_{in}} + \dot{m}_{vol} H_{vol} - \dot{m}_c \left(H_{C_{devol}} - H_{C_{dry}} \right) - \dot{m}_{ash} C_{P_{ash}} \left(T_{devol} - T_{dry} \right) - Q_w$$

The modified devolatilization kinetic rate is given by Hobbes (Hobbs 1990).

$$k_{devol} = 4.02 \times 10^5 e^{-8{,}900/T}$$

Where T is the devolatilization zone temperature.

Drying zone

In this zone, feedstock moisture leaves the fuel and enters the gas phase. In this zone the outlet gas enthalpy is derived from:

$$\dot{m}_{g_{out}} H_{g_{out}} = \dot{m}_{g_{in}} H_{g_{in}} + \dot{m}_{moist} H_{moist} - \dot{m}_c \left(H_{C_{dry}} - H_{C_{in}} \right) - \dot{m}_{ash} C_{P_{ash}} \left(T_{dry} - T_{feedstock_{in}} \right) - \dot{m}_{vol} C_{p_{Feedstock}} \left(T_{dry} - T_{feedstock_{in}} \right) - Q_w$$

The rate of drying is calculated from the heat transfer rate coefficient given by Hobbs (Hobbs 1990).

$$k_{heat_trans} = 2.06 \frac{G C_p}{\varepsilon \rho} Re^{-0.575} Sc^{-2/3}$$

3.3 Model description

The model is developed with Microsoft Excel 2010 and sub-routines developed in Visual Basic Applications (VBA).

The model enables setting of the mass percentages that correspond to each type of materials that constitute the feedstock under consideration. These types including

textile, yard trimmings, food waste, wood, other organic-based biomass, glass, construction and demolition materials, electronic waste, tires, paintings, metals, aluminum, newsprint, papers, containers and packaging, plastics (including PET, HDPE, LDPE, PVC, PP and PS). In addition, the model prompts the user to set the respective moisture fraction for each type of material.

Furthermore, to each type of material are associated the attributes that are listed in Figure 2-2. To this end, the most comprehensive data base of biomass and waste composition, Phyllis, was consulted to have access to these attributes. Proximate, ultimate and calorific values were gathered on a dry basis. Considering the moisture fraction that was previously set by the user, the proximate, ultimate and calorific values are updated accordingly. Finally, considering the respective mass percentage for each material, the average proximate and ultimate composition along with the average calorific content of the feedstock that is supplied to the plant is then derived.

Further optional sorting and drying may be set in the model prior to deriving the final proximate and ultimate composition along with the corresponding calorific content of the feedstock to be used in the gasification island.

Once the feedstock characteristics are set, the operating condition map of the gasification process shall be explored. The feedstock rate is set constant at 20000 kg/hr. The catalyst mass rate ranges from 2% of the feedstock mass rate 6% with five increments of 1% each. The oxidant mass rate ranges from 30% of the feedstock mass rate to 60% with four increments of 10% each. Lastly, plasma power ranges from 2.0

MW to 7.0 MW with an intermediary step at 4.5 MW. Consequently, this leads to a design of experiment of 60 permutations which define the operating condition map of the gasification island.

For each permutation, a complete heat and material balance of the gasification island is calculated by means of a VBA macro designed in Microsoft Excel. Syngas composition is characterized by its constituents, i.e. H_2O, CO, CO_2, N_2, H_2, H_2S, COS, HCl, HCN, NH_3 and CH_4 which are expressed in weight percentages. Syngas mass flow rate is also calculated along with its temperature. Syngas' lower heating value is determined along with its sensible energy. Lastly, slag mass flow rate and temperature are also determined.

Finally, the carbon conversion factor is determined by dividing the carbon mass rate that is contained in the syngas at the outlet of the gasification reactor by the total carbon mass rate fed into the gasification reactor as feedstock and catalyst. Carbon conversion is a statistic that is defined as (Higman and Burgt 2003):

$$carbon\ conversion\ (\%) = \left\{1 - \frac{carbon\ in\ gasification\ residue\ [\frac{kmol}{hr}]}{carbon\ in\ feedstock\ [\frac{kmol}{hr}]}\right\} * 100$$

Should this factor be below 1.00, this means that some carbon is not leaving the gasification reactor as a syngas constituent. There may be two reasons to explain this fact. First, the energy provided to the feedstock is not sufficient to break the elastic bonds of the molecules that constitute the fixed-carbon fraction of the feedstock as entered in the proximate composition. Second, the amount of oxidant injected in the process is too low for the oxygen to bond with the carbon.

Cold gas efficiency statistics are introduced as the ratio of heating value of the syngas to the heating value of the input feedstock (Higman and Burgt 2003).

$$cold\ gas\ efficiency\ (\%) = \frac{heating\ value\ in\ product\ gas\ (MW)}{heating\ value\ in\ feedstock\ (MW)} * 100$$

In this dissertation, we will assume that the overall heating value of the feedstock is the resultant of the heating values of RDF, catalyst and plasma power brought to the gasification process.

3.4 Results and discussions

The composition of the raw materials under consideration is given in Table 3-1.

Table 3-1: Raw MSW composition for base case scenario

	% Wt.	Raw Moisture content
Textile	12.00%	13.50%
Other	15.80%	25.00%
Glass	1.20%	5.00%
Metals Ferrous	3.50%	5.00%
Metals Aluminium	5.70%	5.00%
Paper	26.00%	20.00%
Containers & Packaging	25.80%	20.00%
Plastic mixture	10.00%	0.17%
	100.00%	**16.47%**

The corresponding elemental and proximate compositions along with the heating value are given in Table 3-2.

Table 3-2: Raw MSW elemental and proximate compositions and the related LHV

	Raw Composition		
Inert	16.55		
H	5.00		
C	37.54	VM	56.72
S	0.12	FC	10.26
N	0.51		
Cl	0.05	kJ/kg	15633
O	23.78	kcal/kg	3736
H2O	16.47		
Tot	100.00		

Considering that inert materials do not contribute to syngas production, it is preferable to process a feedstock whose inert content is as small as possible. To this end, feedstock pre-processing facilities could use systems such as magnets and/or optical systems coupled with pneumatic systems to remove inert items such as glass, ferrous metal and non-ferrous metal. Corresponding glass removal efficiency of 50% can safely be assumed, and up to 90% of removal efficiency for ferrous metals and 20% for non-ferrous metals.

As for the non-inert fraction, no drying process was assumed considering its inherent low moisture content.

Consequently, the ultimate and proximate compositions and calorific content of the related feedstock delivered to the gasification reactor are provided in Table 3-3.

Table 3-3: RDF composition (in wt. %) & LHV considered for the gasification base case scenario

RDF Composition	
Inert	12.51
H	5.25
C	39.47
S	0.12
N	0.53
Cl	0.05
O	25.00
H2O	17.06
Tot	100.00

VM	59.64
FC	10.79
LHV (kJ/kg)	16158
LHV (kcal/kg)	3862

The input parameters shown in Table 3-3 are set in the gasification model. As explained in section 3.3, sixty gasification operating cases are run in a design of experiments.

The cases whose carbon conversion does not exceed 99% have been systematically rejected to ensure appropriate operating conditions. Similarly, the cases whose syngas temperature does not exceed 1,200 degree Celsius have been rejected to ensure that no hydrocarbon such as tar would be present in the syngas exiting the gasification reactor.

Out of the sixty cases that correspond to the particular feedstock considered in Table 3-3, only forty four meet the carbon conversion and syngas temperature criteria. Their cold gas efficiency is shown in Figure 3-2.

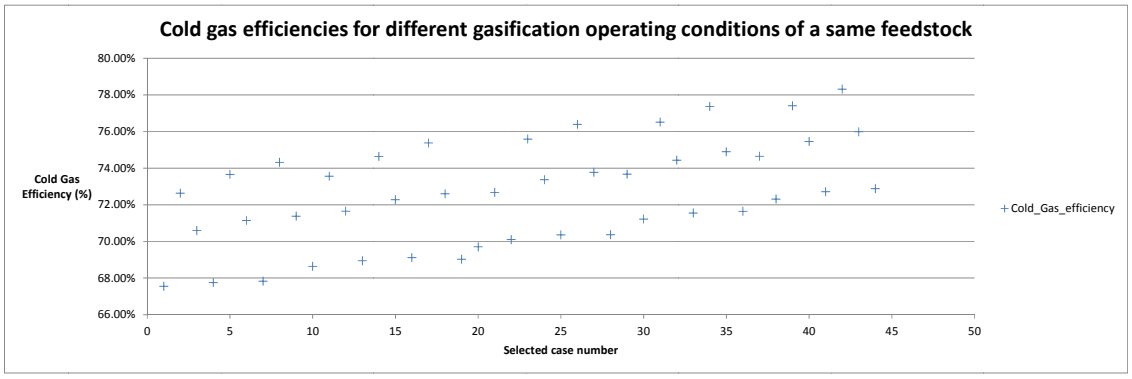

Figure 3-2: Cold Gas Efficiency of a given feedstock under different gasification operating conditions

The best cold gas efficiency case, number 42, is equal to 78% and it corresponds to a high catalyst rate, high oxidant rate and low plasma power rate configuration.

However, this does not necessarily mean that the syngas composition is optimal for a specific syngas application. Should methane be part of the syngas, therefore, the corresponding syngas heating value would certainly increase but the resulting syngas composition is of no use to a FT synthesis system where methane is considered as an inert gas.

Therefore, although cold gas efficiency is a commonly used statistic in gasification processes, it is clear that further statistics should be considered to assist in the selection of the gasification operating parameters. To this end, several syngas molecular ratios have been used and analyzed, as shown in Figure 3-3.

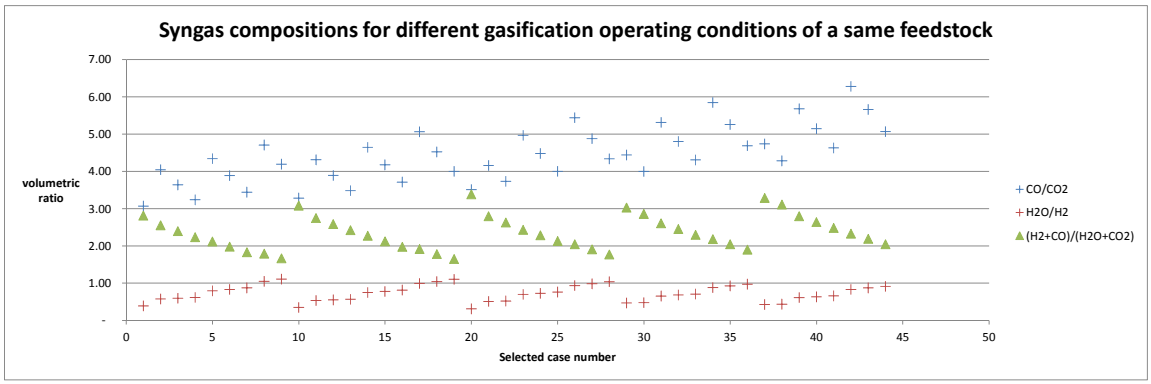

Figure 3-3: Syngas volumetric composition of the selected cases

On this figure, cases that have been selected are numbered on the abscissa axis and their respective syngas volumetric ratio on the ordinate axis. The three volumetric ratios considered are $CO:CO_2$, $H_2O:H_2$ and $(H_2+CO):(H_2O+CO_2)$ to determine the leanest syngas configuration resulting from the gasification process, where "leanest" is defined as the syngas with maximized valuable compounds such as CO and H_2 and minimized inert compounds such as CO_2 and H_2O. The data in blue represents the $CO:CO_2$ ratio, the red one represents the $H_2O:H_2$ ratio and the green one represents the $(H_2+CO):(H_2O+CO_2)$ ratio.

As explained in section 3.3 above, each case corresponds to a specific catalyst rate, oxidant rate and plasma power rating configuration. Several comments can be drawn from Figure 3-3, keeping in mind that a uniform feedstock composition was considered in the gasification process:

1. For a given oxidant and plasma power configuration, the general trend of the $CO:CO_2$ volumetric ratio seems to increase as the amount of catalyst increases, and the general trends of the $H_2O:H_2$ volumetric ratio seems to decrease but to a much lower extent than the $CO:CO_2$ ratio. In the meantime, the $(H_2+CO)/(H_2O+CO_2)$ ratio seems to follow the $CO:CO_2$ ratio tendency to increase.
2. For a given catalyst and oxidant configuration, the trend of the $CO:CO_2$ ratio decreases as the plasma power rating increases. In the meantime, the $H_2O:H_2$ ratio increases and the $(H_2+CO)/(H_2O+CO_2)$ ratio follows the pattern of the $CO:CO_2$ ratio.

3. For a given catalyst and plasma power rate configuration, the trend of the $CO:CO_2$ ratio increases as the oxidant rate increases. In the meantime, the $H_2O:H_2$ ratio increases and the $(H_2+CO)/(H_2O+CO_2)$ ratio decreases.

The $(H_2+CO):(H_2O+CO_2)$ ratio allows identification of the leanest syngas configurations resulting from the gasification process. Best results are obtained when, for each increment of catalyst rate, the oxidant rate is minimized and plasma power rating is maximized. Of these few cases, best results are actually obtained when a greater amount of catalyst is injected in the process, i.e. for cases 1, 10, 20, 29 and 37. It is interesting to note that none of the numbers provided in this batch corresponds to case 42 which has the best cold gas efficiency. The reasons for this apparent discrepancy are multi-fold and could be explained by means of Table 3-4 and Figure 3-4.

Table 3-4: Cold gas efficiencies and (H2+CO)/(H2O+CO2) ratio for selected cases

Case #	1	10	20	29	37	42
Catalyst (kg/hr)	400	600	800	1000	1200	1200
Oxidant (kg/hr)	6000	6000	6000	8000	8000	12000
Plasma (MW)	7	7	7	4.5	4.5	2
Cold gas efficiency	67.55%	68.63%	69.70%	73.67%	74.64%	78.31
(H2+CO)/(H2O+CO2)	2.81	3.08	3.38	3.03	3.29	2.33

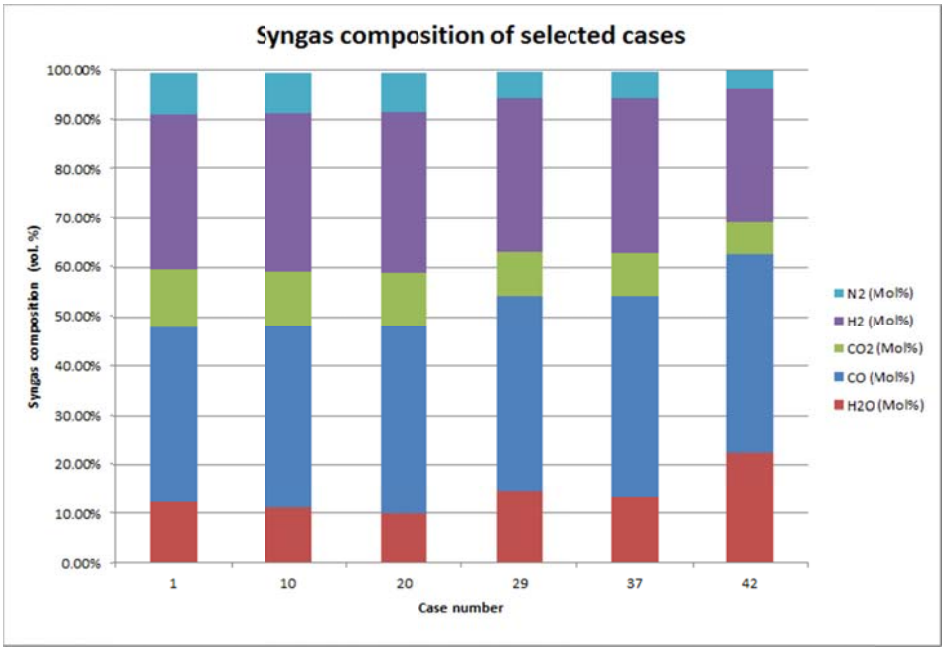

Figure 3-4: Syngas composition of selected cases (vol. % basis)

According to the cold gas efficiency formula, it is clear that the most influential factors are the syngas heating value (numerator) and catalyst heating value along with plasma power (both in the denominator). Therefore, a high cold gas efficiency could result from a high syngas heating value, a low catalyst heating value combined with a low plasma power, or a combination thereof. According to Table 3-4, case 42's highest cold gas efficiency is explained by its lowest plasma power and highest catalyst rate whose carbon content actively participates in syngas' carbon monoxide production. However, the reason that its $(H_2+CO)/(H_2O+CO_2)$ ratio is the lowest is that its syngas composition is not optimized for production of hydrogen and carbon monoxide. More specifically, case 42's catalyst and oxidant rates are higher than the ones for cases 1, 10, 20, 29 and 37. Therefore, more carbon monoxide is expected to be produced in case 42 than for

the other cases. Moreover, its oxidant rate was too high, which inevitably increases the stoichiometric ratio of the gasification process, thus the free oxygen consequently bonds with hydrogen to form additional water vapor. Figure 3-5 confirms this assumption.

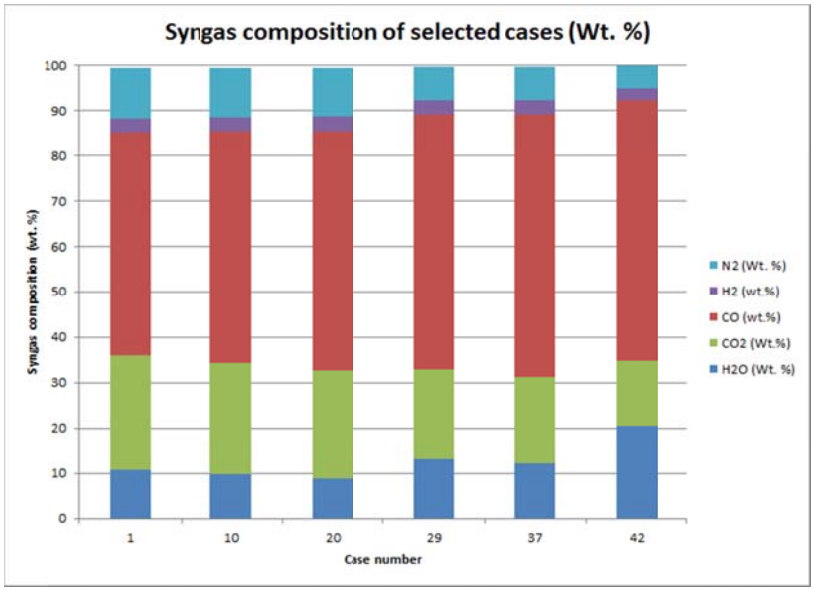

Figure 3-5: syngas composition for selected cases (Wt. % basis)

This gasification model has enabled identification of optimum trends of the operating parameters to manufacture a syngas with specific composition, and for a given feedstock. This study was executed by performing a design of experiments to predict the syngas composition based on three operating parameters, i.e. catalyst rate, oxidant rate and plasma power. However, the current results do not allow predicting the best gasification operating conditions and further research should be performed to resolve this limitation. Nonetheless, prior to proceeding further, the model should be challenged and the predicted syngas characteristics in Figure 3-4 are now compared against information available in the literature.

In her master thesis, Ducharme performed a technical and economic analysis of plasma-assisted waste-to-energy processes (Ducharme 2010). Amongst the several processes taken into consideration in her study, the author analyzed an atmospheric pressure fixed bed plasma gasification process where the waste feedstock is injected on top of a catalyst bed of metallurgical coke that is heated by means of plasma torches. The feedstock mass rate represents 49% of the overall mass entering the reactor. The catalyst feed rate is assumed to be four per cent of the MSW feed rate on a mass basis. In her study, the feedstock is assumed to be municipal solid waste. The oxidant mass rate, which is labeled as air, corresponds to about 44% of the overall mass entering the reactor. However, there is no mention of the air composition in the document. The balance of the entering mass rate corresponds to the plasma air along with limestone that is used to control the chemistry of the slag which is the product of the vitrification of the feedstock's inert fraction. It is further mentioned that the resulting syngas temperature could range between 890 degrees Celsius and 1100 degrees Celsius and the author assumed an average temperature of 1000 degrees Celsius. The corresponding syngas composition is provided in Figure 3-6.

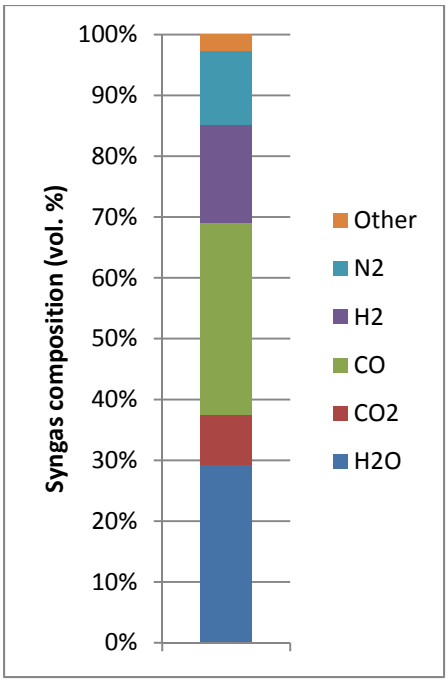

Figure 3-6: Syngas composition (vol. %) of a waste plasma gasification process

Figure 3-4 and Figure 3-6 can then be compared. At first sight, it seems the syngas are composed with the same molecules whose respective ratios are in the same order of magnitude although slightly different. These differences are due to a different feedstock composition, different syngas temperature; and probably different oxidant composition. It should be noted though that the oxidant assumed in her thesis is probably a mixture of enriched air and/or steam considering the low amount of nitrogen present in the syngas. Should the oxidant be only based on air, the amount of nitrogen in the syngas would therefore approach fifty per cent. This approximation is based on literature dealing with biomass gasification whose oxidant is air (Energi E2 2001) (The World Bank 1999) (Faaij, Van Ree, et al. 1997) (Van Swaaij 1981).

In another published document, the authors share their experience from a waste to energy facility in Japan that uses a fixed bed atmospheric pressure plasma gasification

process integrated with a catalytic bed (Willis, Osada and Willerton 2010). A heat and material balance is provided in the document. The feedstock considered is primarily MSW that is blended with some tires. Coke is the catalyst agent fed at a mass rate of 4% of the feedstock rate. The oxidant consists primarily of enriched air at 90% oxygen purity, blended with some air. Plasma power is rated at 2.4% of the input energy, which corresponds to 3.2 MW. The cold gas efficiency is rated at 79%, which is greater than the one obtained with the model developed herein. The difference could be explained by the composition of the syngas, given in Figure 3-7, and particularly the presence of unconverted hydrocarbon in the syngas because of a temperature of only 900 degrees Celsius. It should be noted that the molecular hydrogen to carbon monoxide ratio mentioned in this heat and material balance is close to 0.5 whereas the one that is calculated herein ranges between approximately 0.8 and 1.0.

Lastly, a third document was found to compare syngas compositions resulting from atmospheric pressure plasma gasification systems using a catalyst bed (E4Tech 2009). In this document, the related syngas compositions are provided, but there is no mention of either the syngas temperatures or the operating conditions. Besides, there is no addition of oxidant, which seems inaccurate, since the document focuses on gasification as opposed to pyrolysis. Nevertheless, the syngas compositions that are mentioned have molecular H_2:CO ratios that range between 0.4 and 2.0 depending upon the process selected.

In conclusion, the model that has been developed herein is consistent with the data found in available literature dealing with similar atmospheric pressure plasma gasification of biomass and/or waste.

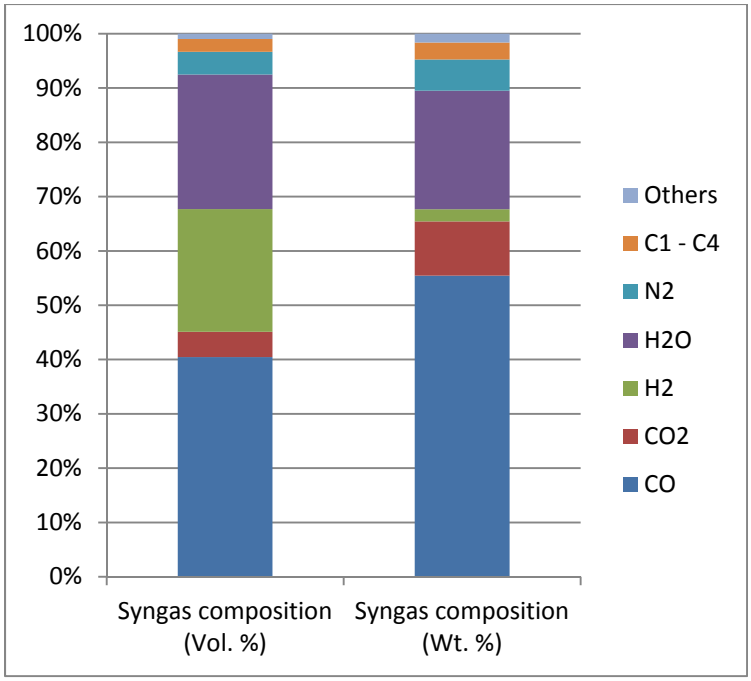

Figure 3-7: syngas composition (vol. and wt. %) of a waste plasma gasification process

Since the model is now validated, we can proceed to further researches to predict the best gasification operating conditions for a given feedstock. To this end, a design of experiment was set with Design-Expert software, version 7.1.6, developed by Stat-Ease, Inc. and the gasification model was used to provide the responses to each run. Considering a design with both mixture and process factors, a D-Optimal design of experiment was chosen. The mixture components represent the ultimate composition of the feedstock and the process factors represent its volatile matter fraction, its lower heating value, along with the catalyst rate, oxidant rate and plasma power. To limit the

number of runs, which was automatically and eventually set at 480, constraints were set to each mixture components and process factors.

A summary of the design is shown in Table 3-5.

Table 3-5: Summary of the Design o Expriment for the Gasification Process

Type	Name	Units	Low Value	High Value
Mixture	Carbon	Wt. %	30	45
Mixture	Hydrogen	Wt. %	3	6
Mixture	Oxygen	Wt. %	21	27
Mixture	Nitrogen	Wt. %	0.1	1
Mixture	Sulfur	Wt. %	0.1	0.5
Mixture	Chlorine	Wt. %	0.05	0.2
Mixture	Inert	Wt. %	7	15
Mixture	Moisture	Wt. %	15	30
Process	Volatile	Wt. %	45	60
Process	LHV	MJ/kg	13	17
Process	Coke	kg/hr	400	1600
Process	Oxidant	kg/hr	6000	12000
Process	Plasma	MW	2.5	7.0

The corresponding responses cover a wide range of data that are summarized in Table 3-6.

Table 3-6: List of responses of the design of experiments

Type	Name	Units
Syngas components	H2O, CO, CO2, N2, H2, H2S, COS, HCl, NO, HCN, NH3, CH4, C2H4, SO2.	Wt. %
Syngas characteristics	Temperature	degree Kelvin
	Mass rate	kg/hr
	LHV	MJ/kg
	Sensible power	MW
	Carbon conversion	%
Slag characteristics	Mass rate	kg/hr
	Sensible power	MW

A statistical analysis was performed for each of the 21 responses in a methodical fashion and iterative process.

First, a fit is determined. Second, the mixture components, process factors and their correlation factors are assigned an order (mean, linear, quadratic,…). Third, the analysis of variance study is performed to determine whether the model and its parameters are statistically significant. This three step process could be iterated as many times as needed to adjust the fit and/or the orders in order to improve the adjusted R-square value of the model. At this point, the final equation for the response is provided as a function of all the mixture components, process factors, and their correlated combinations. The regression formula that predicts the carbon monoxide production is expressed in Appendix A.

The fourth and final step is to verify the normality of the residuals, the studentized residuals versus predicted values to check for constant error and to check for the externally studentized residuals to look for outliers.

Once all the responses have been correctly analyzed, an optimization study is performed to predict the best gasification operating conditions for a given feedstock, while bearing in mind that the objective is to enhance the hydrogen and carbon monoxide production as opposed to cold gas efficiency.

After setting the feedstock composition as per Table 3-3 in Design-Expert, the contour responses for carbon monoxide mass percentage in syngas for different plasma power ratings are depicted in Figure 3-8. From these figures it can be concluded that the higher the plasma power is, the less carbon monoxide is produced and that CO mass percentage in syngas is directly proportional to the amount of coke and indirectly proportional to the amount of oxidant injected in the process. Overall, CO mass percentage in the syngas ranges from 42% to 65%.

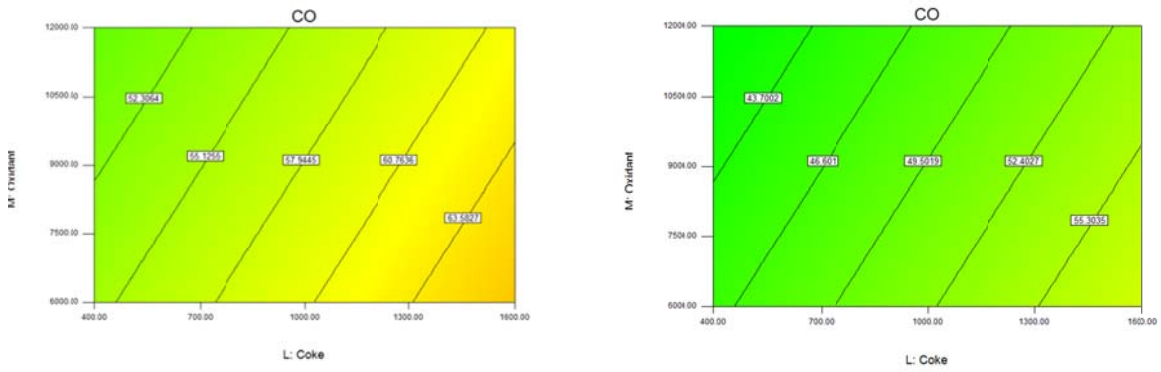

Figure 3-8: CO contour at plasma power 2.5 MW (left) and 7.0 MW (right)

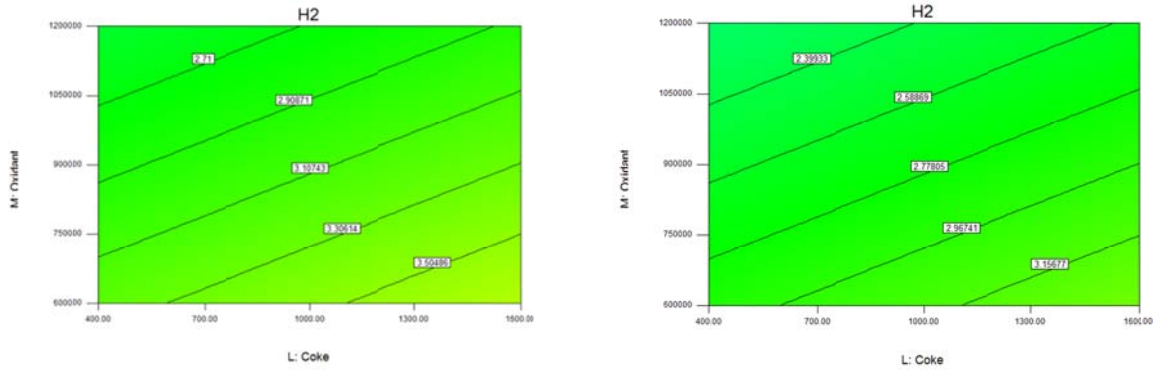

Figure 3-9: H_2 contour response at plasma power 2.5 MW (left) and 7.0 MW (right)

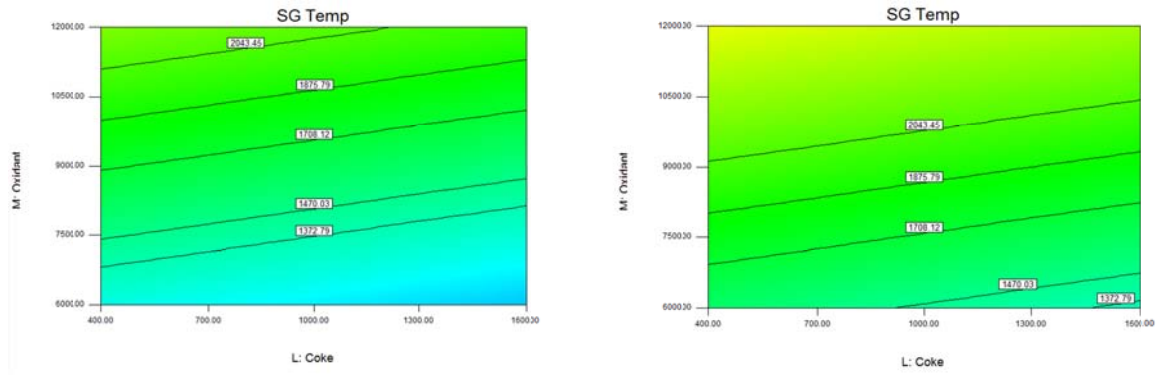

Figure 3-10: Syngas temperature contour response for plasma power 2.5 MW (left) and 7.0 MW (right)

Similarly, the contour responses for hydrogen mass percentage in syngas at different plasma power ratings are depicted in Figure 3-9. From these figures it can be drawn that the higher the plasma power is, the less the hydrogen is produced and that hydrogen mass percentage in syngas is directly proportional to the amount of coke and indirectly proportional to the amount of oxidant injected in the process. Overall, H_2 mass percentage in the syngas ranges from 2.1% to 3.6%.

Lastly, the contour responses for syngas temperature at different plasma power ratings are depicted in Figure 3-10. From these figures it can be drawn that the higher the plasma power is, the hotter the syngas is and that syngas temperature is directly proportional to the amount of coke and oxidant injected in the process. Overall, syngas temperature exceeds 1,200 degree Celsius.

For this particular feedstock, it seems that no optimal gasification operating conditions are obvious and it may be a wise alternative to suggest a compromise between the process factors whilst ensuring high carbon monoxide and hydrogen production.

3.5 Conclusion

A kinetic model was developed to predict syngas characteristics that results from the gasification at atmospheric pressure of biomass in a fixed bed reactor integrated with plasma heating technology process.

Results obtained with this model were compared with data publicly available in the literature. Although a few differences were observed, the results obtained were comparable. It was confirmed that when syngas temperature exceeds 1,200 degrees Celsius then all hydrocarbon molecules are broken down into carbon monoxide and hydrogen, thus ensuring that hydrocarbons containing at least one carbon bond (methane) and above (such as benzene) are not produced. In addition, it was shown that the gasification process is a flexible process enabling the production of a custom-made syngas. When syngas is deemed to be synthesized in a FT process, then the operating conditions should aim at optimizing the carbon monoxide and hydrogen production rather than the gasification process' cold gas efficiency.

Furthermore, this model was used to set a design of experiments. A wide range of feedstock composition, including elemental analysis, proximate analysis and heating values were analyzed along with a wide range of process factors, including catalyst rate, oxidant rate and plasma power. The corresponding statistical responses were then statistically checked and then compared with the kinetic model's responses. Particularly, carbon monoxide, hydrogen and syngas temperature were analyzed. Finally, an optimal map of operating conditions was set for a specific feedstock as a function of process factors. The conclusion is that there is no optimal operating point but instead, compromises amongst the process factors should be agreed to achieve a "smooth operating zone".

This model will then be integrated into the atmospheric-pressure plasma gasification biomass to liquid plant's process model to determine the most energy efficient process configuration.

Chapter 4

4 BIOMASS TO LIQUID AND POWER PROCESS MODEL

4.1 Introduction

The purpose of this chapter is to identify and size the systems located downstream of the plasma gasification island. Subsequently, a plant process model is developed and then used to identify the most efficient process configuration across a wide range of experiments. The best process configuration will then serve as the basis for the economic analysis and the related stochastic study.

4.2 Feedstock characterization

Traditionally, gasification has been associated with coal primarily because it increases the overall process conversion efficiency and, thus, it enhances the environmental acceptability of coal. The idea of using syngas to produce electricity using a gas turbine was reported as early as 1950 (Gumz 1950).

Coal has been formed from biomass. Throughout a several million of year process, and under the effects of pressure and temperature, biomass is subsequently converted into peat, lignite, sub-bituminous coal, bituminous coal and finally anthracite.

To distinguish feedstock, several methods are generally used and the most widely used types of analysis are the proximate and ultimate analyses. The proximate analysis determines the moisture, fixed carbon, volatile matter and inert fractions of the feedstock. Each of these categories is determined according to specific standards to

sample a fuel and they set test duration and operation conditions. It thus provides a qualitative indication of a feedstock's type. The ultimate analysis provides a quantitative concentration of carbon, hydrogen, oxygen, nitrogen, sulfur, chlorine, moisture and inert fractions of the feedstock. From the ultimate composition, the fuel's heating value can be determined per Dulong's formula (Perry and Chilton 1973), although it is mostly applicable for solid fossil fuels on a dry basis:

$$HHV\left(in\frac{MJ}{kg}\right) = 33.86 * C + 144.4 * \left(H - \frac{O}{8}\right) + 9.428 * S \quad (9)$$

where C, H, O and S refer to the mass percentages of feedstock obtained from the ultimate analysis.

Considering the greater content of carbon in solid fossil fuels, equation (9) does not reliably apply to biomass. Other works derived a methodology to determine the higher heating values for solid fuels, including fossil fuels and biomass, per proximate analysis results on a dry basis (Parikh, Channiwala and Ghosal 2005):

$$HHV\ \left(\frac{MJ}{kg}\right) = 0.3536 * FC + 0.1559 * VM - 0.0078 * Ash \quad (10)$$

Other studies focused on predicting higher heating values from proximate and ultimate analysis only for biomass fuels on their dry basis (Yin 2011):

$$HHV\left(\frac{MJ}{kg}\right) = 0.2521 * FC + 0.1905 * VM \quad (11)$$

$$HHV\left(\frac{MJ}{kg}\right) = 0.2949 * C + 0.8250 * H \quad (12)$$

The differences in coefficients between equations (9) and (12), as well as (10) and (11) are explained by the significant differences between proximate and ultimate analysis for biomass and solid fossil fuels. Qualitative studies found that proximate and ultimate analyses of biomass suffer large variations. These variations are explained mostly by the moisture content and ash yields. For instance, the values of natural biomass' volatile matter and fixed carbon range from respectively 30%-80% and 7%-35% on an "as received basis" to 48%-86% and 12%-38% on a "dry basis" (Vassilev, Baxter, Andersen, & Vassileva, 2010). Further, the study compares volatile matter and fixed carbon contents on a dry basis for all varieties of biomass and coal. Respective mean values are 75% and 18% for the former and 33% and 46% for the latter.

Extensive data bases for biomass' proximate and ultimate values are available in literature (Vassilev, et al. 2010) (Yin 2011) (Parikh, Channiwala and Ghosal 2005) (Energy Center of the Netherlands 2011).

Biomass can be broken down into several varieties, such as wood/woody biomass, herbaceous and agricultural biomass, animal biomass, waste biomass and aquatic biomass.

In 2009, 243 million tons were generated in the US, of which 33.8 % were recycled, 11.9 % were combusted and the remaining 54.3 % is disposed in landfills. In other words, 120 million metric tonnes were landfilled in 2009 (US EPA 2010). A material composition breakdown of waste landfilled in 2009 is provided on Table 4-1 where "other" refers to electrolytes in batteries, fluff pulp, feces and urine in disposable diapers (US EPA 2010).

Table 4-1: Material discarded in the municipal solid waste stream, 1960 to 2009

	Percent of Total Discards								
Materials	**1960**	**1970**	**1980**	**1990**	**2000**	**2005**	**2007**	**2008**	**2009**
Paper and Paperboard	30.2%	33.2%	31.7%	30.0%	29.0%	24.9%	22.4%	20.6%	16.1%
Glass	8.0%	11.1%	10.5%	6.0%	5.7%	5.8%	5.7%	5.6%	5.5%
Metals									
Ferrous	12.4%	10.8%	8.9%	5.9%	5.4%	5.8%	6.1%	6.2%	6.5%
Aluminum	0.4%	0.7%	1.0%	1.0%	1.4%	1.5%	1.5%	1.6%	1.7%
Other Nonferrous	0.2%	0.3%	0.5%	0.2%	0.3%	0.3%	0.3%	0.4%	0.4%
Total Metals	*13.1%*	*11.8%*	*10.4%*	*7.2%*	*7.1%*	*7.6%*	*8.0%*	*8.2%*	*8.5%*
Plastics	0.5%	2.6%	5.0%	9.6%	13.9%	15.9%	16.8%	16.7%	17.2%
Rubber and Leather	1.8%	2.4%	3.0%	3.1%	3.4%	3.6%	3.8%	3.9%	4.0%
Textiles	2.1%	1.8%	1.7%	2.9%	4.7%	5.5%	5.9%	6.3%	6.7%
Wood	3.7%	3.3%	5.1%	6.9%	7.1%	7.5%	7.8%	8.0%	8.5%
Other **	0.1%	0.4%	1.5%	1.4%	1.7%	1.8%	1.9%	2.0%	2.1%
Total Materials in Products	59.4%	66.6%	68.8%	67.1%	72.6%	72.6%	72.2%	71.3%	68.6%
Other Wastes									
Food Scraps	14.8%	11.3%	9.5%	13.6%	16.8%	18.1%	18.7%	19.5%	20.8%
Yard Trimmings	24.2%	20.5%	20.1%	17.6%	8.5%	7.1%	6.9%	6.9%	8.3%
Miscellaneous Inorganic Wastes	1.6%	1.6%	1.6%	1.7%	2.0%	2.1%	2.2%	2.3%	2.4%
Total Other Wastes	40.6%	33.4%	31.2%	32.9%	27.4%	27.4%	27.8%	28.7%	31.4%
Total MSW Discarded - %	100.0%	100.0%	100.0%	100.0%	100.0%	100.0%	100.0%	100.0%	100.0%

In the EU, the Landfill Directive 1999/31/EC requires that biodegradable fractions of MSW and used tires must not be disposed in landfills (European Commission 2003). The residual fraction resulting from the sorting process can then be either burned in an incinerator or converted into a refuse-derived fuel (RDF) – the decision often depends on economical parameters. One of the less expensive technologies to produce RDF from MSW is through a mechanical and biological treatment (MBT) process where inert materials are sorted out, organic fractions screened out and high calorific fractions

separated for RDF. The net calorific content of RDF is comprised of between 12 MJ/kg and 16 MJ/kg and has a moisture content that ranges between 15% and 25% by weight (Kallassy, Efremenko and Champel 2008). At that point, RDF is wrapped into bales, ready to be shipped (Efremenko 2008). Solid recovered fuel (SRF) can be obtained from RDF by additional drying by means of an aerobic treatment from which inert fractions and low calorific value components are separated. Consequently, SRF has a greater heating content than RDF, typically comprising between 14 MJ/kg and 18 MJ/kg (Bystrom 2010). In this dissertation, we will assume that waste-derived fuel is delivered at the BTL facility and that it shall not be further processed prior to being fed to the gasification reactors. Composition and characteristics of the corresponding feedstock delivered at the facility are shown in Table 3-3.

4.3 Plasma gasification island

The plasma gasification island will be designed to process municipal solid waste-derived fuel in such quantity that the corresponding power is about 350 MW which falls within the recommended range mentioned in a previous study (Tijmensen, et al. 2002). Considering the heating value of the feedstock as shown in Table 3-3, the corresponding quantity of feedstock needed is:

$$\frac{350\ MW\ \times 3{,}600\ {}^{sec}/_{hr}}{16.158\ {}^{MJ}/_{kg}} = 78{,}000\ {}^{kg}/_{hr}$$

In another industry document, it is said that the capacity of a plasma gasification reactor could range between 830 and 1000 tonnes per day (Westinghouse Plasma Corporation

2012) which corresponds to 35,000 to 42,000 kilograms per hour. Consequently, two of these systems would be needed to ensure complete processing of the feedstock in the gasification island. To strengthen the plant's reliability, a third gasification system will be considered in this study.

Furthermore, the plasma gasification model developed in section 3 is used to determine the expected syngas production rate and composition. This model performs a design of experiments with sixty different operating cases. Only those which have a carbon conversion greater than 99% and a syngas temperature that is equal or greater than 1200 °C are selected. Of these selected cases, those whose syngas temperature is too high could be discarded to ensure that they do not damage the systems located downstream of the gasifiers. Therefore, a third parameter is applied to select the cases whose syngas temperature falls within the range with minimum value of 1,200 degree Celsius and with a maximum value that is set by the user.

4.4 Syngas cooling, cleaning and conditioning

This section describes systems and processes used to cool, clean and condition the raw syngas to make it suitable for the FT process located downstream.

4.4.1 Syngas cooling

Considering the high temperature of the syngas leaving the gasification reactor, it is necessary to cool it down to such a temperature that it can be safely processed downstream. Furthermore, as shown in section 3.4, the syngas contains contaminants such as H_2S, COS, HCl, HCN and NH3 that shall be removed from the syngas prior to

using it as a fuel. The purpose is twofold: to prevent erosion, corrosion and catalyst poisoning of systems located downstream of the plasma gasification reactor and to comply with any environmental regulations. This section provides an overview of the related technologies.

First, the syngas that exits the plasma gasification reactor shall be cooled. To this end, a refractory lined heat recovery steam generator – also known as a boiler - is used and the related conceptual diagram is shown on Figure 4-1.

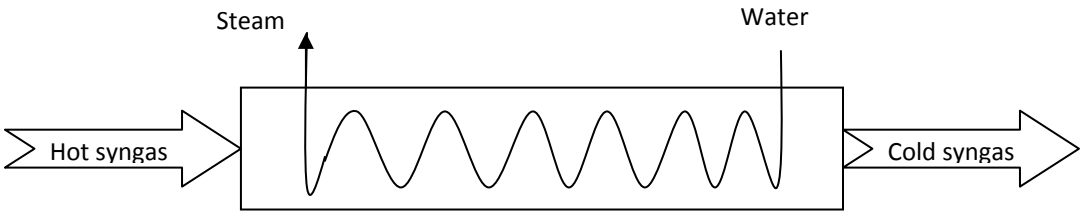

Figure 4-1: Conceptual diagram of a heat exchanger

This process is governed by the heat transfer principle which enables exchange of energy between two fluids. The energy contained in the hot fluid, i.e. syngas, is transferred to the cold fluid, i.e. water, as the former is conveyed through the system. The equations that govern this process are summarized below.

$$Q_e = \dot{m}_{hot} C_{p_{hot}} \left(T_{hot,inlet} - T_{hot,outlet}\right)$$

$$Q_a = \dot{m}_{cold} C_{p_{cold}} \left(T_{cold,inlet} - T_{cold,outlet}\right)$$

$\dot{m}_{hot}$ and $\dot{m}_{cold}$ are the mass flow rate of the hot and cold fluids, respectively.

$C_{P_{hot}}$ and $C_{P_{cold}}$ are the specific heat, at constant pressure, of the hot and cold fluids, respectively.

$T_{hot,inlet}$, $T_{hot,outlet}$, $T_{cold,inlet}$ and $T_{cold,outlet}$ are the temperatures of the hot fluid at the inlet of the system, of the hot fluid at the outlet of the system, of the cold fluid at the inlet of the system and of the cold fluid at the outlet of the system, respectively.

The syngas temperature at the outlet of the system is set in such a way that it remains above the syngas' dew point to avoid acidic components' condensation and subsequent systems' corrosion. A temperature slightly below 300 degrees Celsius is commonly accepted (Van Ree, et al. 1995) and a temperature at 225 degrees Celsius is adopted in this study.

The energy emitted from the syngas shall be absorbed by the water, i.e. |Qe| = |Qa|. In his work, Higman mentioned that only low to medium pressure steam could be obtained when syngas contains tars (Higman and Burgt 2003). Considering the high-temperature syngas resulting from the plasma gasification process, and hence no tar formation, it is safe to assume that medium pressure steam could be produced in the syngas cooler. Consequently, the corresponding amount of water needed can be calculated as shown below.

Version 2.0 of "Steam Tab", a software developed by ChemicalLogic Corporation, was used to calculate the enthalpy of water.

$$\dot{water_needed} = \frac{|Q_a|}{H_{steam} - H_{water}} * 3600$$

4.4.2 Syngas cleaning

Subsequent to cooling the syngas, a conventional wet scrubbing is necessary to remove the contaminants from the syngas. In a previous study, it is reported that reduced halogen gas such as HCl, reduced nitrogen compounds such as HCN and NH_3 and reduced sulphur compounds such as H_2S and CO_2 dissolve in the scrubber medium. When the medium is water, then mainly halogen gas and reduced nitrogen compounds dissolve in the scrubbing system. This is explained by the aqueous solubility factor which is about two orders of magnitude lower for CO_2 and H_2S than for HCl, HCN and NH_3. Carbon monoxide CO and hydrogen H_2 are even less soluble by four orders of magnitude (Van Ree, et al. 1995). Figure 4-2 depicts the aqueous solubility of these components in a scrubbing system operating at atmospheric pressure. It is also possible to enhance the process efficiency by scrubbing halogen gas and nitrogen compounds in separate systems and adjusting the scrubbing medium accordingly. For instance, it is reported that using a 3% to 6% NaOH solution could significantly improve the HCl scrubbing efficiency (Val'dberg, Lazarev and Kuzina 2003). Furthermore, another study mentions that to enhance the reduced nitrogen compounds scrubbing, a H_2SO_4 solution could be used (Van Ree, et al. 1995).

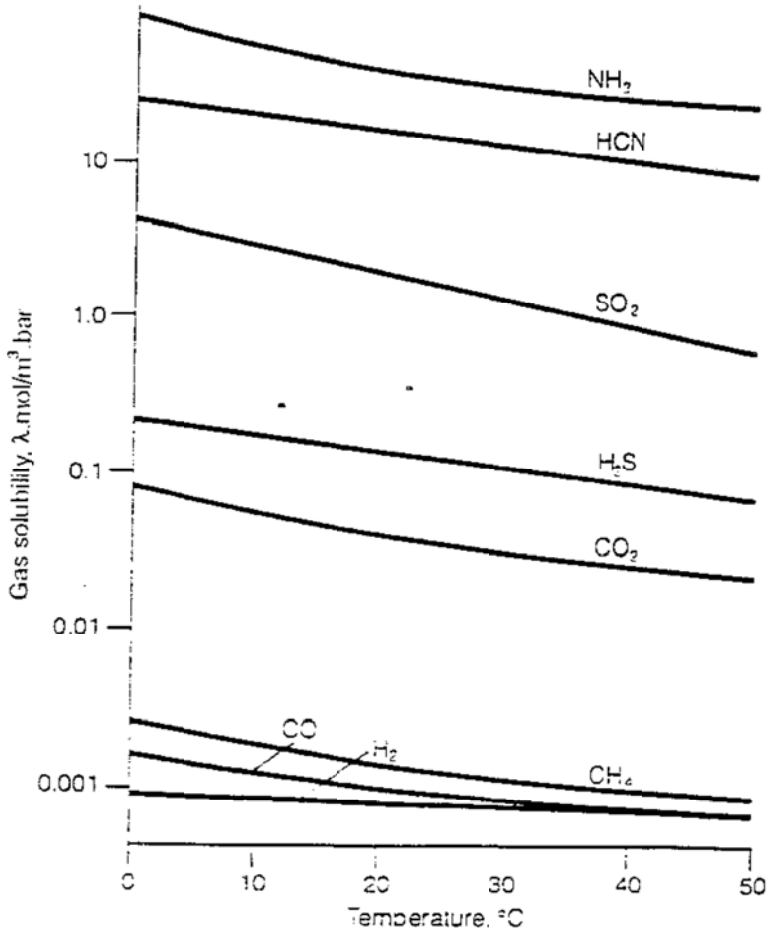

Figure 4-2: Aqueous solubility of syngas components at 1 bar (Van Ree, et al. 1995)

Subsequent to cooling the syngas temperature and removing HCl and NH_3 traces, sulfur compounds such as hydrogen sulfide and carbonyl sulfide should be removed to avoid FT catalyst deactivation (Van der Laan 1999) (Andrews and Logan 2008). These acid gases, along with carbon dioxide, are generally removed by processes using either chemical or physical absorption solvents (National Renewable Energy Laboratory 2009).

Most of these chemical or physical processes operate at pressurized atmospheres. Since this work considers an atmospheric pressure syngas, it is necessary to compress it. Prior to compressing it, the syngas should be further cooled to drop its temperature below

the dew point and knock out its water content, resulting in less syngas volume to compress and therefore leading to less energy required for the compression. In this process, it is assumed that 97% of the water vapor contained in the syngas actually condenses into liquid water. The resulting syngas is then ready to be compressed.

Previous studies report syngas pressure at the inlet of the Selexol unit as low as 418 psia which corresponds to approximately 29 bara (WorleyParsons Group, Inc. 2006) and as high as 65 bar (Larson and Tingjin, Synthetic fuel production by indirect coal liquefaction 2003). In this study, we will consider the syngas pressure at the inlet of the Selexol unit at 33 bars since the required pressure at the inlet of the FT unit is about 30 bars. The difference accounts for pressure drops through different systems between the compressor and the FT unit. We will assume that the compressor is an adiabatic system and therefore we can use the ideal gas law to determine the syngas temperature at the outlet of the compressor (Walas 1990):

$$T_o = T_i \left(\frac{P_o}{P_i}\right)^{\left(\frac{Cp}{Cv}\right)-1 \Big/ \frac{Cp}{Cv}}$$

Where Ti is the syngas temperature at the inlet of the compressor; Pi is the pressure at the inlet of the compressor; Po is the syngas pressure at the outlet of the compressor and Cp and Cv are the heat capacities of the syngas at constant pressure and constant volume respectively.

The compressor's theoretical adiabatic power is calculated as (Walas 1990):

$$THP = \frac{(Syngas_SCFM) \times T_i}{8130 \times \left[\frac{\frac{Cp}{Cv} - 1}{\frac{Cp}{Cv}}\right]} \times \frac{Po}{Pi}^{\left[\frac{\frac{Cp}{Cv}-1}{\frac{Cp}{Cv}}\right]} - 1$$

Where Syngas_SCFM is the syngas volumetric flow rate in standard cubic feet per minute.

Furthermore, the coupling power is calculated as the theoretical adiabatic power minus the heat dissipated in the compressor, the latter being determined as:

$$heat\ dissipated = \dot{m_{syngas}} \times C_P \times (To - Ti)$$

The recommended compressor motor power shall be rated for 10% above the coupling power:

$$recommended\ motor\ power$$
$$= (theoretical\ adiabatic\ power - heat\ dissipated) \times 1.1$$

The resulting cool, clean, dry and compressed syngas is now suitable to be processed in the sulfur removal system.

In a chemical absorption process, acid gases react with a solvent to produce a chemical compound. The solvent can be regenerated by application of heat to strip the absorbed gases. Typical chemical absorption processes use an amine solvent such as monoethanolamine (MEA), diethanolamine (DEA), methyldiethanolamine (MDEA) or others. A chemical absorption process performance summary for solvents is provided in Table 4-2.

Table 4-2: Chemical absorption process performance summary (National Renewable Energy Laboratory 2009)

	MEA	DEA	MDEA
H_2S (ppmv)	1	4	10
CO_2 (ppmv)	15	200	Bulk removal

CO_2 absorption is preferred but not mandatory since this is not a poisonous compound to the FT catalyst. Besides, any CO_2 absorbed would result in a smaller volume of syngas fed to the FT reactor and this would be considered favorable. Therefore, MDEA seems to be a legitimate solvent for chemical absorption process, particularly considering that it has already been integrated into a gasification process (Department of Energy 2004).

In a physical absorption process, an organic solvent is used to absorb the acid component without chemical reaction. Each acid component is absorbed in proportion to its concentration and solubility – high solubility of acid gases being the driving force in this process. Amongst their advantages, physical absorption processes enable H_2S vs. CO_2 selective recovery, removal of impurities such as COS and mercaptans and solvent regeneration. The main drawback though is the high operating pressure combined with low operating temperatures to get a most efficient and economical process (National Renewable Energy Laboratory 2009). A physical absorption process performance summary is provided in Table 4-3.

Table 4-3: Physical absorption process performance summary (National Renewable Energy Laboratory 2009)

	Selexol	Rectisol
H_2S (ppmv)	1	0.1
CO_2 (ppmv)	300	10-100
Selective H_2S removal	yes	yes
Removal of COS, mercaptans	partial	yes
Typical solvent losses (Lb /MMSCF sweet gas)	0.5	Not reported
Commercial experience with gasification (coal & petcoke)	yes	Yes

One of the advantages of physical processes versus amine-based processes is that the former do not react chemically with the absorbed gases, thus avoiding formation of heat-stable salts (Breckenridge, et al. 2000). Further, a Claus process system could be integrated downstream of the acid gas removal system to convert the hydrogen sulfide to elemental sulfur. The process involves a multistage catalytic oxidation according to the following overall equation:

$$2\ H_2S + \ O_2 \rightarrow 2S + 2\ H_2O$$

The Claus processes consists of burning one-third of the hydrogen sulfide to produce sulfur dioxide according to the following reaction:

$$2\ H_2S + \ 3\ O_2 \rightarrow 2\ SO_2 + 2\ H_2O + heat$$

The remaining uncombusted two-thirds of the hydrogen sulfide undergoes the following reaction to form elemental sulfur:

$$2\,H_2S + \,SO_2 \rightarrow 3S + 2\,H_2O$$

It is estimated that about 95% to 97% overall recovery can be achieved, depending upon the number of catalytic reaction stages (Environmental Protection Agency 2009).

Given that sulfur compounds are poisonous to the FT catalyst, and taking into consideration their respective performances, a physical process is therefore preferred versus a chemical process. A Selexol process will be considered in this study to reach 1 ppmv total sulfur level and a sulfur guard will be placed downstream to reach ppbv levels at the FT reactor inlet. Previous feasibility studies explored the use of a Selexol unit integrated in integrated coal gasification in a combined cycle process (Larson and Tingjin, Synthetic fuel production by indirect coal liquefaction 2003). In their works, Larson and Tingjin processed a syngas carrying about 16,500 kmol / hr into a Selexol unit to remove both H_2S and CO_2. Another study refers to using a Selexol unit for H_2S and CO_2 removal simultaneously (Kreutz, et al. 2005). In their study, Kreutz et al. indicate that H_2S levels in the syngas leaving the Selexol are generally contained within a 20 – 50 ppmv level. They mention however that it is possible to achieve levels of about 1 ppmv and possibly to reach the ppbv levels by integrating a sulfur guard to the previously mentioned system.

The stream of H_2S captured in the Selexol is subsequently processed into a Claus unit to produce elemental sulfur, therefore avoiding having to flare sulfur compounds in the atmosphere.

4.4.3 Syngas conditioning

Thus far, this chapter has dealt with syngas cooling, cleaning, drying and compressing. However, its primary components have not yet been addressed to ensure that their volumetric ratio matches with the FT system's requirement. To this end, two systems are used: a steam methane reformer (SMR) and a water-gas-shift-reactor (WGSR). Their respective main stoichiometric reactions are:

$$CH_4 + H_2O + heat \rightarrow CO + 3H_2 \qquad with\ heat = 206\ kJ$$ (Stipanovitch 2006)

$$CO + H_2O \rightarrow H_2 + CO_2$$

It is therefore possible to adjust the hydrogen to carbon monoxide molecular ratio of the syngas entering the FT unit by controlling the amount of natural gas fed to the SMR unit and the amount of syngas entering the WGSR along with the corresponding quantity of water vapor. In this conditioning process, the reformed natural gas is blended with the syngas exiting the acid gas removal unit, prior to being processed in the WGSR. In addition, the model enables the user to set a target amount of carbon monoxide at the FT inlet and divert the resulting excess syngas to the power generation system. The second objective is to set the H_2:CO molecular ratio. A subroutine is developed in VBA to perform the calculation. A loop sets the quantity of natural gas by

increments of 100 kg/hr until the final H_2:CO mole ratio reaches the target value. Within this loop, another loop calculates the amount of carbon monoxide that shall react with water vapor within the WGSR to ensure the required production of hydrogen. Within this loop, the amount of carbon monoxide reacting in the WGSR is set by increment of 500 kg/hr.

In some instances set by the design of experiments, the syngas entering the conditioning island may have enough or more CO and H_2 than is needed to match with the FT H_2:CO mole ratio requirement. Therefore no additional syngas resulting from the SMR operation would be needed. It is also possible that the syngas, once conditioned to the appropriate H_2:CO mole ratio, has a quantity of CO and H_2 that exceeds the corresponding target and therefore any excess syngas would be directed to the gas turbine to be combusted.

In the other cases, the SMR shall provide enough carbon monoxide and hydrogen necessary to saturate the FT reactors. The SMR must be sized to process the maximum amount of natural gas amongst these cases selected by the design of experiments. Similarly, the WGSR shall be sized to process the maximum amount of carbon monoxide and steam amongst these cases selected by the design of experiments. In this analysis, we will consider that natural gas is composed solely of methane and that stoichiometric conversion is observed as opposed to equilibrium. This means that the methane will be converted into production of only carbon monoxide and hydrogen.

Another objective of the SMR is to split its syngas produced in two streams; one is blended with the syngas exiting the Selexol unit and the resulting mixture is processed through the WGSR. The second stream is conveyed to a pressure swing adsorption (PSA) unit where impurities and carbon monoxide are removed to produce very pure hydrogen that is needed by the hydrocracking facility. Since the SMR is an endothermic process, heat must be provided to the system (Yang and Ogden 2007) (Stipanovitch 2006). This heat will actually be provided by burning additional natural gas in a furnace since the residual gases from the PSA are mainly composed of carbon monoxide and may not provide enough heat. A schematic of the conditioning island is depicted in Figure 4-3. Hydrogen and carbon dioxide are the products resulting from the inherent stoichiometric reaction in the WGSR. Although hydrogen is a desired product, carbon dioxide increases the volume of conditioned syngas to be delivered to the FT facility and is therefore not necessarily desired. In the section dealing with syngas cleaning, it was mentioned that a CO_2 removal unit could be integrated with the Selexol unit. This could reduce the overall volume of the FT reactors and consequently the related FT capital expenditures. The model enables the user to set a target for total inert content in the syngas at the FT inlet and a VBA routine subsequently determines the corresponding amount of CO_2 to remove. For the FT process, H_2O, CO_2, N_2 and CH_4 are considered inert.

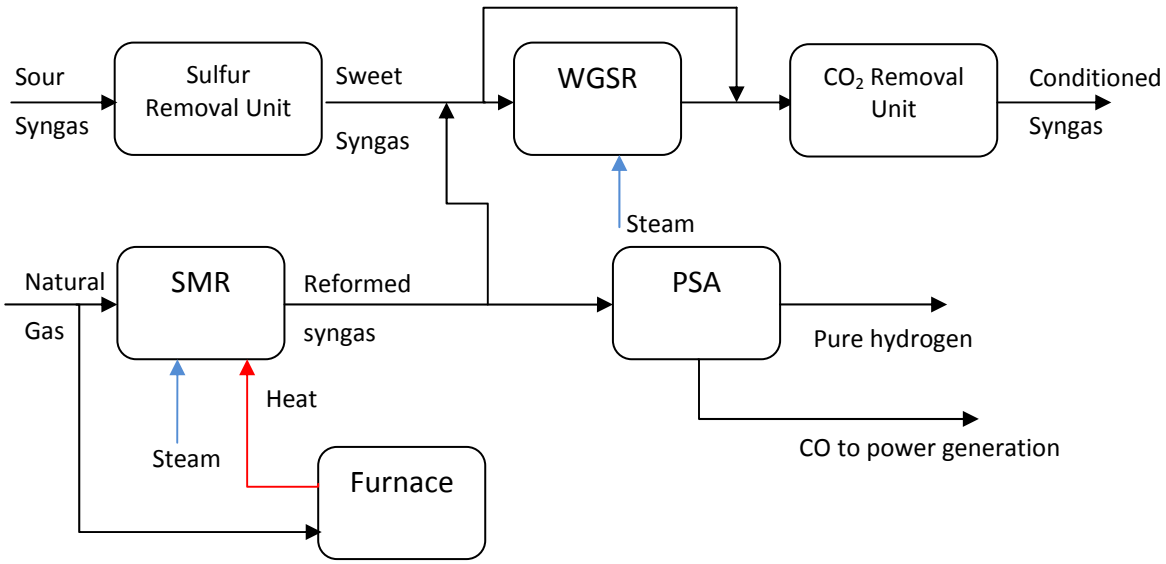

Figure 4-3: Block flow diagram of the conditioning island

4.5 Fischer-Tropsch and FT-products hydrocracking

As explained in section 2.2.3, the principle of the FT synthesis is to produce long chain hydrocarbons from a mixture of carbon monoxide and hydrogen. The main reaction governing this synthesis is provided below and corresponds to paraffinic waxes (Leviness, et al. 2011):

$$n\,CO + (2n+1)\,H_2 \rightarrow C_nH_{2n+2} + n\,H_2O + \Delta H$$

This synthesis is exothermic and the corresponding enthalpy ΔH = -165 kJ/mol.

This means that the carbon monoxide contained in the syngas interacts with the FT catalyst and participates in the paraffinic wax production. However, in fact, only a

fraction of the carbon monoxide reacts with the FT catalyst and therefore some carbon monoxide does not participate in wax production and passes through the reactor. This unconverted fraction of carbon monoxide, along with the light hydrocarbons resulting from the FT synthesis – typically those molecules with carbon number ranging from 1 to 4 – constitute a "tail gas".

Furthermore, the paraffinic wax production mechanism follows the Flury-Schultz polymerization kinetics which is characterized by a probability of chain growth (α). Consequently, the carbon number distribution of the FT products can be described by a statistical model known as the Anderson-Flory-Schultz (AFS) distribution (Tijm 1994). This distribution is described in section 2.2.3 as:

$$\log\left(\frac{W_n}{n}\right) = n\log\alpha + \log\frac{(1-\alpha)^2}{\alpha}$$ (Green and Perry 2007)

In his works, Tijm states that the probability of chain growth could range between 0.70 and 0.95. Figure 4-4 depicts the AFS distribution for two different α values, 0.85 and 0.91. It can be observed that the greater the α value, the fewer light hydrocarbons are likely to be produced and the more heavy hydrocarbons are likely to be produced. In this work, we will assume a base case alpha value of 0.91 as suggested in Hammond's works (Hammond, et al. 2009).

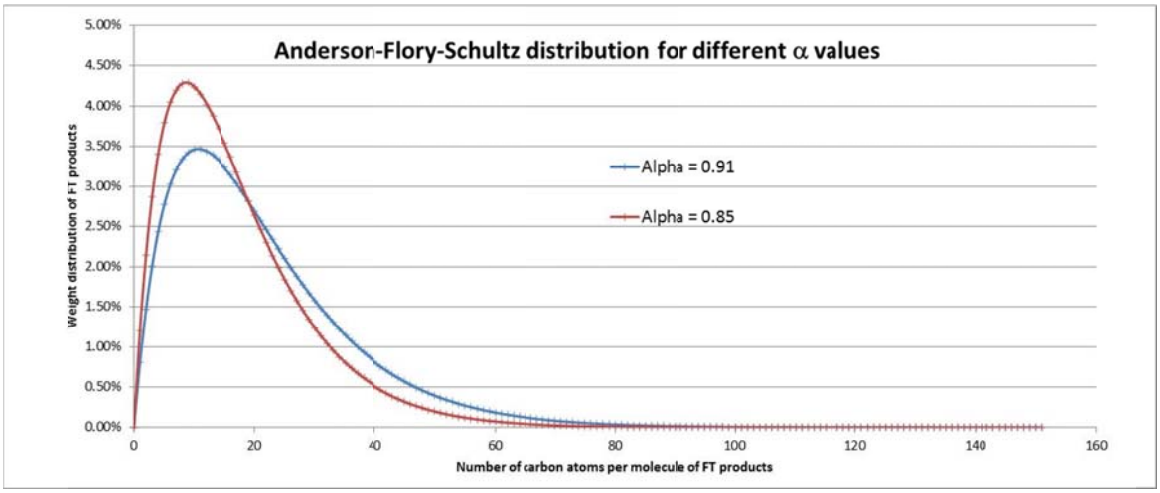

Figure 4-4: Anderson-Flury-Schultz distribution for 2 alpha values

The FT synthesis could be conceptually broken-down as shown in Figure 4-5.

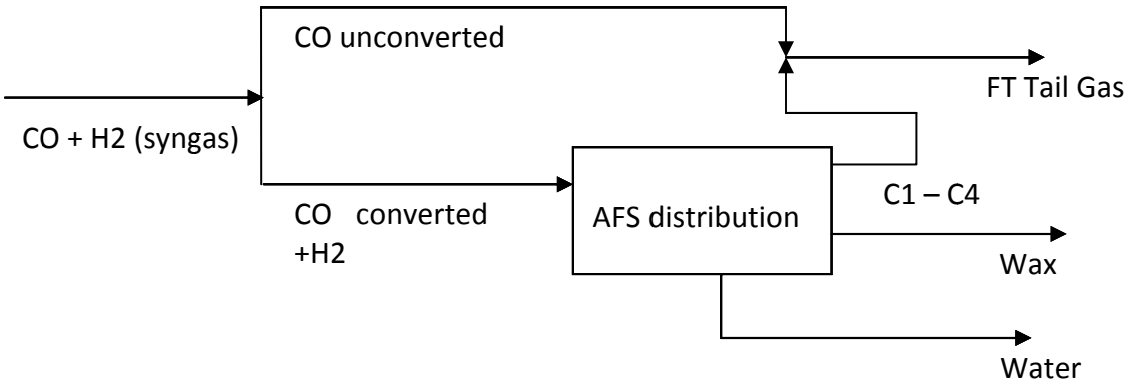

Figure 4-5: Schematic of the FT synthesis concept

Figure 4-5 can be used to track the carbon and hydrogen atoms entering the FT process and ultimately to determine the FT tail gas composition and flow rate, wax composition and flow rate by carbon number and water flow rate.

Most of the FT processes use either a fixed bed reactor or a slurry bed reactor. In this study, we will consider a microchannel process technology such as the one described in a recent natural gas to liquid techno-economic study (Hammond, et al. 2009) mainly because of the very interesting CO conversion rate and alpha value that can be achieved. Operating and performance parameters of such a system are summarized in Table 4-4.

Table 4-4: Microchannel FT technology operating and performance parameters

Parameter	***Results***	***Source***
CO conversion	>70%	(Nexant, Inc. 2008)
α	0.89 – 0.91	(Nexant, Inc. 2008)
Temperature (° C)	210 – 240	(Nexant, Inc. 2008)
Pressure (psig)	350	(Dritz 2011)
H_2:CO ratio	2.1 : 1.0	(Nexant, Inc. 2008)
Contact time (ms)	<250	(Nexant, Inc. 2008)
Catalyst life (years)	2	(Dritz 2011)

Since the amount of carbon monoxide converted into FT products has been determined, the heat released during the FT synthesis can be calculated along with the quantity of water to be supplied to maintain the adequate FT operating temperature.

The wax product shall then be hydrocracked to produce drop-in fuels, e.g. diesel and kerosene. Figure 4-6 depicts a typical process flow diagram. The hydrocracking facility is composed of reactors containing a catalyst to maximize the production of desired products. The effluents of the reactors are flashed in a hot separator to split the hot

liquid bottoms from the overhead product. The reason for integrating a hot separator is to prevent cold parts of the facility to be fouled by hot liquid bottoms. The overhead product is then processed in a cold separator to split the recycle gas from the product. The latter is then sent to the fractionator.

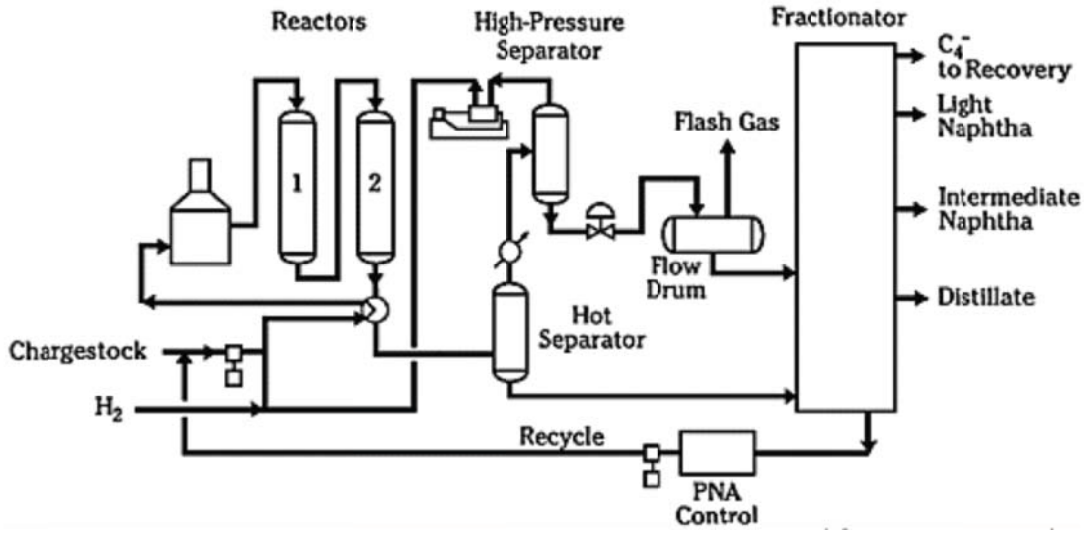

Figure 4-6: Hydrocracking process flow diagram (Meyers 2004)

Besides the wax product, referred to as chargestock on Figure 4-6, high purity hydrogen is needed to perform the hydrocracking process.

Typical operating parameters are summarized in Table 4-5.

Table 4-5: Hydrocracking facility typical operating parameters

Parameter	***Results***	***Source***
LHSV (hr^{-1})	1 – 3	(Shah, et al. 1988)
Pressure (bara)	8 – 42 35 – 70 55 - 100	(Miller, et al. 2001) (Shah, et al. 1988) (Hilbert, et al. 2008)
Hydrogen (SCFB)	1000 – 10000 456 – 748 500	(Miller, et al. 2001) (Shah, et al. 1988) (Speight and Ozum 2002)
Hydrogen (Nm^3/m^3)	90 – 219	(Hilbert, et al. 2008)
Fired fuel (BTU/hr)	2 – 6 per 1000 BPD of wax	(Meyers 2004)

Where SCFB refers to standard cubic feet of hydrogen per barrel of wax and Nm^3/m^3 refers as normal cubic meter of hydrogen per cubic meter of wax.

Where the liquid hourly space velocity (LHSV) is a process variable that measures volumetric rate per unit volume of catalyst.

In their works, Shah et al. performed several hydrocracking experiments to determine the effect of some operating parameters on product yields and characterization along with the corresponding hydrogen consumption. These are summarized in Table 4-6.

Table 4-6: Wax hydrocracking yields from (Shah, et al. 1988)

Run #	901	902	903	904	905	906
Pressure (psig)	507	1000	751	1000	998	999
LHSV (hr^{-1})	0.99	1.00	1.00	1.99	2.99	2.98
Catalyst type	A	A	A	A	A	A
H_2 (SCFB)	456	581	531	581	677	748
C1 (wt. %)	0.05	0.05	0.05	0.05	0.06	0.05
C2 (wt. %)	0.07	0.07	0.08	0.08	0.07	0.80
C3 (wt. %)	0.50	0.45	0.48	0.39	0.55	0.72
C4 (wt. %)	4.53	3.46	2.98	4.05	7.28	7.44
C5 (wt. %)	4.81	3.74	3.43	4.44	6.59	7.86
C6 (wt. %)	5.52	4.41	3.87	4.74	6.57	7.95
C7 – 300 (wt. %)	16.10	14.66	13.05	13.91	16.50	18.59
300 – 550 (wt. %)	35.50	43.23	39.81	40.50	37.31	35.33
550 – EP (wt. %)	32.82	31.09	37.16	33.08	27.41	23.25
Sub-total C7 +	*84.42*	*88.98*	*90.02*	*87.49*	*81.22*	*77.17*
Total (wt. %)	99.9	101.16	100.91	101.24	102.34	101.99

C1 to C7 refer to hydrocarbon molecules with 1 to 7 atom of carbon respectively. Consequently, C1 to C4 refer to light gases with carbon number ranging from 1 to 4. C5 and C6 refer to light naphtha. Heavy naphtha is referred to C7 – 300 °F. Jet fuel refers to the 300 °F – 550 °F boiling range cut and diesel fuel refers to the 550 – 700 °F boiling range cut.

Note that the total sum of cuts does not add up to 100% because it takes into consideration hydrogen consumption.

From Table 4-6, several observations can be made:

1. At same pressure, same catalyst type and same hydrogen consumption, then more C7 and heavier products are produced if the LHSV decreases. Consequently, if more wax is processed, more light products tend to be produced.
2. At same pressure, same catalyst type and same LHSV, then more C7 and heavier products are produced if the hydrogen consumption decreases and [jet + diesel] production seems favored against [light naphtha + heavy naphtha].
3. As reactor pressure increases, the overall C7+ product yield increases and it seems to decrease as the pressure keeps increasing.

In this study, process conditions and product yields for the FT and hydrocracking facilities are summarized in Table 4-7.

Table 4-7: FT and hydrocracking process parameters and product yields

Process conditions		Hydrocracking product yields (wt. %)	
CO conversion (%)	70	C_1-C_4	3.98
α-level	0.9	C_5 – 300 °F	22.55
H_2 to hydrocracking (SCFB)	580	300 °F – 550 °F	30.73
		550 °F – EP.	42.73

To determine the quantity of hydrogen required by the hydrocracking process, the volume of wax shall first be calculated. The model tracks every paraffinic wax compound with carbon number ranging from 5 to 151. Each of these compounds has its own density which is used to compute the corresponding volumetric flow rate as per the following equation:

$$Volume_{wax_n} = \frac{Mass_rate_{Wax_n}}{density_{Wax_n}}$$

Where wax_n refers to a molecule of wax with carbon number n.

The final FT products' lower heating values are summarized in Table 4-8.

Table 4-8: FT fuels LHV

FT Fuels lower heating content (MJ/kg)		
LPG	46.6 46	(Boundy, et al. 2011) (Dinçer and Zamfirescu 2011)
Naphtha	44.38 44	(Boundy, et al. 2011) (Dinçer and Zamfirescu 2011)
Jet	44.1 43.2 42.8	(NETL 2010) (Dinçer and Zamfirescu 2011) (International Air Transport Association 2012)
Diesel	44 42.8	(Kalnes, et al. 2008) (Dinçer and Zamfirescu 2011)

4.6 Power Generation

As explained in previous sections of this document, three gaseous streams are directed to the power generation system to produce electricity, namely the FT tail gas, the residual carbon monoxide from the hydrogen pressure swing adsorption system and any excess syngas that would be available.

In a previous study, Tijmensen explored the possibility of burning the residual gases, such as the FT tail gas. He noted that it is possible to use commercial gas turbines if the lower heating value (LHV) of the gas is greater than 4 to 6 MJ/Nm^3 (Tijmensen, et al. 2002). Consequently, should the mixture of gas sent to the gas turbine have a LHV lower

than 6 MJ/Nm3, then this mixture shall be blended with supplementary natural gas until the related LHV reaches the required threshold.

Knowing the heating content of the fuel gas processed in the gas turbine and its mass rate, the corresponding power content at the inlet of the gas turbine can be determined. Furthermore, taking into consideration the gas turbine's heat rate, the amount of electricity produced can be computed. For a General Electric 6B heavy-duty gas turbine, power generation is quoted 42.1 MW with a turn-down ratio as low as 50% (General Electric Energy 2013) and the corresponding heat rate is 11227 kJ/kWh (GE Power and Water 2013).

It is further assumed that the flue gas resulting from the combustion of the fuel gas in the turbine enters a heat recovery system to produce steam by cooling the flue gas temperature. The amount of steam produced is calculated as :

$$Steam\ produced\ (MW) = \frac{Fuel\ gas\ energy - electricity\ produced\ (MW)}{heat\ recovery\ efficiency}$$

Where the heat recovery efficiency is assumed 95%.

This steam, along with the steam generated from residual heat of other systems such as the syngas cooling system, is subsequently processed in a steam turbine integrated with a generator to produce additional electricity. Additional information is also available regarding the MS6001B combined cycle performance (GE Power and Water 2013). The overall combined cycle process heat rate is 7340 kJ/kWh. From this, it follows that the steam turbine's heat rate is 14400 kJ/kWh.

4.7 Balance of the plant

An air separation unit (ASU) is necessary to provide the gasification island with the necessary amount of oxygen. The power requirements for this system are estimated at 0.25 kWh / Nm3 of 95% purity oxygen (Beysel 2009).

A steam methane reformer will generally provide sufficient hydrogen to the hydrocracking process. The related main reaction is stated below:

$CH_4 + H_2O + heat \rightarrow CO + 3H_2$ $with\ heat = 206\ kJ/mol$ (Stipanovitch 2006)

The necessary amount of heat required will be produced by natural gas combustion in a dedicated furnace.

4.8 Results and discussion

The design of experiments developed in the Plasma gasification process model section is integrated with the process model described in this section. For each case selected by the design of experiments, a mass and energy balance is developed. The operating parameters that were assumed in the analysis are summarized in Table 4-9.

The feedstock rate of 78,000 kg/hr is chosen in such a way that its energy content is close to the 350 MW recommended by Tijmensen (Tijmensen, et al. 2002).

Several process configurations are then explored to improve the overall plant energy efficiency by adjusting the target carbon monoxide volumetric rate at the inlet of the FT

unit. To this end, alternative process configurations are analyzed across a spread of carbon monoxide targets that range from 1000 to 1400 kmol/hr.

Table 4-9: Operating and performance parameters of the BTL process

Feedstock (MJ/kg)	16.158
Feedstock mass rate (kg/r)	78000
Max syngas temperature (°C)	1500
Syngas pressure at compressor outlet (bara)	33
Natural Gas LHV (MJ/kg)	45.5
Target amount of CO at FT inlet (kmol/hr)	1000 – 1400
H_2:CO ratio at FT inlet	2.1 : 1.0
Max inert content at FT inlet	15%
CO conversion	70%
α-level	0.9
hydrogen to hydrocracking (scf / barrel of wax)	580
Hydrocracking product cut (%) C1 – C4 Naphtha Diesel jet	 4.98 22.55 30.73 42.73
Minimum fuel gas LHV to gas turbine (MJ/Nm^3)	6
Gas turbine heat rate (kJ/kWh)	11227
Steam turbine heat rate (kJ/kWh)	14400

Table 4-10: Plant energy efficiency vs. CO vol. rate target at FT inlet

Target CO vol. rate at FT inlet (kmol/hr)	NG for additional SG (kg/hr)	Best plant energy efficiency (%)
1000	0	46.50%
1050	0	47.00%
1100	0	47.60%
1150	0	48.10%
1200	0	48.60%
1250	0	49.20%
1300	0	49.60%
1350	600	50.20%
1400	800	50.80%
1450	1800	51.30%

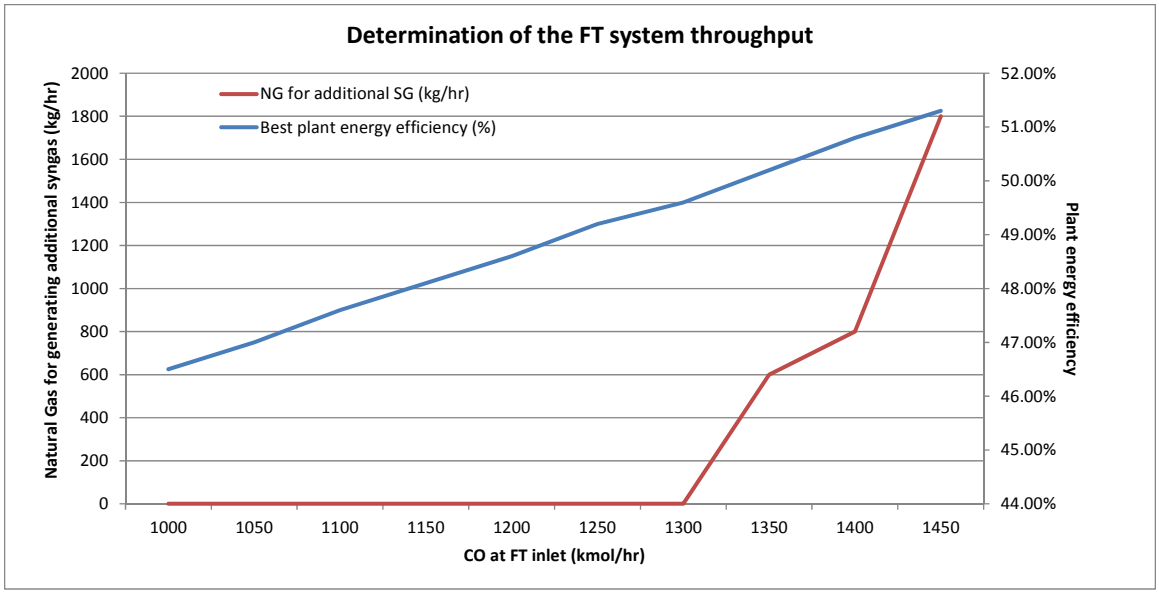

Figure 4-7: Determination of the FT system throughput

The plant process model and its subroutines in VBA is used to perform the study. For each value of the carbon monoxide target, the analysis is performed across the entire map set by the design of experiments which corresponds to sixty operating conditions. The highest plant energy efficiency is selected for each case along with the corresponding amount of natural gas needed to produce additional syngas, should it be needed to match with the required CO target value at the inlet of the FT unit.

The plant's energy efficiency is calculated as follows:

$$Efficiency = \frac{Energy\ (naphtha + \ jet + diesel + electricity\ produced)}{E\ (electricity\ consummed + natural\ gas + feedstock + catalyst)}$$

Where all energy contents are expressed on a LHV basis.

From Table 4-10, it can be observed that with a low CO volumetric rate target at the inlet of the FT unit, plant energy efficiency is lower. This could be qualitatively explained as follows. Since less syngas is to be processed in the FT system, then more syngas is actually diverted to the power generation system. Consequently, less FT liquid fuel is produced and more electricity is generated. Since the energy efficiency of an integrated FT + hydrocracking system is greater than a power generation system, values summarized in Table 4-10 do make sense.

Figure 4-7 depicts the values from Table 4-10 and is used to provide a quantitative analysis of the natural gas needs for additional syngas production. Until the CO target of 1300 kmol/hr is reached, no additional syngas is necessary to saturate the FT system and therefore no natural gas is required. The ebb occurs at CO = 1300 kmol/hr. As the CO target has been reached and exceeds this threshold, the quantity of natural gas rises in a proportional fashion to the amount of CO required and the related coefficient of proportionality is 0.083 kg/hr of natural gas per kmol/hr of CO.

In general, a trade-off between a carbon monoxide target and natural gas consumption would be made. In particular, the threshold is set at CO = 1250 kmol/hr to ensure a minimum amount of natural gas needed for the process.

Since the plant's main systems have been sized and the process scheme set, the sensitivity of the plant energy efficiency can now be analyzed by varying the plant operating parameters. To this end, the gasification design of experiments is integrated with the BTL process model.

From the initial sixty cases generated by the model, only fourteen match with the criteria as set above and they are therefore selected for further analysis. The gasification island's and the BTL's operating parameters are summarized in Table 4-11.

Table 4-11: Base case process model operating parameters

Gasification catalyst rate (% of feed rate)	2% - 6%
Gasification oxidant rate (% of feed rate)	30% - 60%
Plasma power (kW/tonne of feed)	100 – 350
CO target at FT inlet (kmol/hr)	1250
Rest of operating parameters	See Table 4-9

Results of this study are shown on Figure 4-8. The best case is obtained for a gasification catalyst rate of 5%, an oxidant rate of 50% and a plasma power of 100 kW/tonne. The corresponding material and energy balance is shown in Appendix B and the corresponding wax composition is provided in Appendix C.

The resulting liquid FT fuel mass rates are shown in Table 4-12.

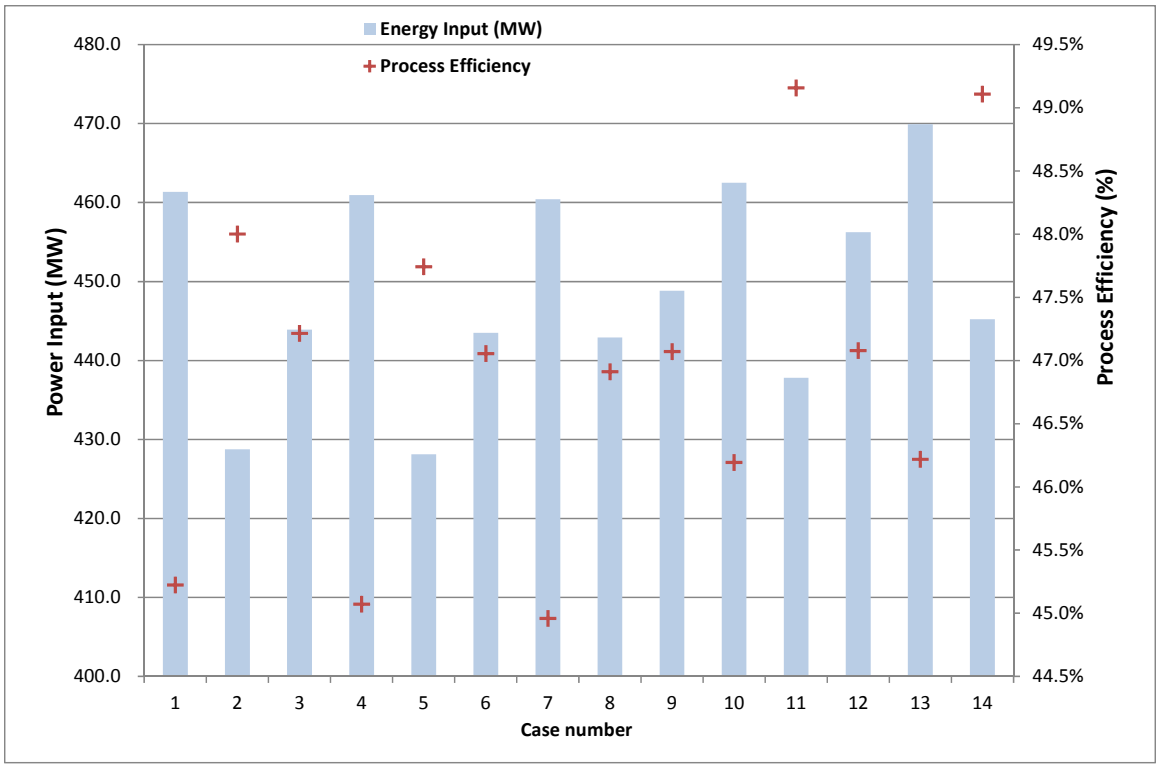

Figure 4-8: Energy efficiency for the process configurations selected

Table 4-12: FT fuel production rate (barrels/day)

	mass flow rate		density		vol. rate		vol. prod. Rate		vol. prod. Rate	
Naphtha	2,599.5	kg/hr	670.0	kg/m3	3.88	m3/hr	24.4	bbl/hr	586	bbl/day
Jet	3,543.1	kg/hr	780.0	kg/m3	4.54	m3/hr	28.6	bbl/hr	686	bbl/day
Diesel	4,926.6	kg/hr	790.0	kg/m3	6.24	m3/hr	39.2	bbl/hr	941	bbl/day
	11,069.1	kg/hr			14.7	m3/hr	92.2	bbl/hr	2,213	bbl/day

In order to identify which of the operating parameters have the greatest effects on the plant's energy efficiency, a sensitivity analysis was performed with TopRank, version 6.0 which is a software licensed by Palisade Corporation.

The input parameters under consideration, along with their distribution function and characteristic values, are listed in Table 4-13.

Table 4-13: Input parameters for process sensibility analysis

Input parameters	Unit	Distribution	Min value	Base	Max.
Coke rate	% of feedstock rate	Normal	-20%	5	+20%
Oxidant rate	% of feedstock rate	Normal	-20%	50	+20%
Plasma power	kW/tonne of feedstock rate	Normal	-20%	100	+20%
Feedstock rate	tonnes per hour	Normal	-20%	78	+20%
H_2:CO ratio in syngas at FT inlet	Mol. %	Normal	1.9	2.1	2.3
CO_2 to remove form syngas	kg/hr	Normal	-20%	46000	+20%
CO conversion	%	Normal	-20%	70%	+20%
α-level	none	Triangular	0.87	0.90	0.92
Hydrogen to hydrocracking	SCF/barrel of wax	Normal	-20%	580	+20%
Gas turbine heat rate	kJ/kWh	Normal	-20%	11227	+20%
Gas turbine heat rate	kJ/kWh	Normal	-20%	14400	+20%

From this analysis, a tornado graph and a spider graph were generated and they are shown on Figure 4-9 and Figure 4-10 respectively.

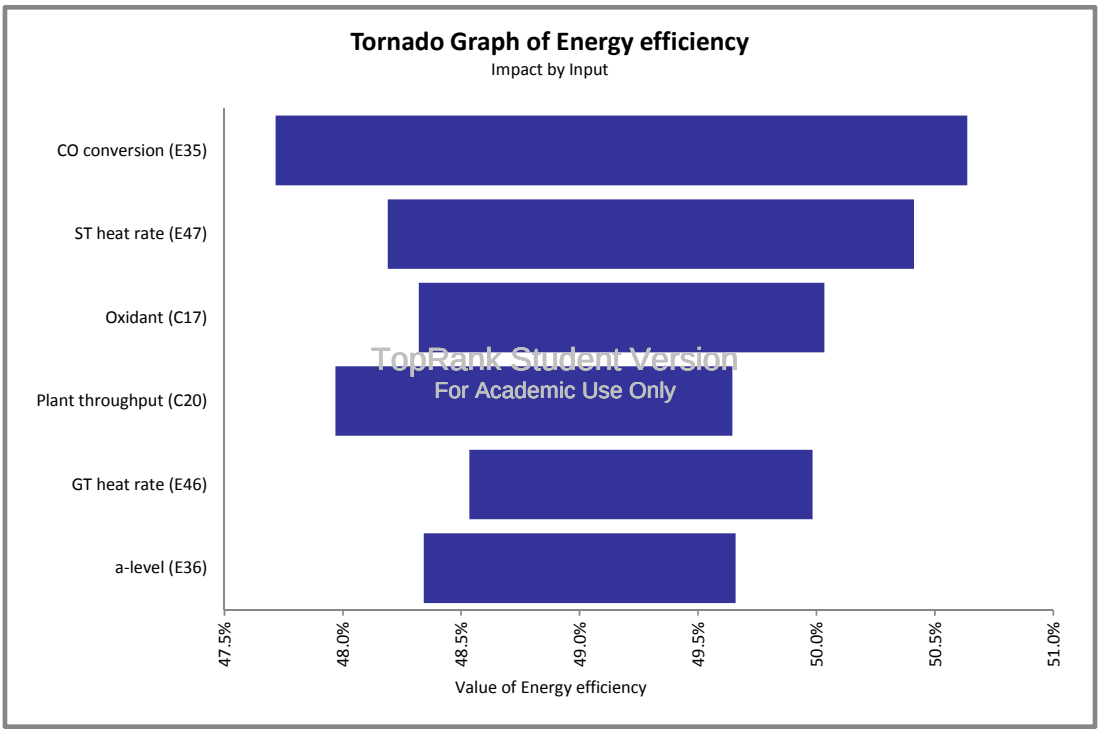

Figure 4-9: Tornado graph of plant energy efficiency for BTL base case

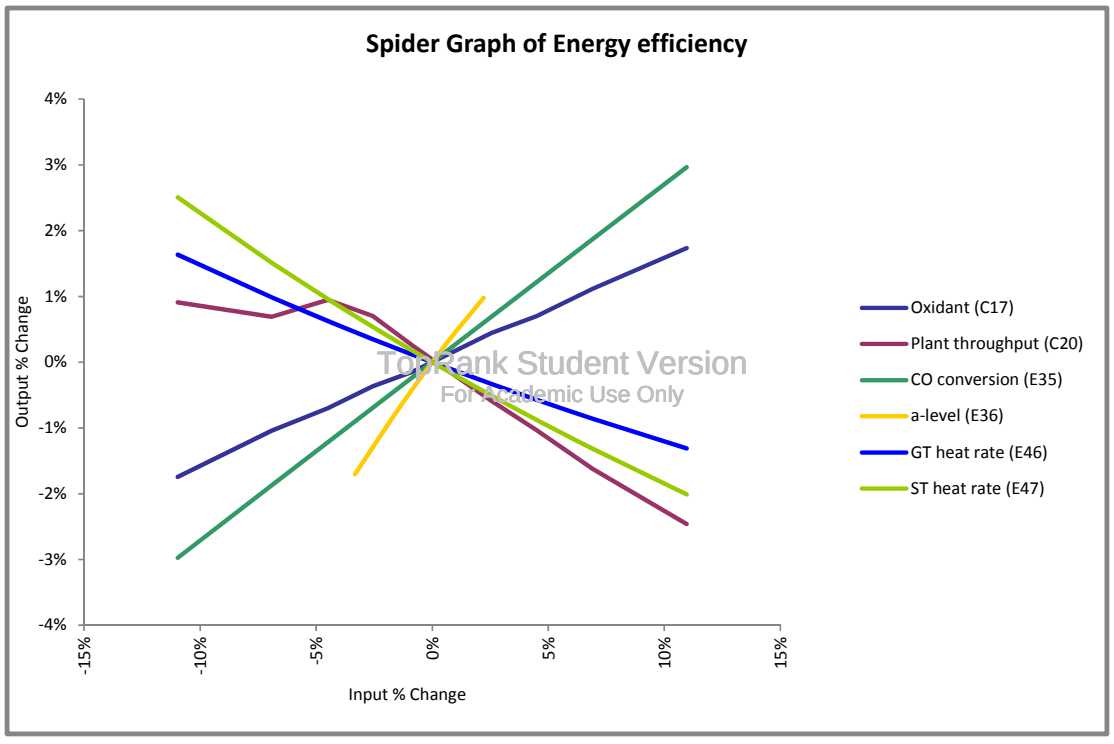

Figure 4-10: Spider graph of the plant energy efficiency for BTL base case

The first observation is that five input parameters were discarded due to their insignificant impact on the plant energy efficiency, and notably the CO_2 removal system has no effect on plant energy efficiency.

α-level is the most influential parameter and this is the reason why its range of variation was restricted to [0.87 – 0.92]. Its behavior is clearly identified on the spider chart. As dictated by the Anderson-Flory-Schultz law, the higher the α-level, the more carbon is synthesized in longer hydrocarbon chains instead of lighter ones that would subsequently be contained in the tail gas. This observation concurs with our previous conclusions drawn while sizing the optimum FT system by adjusting the amount of carbon monoxide.

The second most influential parameter is the CO conversion factor. The α-level's conclusions apply for this parameter as well.

The third most influential parameter is the steam turbine heat rate, which is inherent to the power generation system. It is interesting to notice that the steam turbine's heat rate is more influential than the gas turbine's which means that more electricity is generated by the steam turbine than by the gas turbine. This emphasizes the importance and the benefits of steam management and heat recovery in the plant.

Not surprisingly, the plant energy efficiency drops as the feedstock mass rate increases for the reasons that were discussed above, i.e. any excess syngas above the CO target at the FT inlet is rerouted to the gas turbine.

4.9 Conclusion

In this chapter, the main systems located downstream of the gasification island were identified and sized. A process model, based on chemical engineering parameters, was developed by integrating the related volumes and operating parameters of these systems.

This model assumed a FT's once-through process configuration and it was subsequently used to optimize the plant process configuration. The main drivers for this analysis were to maximize the plant energy efficiency while reducing as much as possible the supplemental amount of natural gas. Accordingly, it was determined that best results were obtained if the maximum amount of carbon monoxide at the FT system inlet was set at 1250 kmol/hr. In such case, no natural gas is needed.

Moreover, a sensitivity analysis was performed to identify the most influential operating parameters. It was concluded that the FT system has the most influential operating parameters, followed by the power generation, itself followed by the gasification system.

Finally, assuming that 78 tonnes per hour of feedstock are processed in the plant, which corresponds to 350 MW, the best plant energy efficiency achieved was 49.2% and the corresponding FT liquid fuels production rate was estimated at 11069 kg/hr which is equivalent to 2213 barrels per day.

Lastly, a process flow diagram and a material balance were generated by the process model for the best process configuration.

Chapter 5

5 TECHNO-ECONOMIC MODEL

5.1 Introduction

The aim of this chapter is to determine the internal rate of return (IRR) and the FT liquid fuels products value for a biomass to liquid facility similar to the one described in the previous chapter.

To this end, a discounted cash flow model will be developed and the calculation will be performed to reflect the optimized process scheme identified in the previous section of this work.

First, the methodology used to develop the discounted cash flow model will be described, along with the method to determine the product value. Then, the capital costs, financial assumptions, variable costs and economic assumptions will be developed.

Lastly, a discounted cash flow rate of return analysis will be performed to quantify the uncertainty related to the IRR, and a discussion will follow.

5.2 Methodology

The methodology to assess the product value is described in Swanson's thesis (Swanson 2003). A discounted cash flow model is developed and takes into account project investments, revenues, fixed costs, variable costs and depreciation. The analysis is performed over the planned lifetime of the project and product value is determined to set the plant net present worth at zero.

To do this, in consideration of the variety of FT liquid fuel products manufactured, a correlation factor will apply between naphtha, diesel and jet prices in order to refer to only one type of product variable.

More specifically, a factor of $\frac{\$_{kerosene}}{\$_{diesel}} = \frac{1.066}{1.000}$ is assumed and based on current spot prices (Platts 2013) (Freigth Transport Association 2013). Similarly, a factor $\frac{\$_{diesel}}{\$_{naphtha}} = 0.941$ according to current spot prices (Freigth Transport Association 2013) (Bloomberg 2013).

As shown on Figure 5-1, diesel and kerosene prices are strongly correlated which supports the assumption of dealing with only one product variable in this analysis. The differential price of cracking crude oil into jet has increased over the last decade, as depicted more explicitly on Figure 5-2.

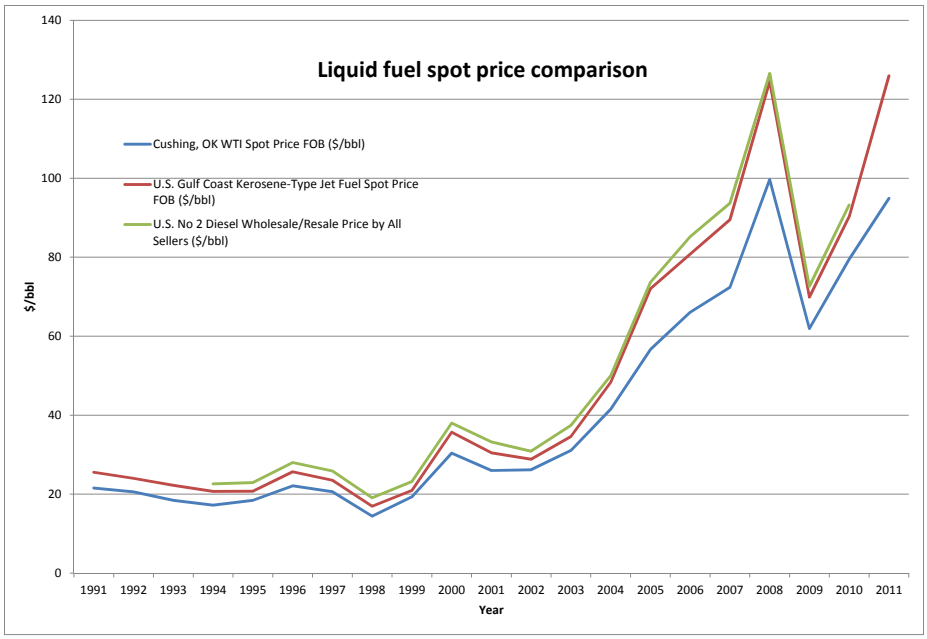

Figure 5-1: Liquid fuels spot price comparison. Data derived from (US EIA 2013) (US EIA 2013)

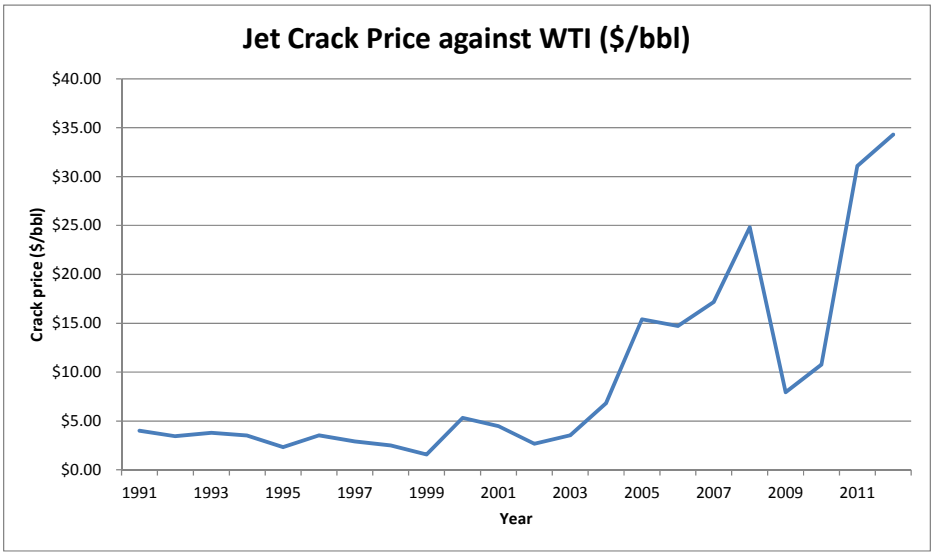

Figure 5-2: Jet crack price vs. WTI. Data from (Airlines for America 2013)

Table 5-1: Plant total capital cost methodology

Direct Capital Costs	
Inside Battery Limit (ISBL)	
Process Unit 1	Cost 1
Process Unit 2	Cost 2
Process Unit n	Cost n
Total ISBL	*Cost_ISBL*
Outside Battery Limit (OSBL)	Cost estimate (% of Cost_ISBL)
Instrumentation & Controls	5.0
Buildings	1.5
Grid Connections	5.0
Site preparation	0.5
Civil works (including waste water treatment plant)	10.0
Electronics	7.0
Piping	4.0
Total OSBL	*Cost_OSBL*
Total Direct Capital (TDC)	**Cost_ISBL + Cost_OSBL**
Indirect Capital Costs (% of TDC)	
Engineering	15
Contingency	10
Fees / Overhead / Profits	10
Start-Up	5
Total Indirect Capital (TIC)	**= TDC * 40%**
Total Capital Costs (TCC)	**TDC + TIC**

In their works, Ng and Sadhukhan analyzed the techno-economic performances of a bio-oil FT and CHP synthesis platform. The systems used in their analysis are very similar to the ones assumed in this work. A similar methodology was applied to determine the plant's total capital costs (Ng and Sadhukhan 2011). This methodology is summarized in Table 5-1.

The cost of a process unit can be derived based upon a similar reference process unit with known capacity and cost, using the following formula:

$$\frac{Cost_{\ system}}{Cost_{\ reference}} = \left(\frac{Capacity_{\ system}}{Capacity_{\ reference}}\right)^{n}$$

Where n is a size factor, specific to each system and found in specialized literature.

When the sole equipment cost is found, an installation factor is therefore applied to determine the corresponding Inside Battery Limit cost. Silla summarizes these installation factors based upon the type of process – solid to solid, solid to fluid or fluid to fluid – and distinguishes the primary materials – whether primarily carbon steel or alloy equipment (Silla 2003).

Unless otherwise noted, all monetary values are expressed in 2013 US $. All monetary values are adjusted to take into consideration the consumer price index provided by the U.S. Bureau of Labor Statistics (U.S. Department of Labor 2013). The currency exchange rates used in this study were taken from the Yahoo! Finance website.

5.3 Product value analysis

The product value is determined by means of a discounted cash flow model which is based on the expected expenses and revenues of a plant throughout its whole life. The first part of this section will break down the associated expenses and revenues, along with the corresponding assumptions. In a second part, results will be discussed and a sensitivity analysis will be performed to identify the most influential parameters.

5.3.1 Capital costs estimation and financial assumptions

Capital costs references are shown in Table 5-2. A summary of the total capital costs and the related financial assumptions are provided in Table 5-3 and Table 5-4 respectively.

Table 5-2: Reference process units' capital costs

Process Unit	Reference Cost (million)	Reference Capacity[1]	Reference year	Power factor	Source
Gasification	CAN $ 22	1000 TPD	2011	1	(Bloomberg Businessweek
HRSG	€ 2.87	47.5 TPH	1999	0.8	(Ng and Sadhukhan 2011)
ASU – O_2 plant	€19.6	24 TPH	1999	0.75	(Ng and Sadhukhan 2011)
Compressor	€10.2	13.2 MW	1999	0.85	(Ng and Sadhukhan 2011)
WGSR	€0.38	2400 kmol/hr of	1999	0.6	(Ng and Sadhukhan 2011)
AGR - Sulfur	US $ 44	81 TPD	2002	0.67	(Larson and Tingjin, Synthetic fuel production by indirect coal liquefaction 2003)
AGR – CO_2	US $ 43.38	327 TPH	2002	0.67	
AGR - Claus Unit	US $ 22.9	81 TPH	2002	0.67	
FT	See Appendix D		2009	-	(Hammond, et al. 2009)
Hydrocracking	US $ 45	4 MBPD	2005	1	(Gary, Handwerk and Kaiser 2007)
SMR	US $ 3.2	1500 kg H_2 per day	2007	0.7	(Yang and Ogden 2007)
Gas Turbine	€ 6.5	25 MW	1999	0.7	(Ng and Sadhukhan 2011)
Steam Turbine	€ 3.8	12.3 MW	1999	0.7	(Ng and Sadhukhan 2011)

[1] TPH = tonnes per hour, TPD = tonnes per day, MW = Mega Watt,

Table 5-3: Plasma Gasification Biomass to Liquid Total Capital Costs estimation

DIRECT CAPITAL COST			
ISBL			
Gasification island	$	65,455,236	
ASU / O2 plant	$	42,043,507	
HRSG (Syngas cooling + Power Gen)	$	13,582,763	
Compressor	$	19,899,578	
Sulfur + CO2 removal (incl. elemental S unit)	$	25,321,601	
Water-Gas-Shift-Reactor	$	773,719	
FT Island	$	20,956,502	
Hydrocracking facility	$	29,374,403	
Steam Methane Reformer	$	6,264,196	
Power Island (GT+ST)	$	26,787,182	
Balance of the plant	$	37,568,803	15.0%
Total ISBL	$	288,027,490	
OSBL			*% of ISBL*
Instrumentation & Controls	$	14,401,374	5.0%
Building	$	4,320,412	1.5%
Grid connection	$	14,401,374	5.0%
Site preparation	$	1,440,137	0.5%
Civil works (incl. waste water treatment)	$	28,802,749	10.0%
Electronics	$	20,161,924	7.0%
Piping	$	11,521,100	4.0%
Total OSBL	$	95,049,072	
TOTAL DIRECT CAPITAL (TDC = ISBL + OSBL)	$	383,076,562	
INDIRECT CAPITAL COSTS			*% of TDC*
Engineering	$	57,461,484	15.0%
Contingency	$	38,307,656	10.0%
Fees / Overhead / Profits	$	38,307,656	10.0%
Start-Up	$	19,153,828	5.0%
TOTAL INDIRECT CAPITAL (TIC)	$	153,230,625	
Total Capital Costs (TCC = TDC + TIC)	**$**	**536,307,186**	

Table 5-4: Financial assumptions

Debt	$	-	0%
Equity	$	536,307,187	100%
Investment spent during 1st year of construction		60%	
Interest rate		7%	
Debt term		10	years
MARR (A$ after-tax, combined market rate)		12.64%	
General Inflation Rate		2.40%	
MARR (R$ after-tax, combined market rate)		10.00%	
Marginal Tax rate		30%	
Escalation rate		2%	per year
O&M annual cost - year 0	$	7,661,530.03	2% ot TDC
Plant availability during 1st year		50%	
Plant availability		8000	hours per year
Study period		20	years
Interest rate for sinking fund		3%	
End of life demolition cost		2%	of TDC
End of life demolition cost - year 0	$	7,661,530.03	
Demolition costs - year 20	$	12,311,604.08	
Depreciation ratio		100%	
Depreciation method	MACRS - 7 years		

It is assumed that the construction of the plant will last for two years, with 60% of the investment spent during the first year and the remaining 40% spent during the second year. Capital costs are escalated during construction.

It is further assumed that the plant production rate will be only 50% during the first of operation and will reach maximum capacity during the second year.

In order to compare this plasma gasification biomass to liquid plant's product costs with results from other articles, the same financial assumptions should be made. Accordingly, the plant shall be financed 100% with equity funds for this analysis.

5.3.2 Variable costs and utilities assumptions

The variable costs of the plant include the chemicals, direct labor, operation and maintenance. A summary of the chemicals' costs is provided in Table 5-5. Salaries with benefits and overhead, along with operation and maintenance account for 2% of the total direct costs of the plant, at year 0.

Table 5-5: Variable operating costs per process unit

Process Unit	Chemical	Costs	Source
Gasification	Pet Coke	$ 33 / tonne	(Loutfi and Harriz 2006)
Cleaning	NaOH	$ 1300 / tonne	(Tijmensen, et al. 2002)
Cleaning	H_2SO_4	$ 500 / tonne	Assumed
Selexol	Solvent	$ 12 / gallon	(WorleyParsons Group, Inc. 2006)
FT	Cobalt	$ 25000 / tonne	(London Metal Exchange 2013)
Balance of the plant	Boiler feed water	$ 2.5 / tonne	(West Virginia University 2013)
Balance of the plant	Electricity from grid Electricity to grid	$ 38.4 / MWh $ 73.0 / MWh	(Tijmensen, et al. 2002) corrected by inflation factor
Balance of the plant	Natural Gas	$ 4 / MMBTU	Henry Hub Gulf Cost Natural gas Spot price

5.3.3 Results and discussion

The discounted cash flow is shown in Appendix E. At net present value of zero, product value of 16.44 US$/GJ is achieved. This result is in the same range of those reported in Tijmensen's (Tijmensen, et al. 2002) who obtained 16 US$ / GJ. Taking into consideration the inflation rate, Tijmensen's production rates correspond to 21.40 $2013 / GJ. Moreover, Tijmensen did not consider a hydrocracking system in his study. This should, according to his estimation, increase the product value by about 0.72 $2000 / GJ, or about 0.96 $2013 / GJ, leading to a total product value of 22.36 $2013 / GJ.

Table 5-6: Comparison of assumptions and results with Tijmensen study

Parameter	(Tijmensen, et al. 2002)	**Present study**
Biomass input (MW)	367	350
Biomass cost ($/GJ)	2.0	0.0
Total Investment Costs (MM US$)	380	536
Real interest rate	10%	10%
Electricity value ($/MWh)	57	72
Efficiency (% - LHV based)	50.1	49.2
Load factor (hours / year)	8000	8000
Depreciation period	15	10
Cost reference year	2000	2013
Product value ($/GJ)	16.50	16.44

Table 5-6 summarizes assumptions and results between this study and Tijmensen's. After correcting his values for inflation, total investment costs are similar on a biomass input basis. Consequently, the product value difference results from the annual operating expenses in general, and biomass in particular.

This could be quickly demonstrated by performing a product value analysis and assuming a biomass price that corresponds to Tijmensen's assumption. Considering that he assumed 367 MW of biomass with a corresponding price of 2$ / GJ, then the resulting biomass annual expenses corrected by the inflation factor is 28,220,832 US$ 2013. Considering that the present study processes 78 tonnes per hour of biomass, the resulting biomass price would be 45 US$ / tonne. Under this configuration, the resulting product value is 23.5 $/GJ, which is very close to 22.36 $/GJ which was predicted above.

Then, a Monte Carlo analysis is performed to quantify the uncertainty of the plant's internal rate of return and identify the related most influential parameters. This study is performed by using @Risk software, version 6.0. The inputs, along with their distribution and range of value, are summarized in Table 5-7.

Table 5-7: Input parameters for Monte-Carlo simulation

Input parameters	**Distribution type**	**Range of value / Parameters**	**Units**
Biomass	Triangle	Min: 0 Most likely: - 20 Max: - 40	$ / tonne
Coke rate	Normal	μ = 5% σ = 0.5%	Of biomass rate
Oxidant rate	Normal	μ = 50% σ = 5%	Of biomass rate
Plasma power rate	Normal	μ = 100 σ = 10	kW / tonne of biomass

Amount of CO_2 removed	Uniform	Min: 26000 Max: 66000	tonnes per hour
CO conversion rate	Normal	μ = 70% σ = 7%	None
α-level	Triangle	Min: 0.89 Most likely: 0.90 Max: 0.92	None
H_2 to hydrocracking	Normal	μ = 580 σ = 58	SCF / barrel of C5+ products
Gas turbine heat rate	Normal	μ = 11227 σ = 1122.7	kJ/kWh
Steam turbine heat rate	Normal	μ = 14400 σ = 1440	kJ/kWh
ISBL direct capital costs[2]	Normal	μ $\sigma = 0.1 * \mu$	$
OSBL direct capital costs	Normal	μ = 33% σ = 3.3%	$
Indirect capital costs	Normal	μ = 40% σ = 4%	$
Marginal tax rate	Triangle	Min: 15 Most likely: 30 Max: 40	%
Plant availability	Triangle	Min: 7600 Most likely: 8000 Max: 8300	Hours per year
Electricity price	Normal	μ = 73 σ = 7.3	$ / MWh

[2] For all main system: gasification, HRSG, ASU, compressor, WGSR, Selexol sulfur, Selexol CO_2, elemental sulfur – Claus unit, FT, Hydrocracking, SMR, Gas turbine and Steam turbine.

The simulation has 28 inputs, described shown in Table 5-7, and one output that represents the project's IRR. The simulation runs 5000 iterations, which exceeds the convergence threshold.

The results are depicted as probability density in Figure 5-3. The IRR has a mean value of 10.14% with a standard deviation of 1.34%. The IRR corresponding to the 5% percentile equals 7.93%.

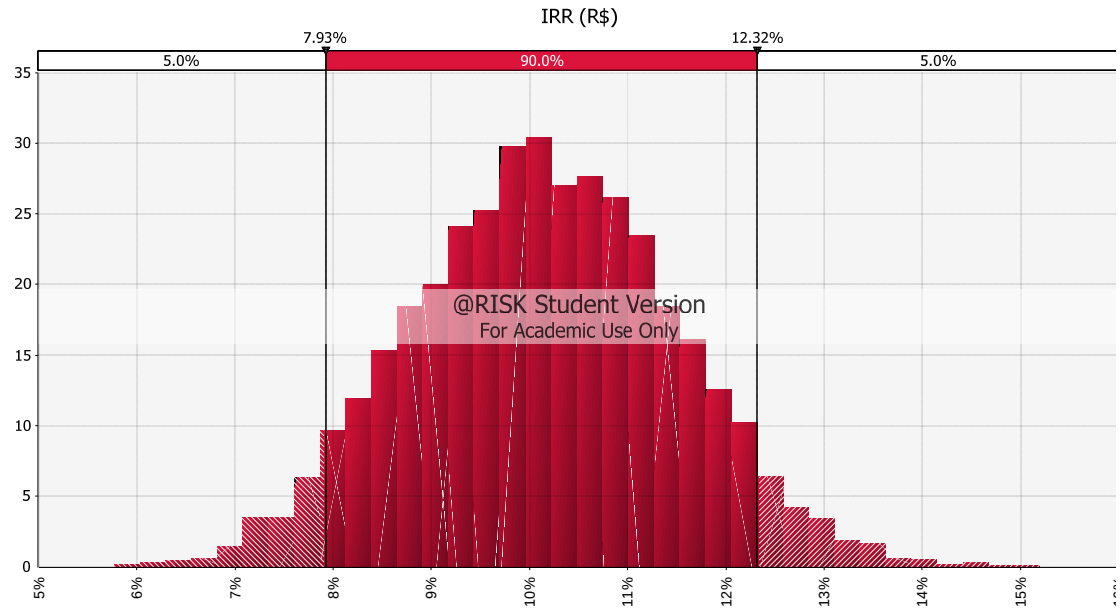

Figure 5-3: Project's IRR resulting from the Monte-Carlo simulation

In order to decrease the standard deviation as much as possible, and therefore to decrease the project risks, it is necessary to identify the most influential parameters. To this end, a Tornado graph is created and summarized on Figure 5-4.

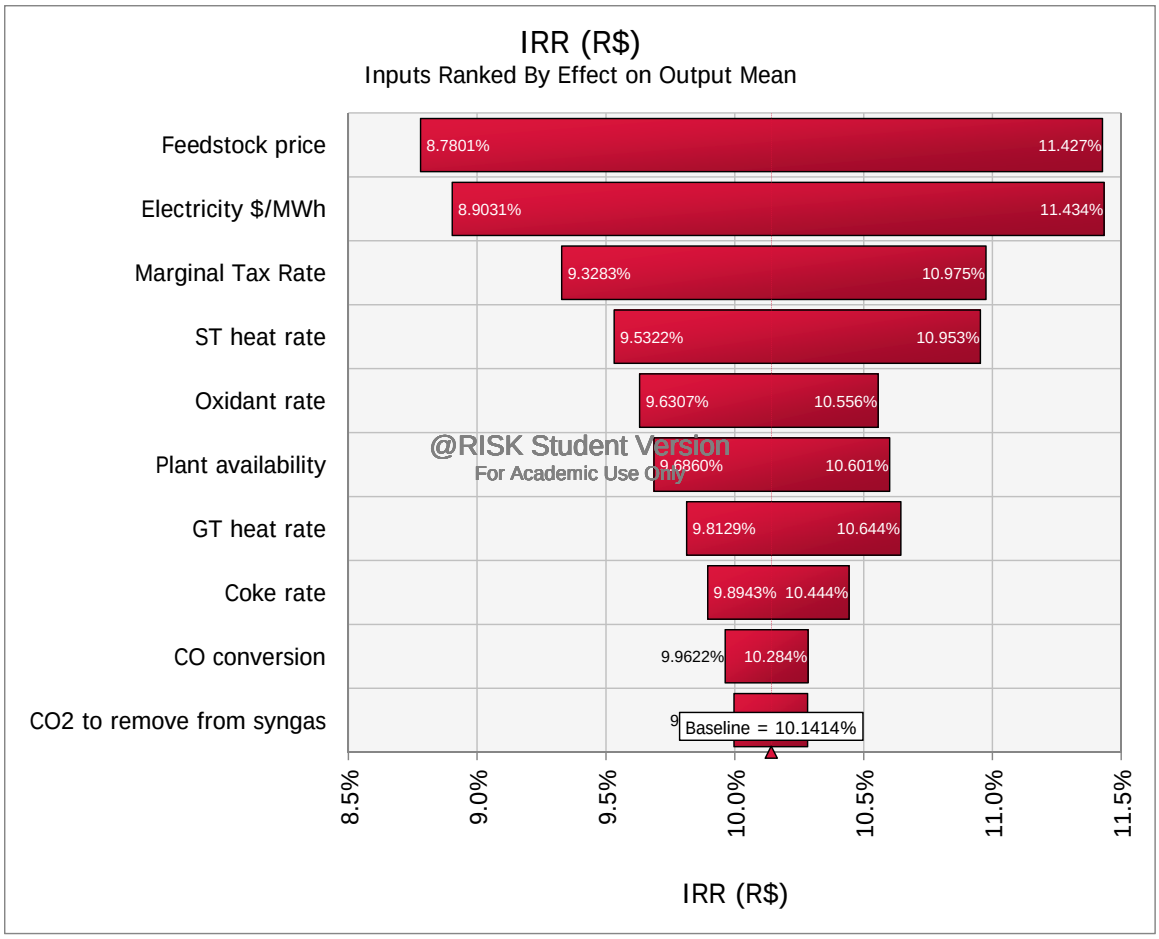

Figure 5-4: Tornado chart resulting from the Monte Carlo simulation

On Figure 5-4, two types of parameters can be identified. Those related with process operating conditions and those related with business conditions.

The most influential parameters are business related, emphasizing the importance of possibly securing long-term contract agreements with suppliers and clients to minimize project risk.

From a process standpoint, it seems that the steam turbine's heat rate is the most important parameter. This is because of the large amount of steam raised throughout

the process. Specifically, the three major sources of steam are the syngas cooling system, the gas turbine heat exchanger system and the FT system respectively.

The gas turbine's heat rate is also important, although third in rank.

The second and fourth most important process parameters are the oxidant and coke rates as part of the gasification system. These independent variables have an immediate impact on syngas composition, which could be beneficial to adjust for any feedstock composition variation. This emphasizes the importance of developing an accurate and reliable integrated gasification control system to ensure as much as possible a stable syngas production.

Finally, it is shown that the CO_2 removal unit might not be of great importance in this process and it could potentially be removed without affecting much the project IRR, which is a result in line with one of Tijmensen's conclusions. Several direct benefits would be to decrease capital and operating expenditures along with increasing process reliability since fewer systems would be integrated.

5.4 Conclusion

In this chapter, a discounted cash flow model was developed to determine the product value of FT products manufactured from a plasma gasification biomass to liquid plant.

Product value of about 16.2 $2013/GJ were achieved which is less expensive than those found in the literature at about 22.4 $2013/GJ (Tijmensen, et al. 2002) (Saynor, Bauen and Leach 2003). It was found that the energy conversion of the process described in

this work was very similar to other biomass gasification to liquids facility analyzed by others (Tijmensen, et al. 2002) (Swanson 2003). So were the project investment costs (Tijmensen, et al. 2002). It was demonstrated that the main product value difference was because of the price of the feedstock considered.

A Monte-Carlo analysis was subsequently performed to determine the uncertainty of the IRR and to identify the related most influential parameters. A mean rate of return of 10.14% with a standard deviation of 1.34% was achieved.

The most influential type of parameters deals with business related issues such as the price of electricity and feedstock. It is therefore recommended to seek long-term contractual agreements with suppliers and off-takers to limit as much as possible the project's return uncertainty.

The second most influent type of parameters deals with process operating conditions. Of these, the power generation systems are the most influential along with the gasification system. The CO_2 removal unit appeared to not be a critical system and could potentially be removed from the process.

Chapter 6

6 CONCLUSION

An atmospheric pressure plasma gasification process model was developed and used to predict syngas characterization resulting from biomass gasification. The results obtained confirmed that 100% of the carbon contained in the feedstock is converted into syngas, resulting in a tar-free high temperature syngas with no bottom or fly-ashes. It was further concluded that such a gasification process provides flexible operating conditions to monitor the syngas characterization, and therefore optimize the carbon monoxide and hydrogen content in the syngas as opposed to the usual gasification performance metrics such as cold gas efficiency.

The gasification process model was then integrated into a biomass to liquids process model. The syngas, once cooled, cleaned and conditioned, is synthesized into a FT system to produce paraffinic wax. The FT system is designed as a once-through configuration which means that the unconverted syngas is directed to a gas turbine to contribute to power generation. The syngas conditioning process is designed in such a way that the model enables to user to set the H_2:CO ratio and syngas flow rate at the FT system inlet. Any potential excess syngas at the FT system inlet is rerouted to the gas turbine for additional power generation. On the other hand, should the syngas flow rate target at the FT system inlet be set too high, supplemental natural gas would be

processed in a steam methane reformer to supply the FT unit with the right amount of carbon monoxide and hydrogen.

The biomass to liquid process model was then used to perform a case study. Previous researches that investigated the economics of a biomass to liquids plant recommended designing plants that process about 350 MW of biomass. In our case study, the corresponding quantity of refuse derived fuel is 78 tonnes per hour. The best plant process configuration is obtained for setting the syngas flow rate at 1250 kmol/hr of carbon monoxide at the inlet of the FT system which ensures avoidance of processing any natural gas in the steam methane reformer for supplemental syngas production. The corresponding FT liquid fuels production is 2200 barrels per day of naphtha, jet and diesel and the related plant efficiency is 49%.

Finally, a discounted cash flow was developed and product costs in the range of 16 $/GJ were obtained for the base case model assumptions. A Monte-Carlo analysis further defined the project IRR distribution with a mean value of 10.14% and with a standard deviation of 1.34 %. The Monte-Carlo simulation was used to identify the most influential parameters that affect the IRR value.

This analysis shows that the price of feedstock and electricity are the most influential parameters. Negotiating long-term contractual agreements with suppliers and product off-takers should therefore help to reduce the project risk. Second to these business parameters are the technical parameters. The power generation system's efficiencies are considered critical variables. Gasification oxidant and catalyst rates are also

considered critical independent variables and should be able to compensate for any feedstock composition fluctuation. This flexibility was highlighted in section 3 of this work. Lastly, the CO_2 removal unit appeared not to be a critical system and could potentially be removed from the design.

Further improvements to this model could include the possibility of designing the FT system in either a once-through or recycle configuration. The resulting model could be used to explore a wider range of process conditions and therefore to enhance the analysis.

Further researches could focus on investigating the optimized feedstock composition.

7 WORKS CITED

Agence Internationale de l'Energie. "From 1st to 2nd generation biofuel technologies." *IEA Bioenergy.* November 2008. http://www.iea.org/publications/freepublications/publication/2nd_Biofuel_Gen_Exec_Sum.pdf (accessed September 2012).

Air Transport Action Group (ATAG). *Facts & Figures.* March 2012. http://www.atag.org/facts-and-figures.html (accessed September 29, 2012).

Airlines for America. *Annual crude Oil and jet Fuel Price.* 2013. http://www.airlines.org/Pages/Annual-Crude-Oil-and-Jet-Fuel-Prices.aspx (accessed March 06, 2013).

Andrews, A., and J. Logan. *Fischer-Tropsch Fuels from Coal, Natural Gas, and Biomass: Background and Policy.* Report for Congress, Congressional Research Center, 2008.

Beysel, G. "Enhanced cryogenic air separation - a proven process applied to oxyfuel." *International Energy Agency - Greenhouse Gas.* 09 08, 2009. http://www.ieaghg.org/docs/oxyfuel/OCC1/Plenary%201/Beysel_ASU_1stOxyfuel%20Cottbus.pdf (accessed 02 21, 2013).

Bloomberg Businessweek. *Company Overview of Westinghouse Plasma Corporation.* 12 21, 2011.

http://investing.businessweek.com/research/stocks/private/snapshot.asp?privcapId=33928056 (accessed 01 08, 2013).

Bloomberg. *Market Data - Naphtha FOB Amsterdam Rotterdam Antwerp Spot Barges.* March 01, 2013. http://www.bloomberg.com/quote/NAPHNEFB:IND (accessed March 02, 2013).

Booz & Company. *Press Media.* May 29, 2011. http://www.booz.com/me/home/press_media/management_consulting_press_releases/article/49572381?tid=39979829&pg=all (accessed September 2012).

Boundy, B., S. Diegel, L. Wright, and S. Davis. *Biomass Energy Data Book.* 4. US DOE - EERE, 2011.

Breckenridge, W., A. Holiday, J, Ong, and C. Sharp. "Use of SELEXOL Process in Coke Gasification to Ammonia Project." *Laurance Reid Gas Conditioning Conference.* Norman, Oklahoma: http://www.dow.com/PublishedLiterature/dh_003d/0901b8038003d131.pdf, 2000.

Bystrom, J. *Mechanical biological treatment plants.* JASPERS, Solid waste and energy division - , European Investment Bank, 2010.

Byun, Y., Cho, M., Chung, J., Namkung, W., Lee, H., Jang, S., et al. "Hydrogen recovery from the thermal plasma gasification of solid waste." (Journal of hazardous materials) 190 (2011).

Cao, C., Y. Wang, J. Hu, D. Elliott, S. Jones, and D. Stevens. "Microchannel catalytic process for converting biomass derived syngas to transportation fuels. ." *Pacific Northwest National Laboratory.* September 08, 2003. http://www.pnl.gov/biobased/docs/acs2003presentation.pdf (accessed October 23, 2011).

Davis, B. "Fischer-Tropsch synthesis: Comparison of performances of iron and cobalt catalysts." *Industrial & Engineering chemistry research* , 2007: 8938-8945.

Demirbas, A. "Progress and recent trends in biofuels." *Progress in Energy and Combustion Science* (Science direct) 33, no. 1 (February 2007): 1-18.

Department of Energy. *Tampa Electric Integrated Gasification Combined Cycle Project.* Clean Coal Technology Demonstration Program , DOE, 2004.

Dinçer, I., and C. Zamfirescu. *Sustainable Energy Systems and Applications.* Springer, 2011.

Dritz, T. "Microchannel technology enabled distributed fuel production: deployment update." *Energy Frontiers International - Gas-to-Market and energy conversion forum.* 10 26, 2011. http://www.energyfrontiers.org/index.asp?bid=271&efg=1 (accessed 07 30, 2012).

Ducharme, C. *Technical and economic analysis of plasma assisted waste-to-energy processes.* M.S. thesis, New York, NY: Columbia University, 2010.

E4Tech. "Review of technologies for gasification of biomass and wastes." Report to NNFCC - project 09/008, 2009.

Efremenko, B. "The status of mechanical and biological treatment." *ISWA Beacon - the global challenge: optimising the cycle of biological treatment of biowaste.* Perugia, Italy: International Solid Waste Association , 2008.

Energi E2. *Straw gasification for co-combustion in large CHP-plants.* technical report from contract # ERK5 – CT – 1999 – 0004, European Community, 2001.

Energy Center of the Netherlands. *Phyllis.* 2011. www.ecn.nl/phyllis.

Environmental Protection Agency. "AP 42 Emissions Factors by Chapter." *EPA - Technology Transfer Network - Clearinghouse for Inventories & Emissions Factors.* december 31, 2009. http://www.epa.gov/ttn/chief/ap42/ch08/final/c08s13.pdf (accessed February 10, 2013).

European Central Bank. *Euro Exchange Rates USD.* 2013. http://www.ecb.int/stats/exchange/eurofxref/html/eurofxref-graph-usd.en.html (accessed 2013).

European Commission. *Refuse Derived Fuel, Current practice and perspectives.* European Commission, Directorate General Environment, 2003.

Faaij, A. "Modern biomass conversion technologies." *Mitigation and adaptation strategies for global change* 11 (2006): 343-375.

Faaij, A., R. Van Ree, L, Waldheim, E. Olsson, A. Oudhuis, and A. Van Wijk. "Gasification of biomass waste and residues for electricity production." *Biomass and Bioenergy* (Elsevier Sciences) 12, no. 6 (1997): 387-407.

Freigth Transport Association. *Fuel price information / weekly fuel prices.* January 2013. http://www.fta.co.uk/policy_and_compliance/fuel_prices_and_economy/fuel_prices/weekly_fuel_prices.html (accessed March 03, 2013).

Gary, J., G. Handwerk, and M. Kaiser. *Petroleum Refining: Technology and Economics.* CRC Press, 2007.

GE Power and Water. *MS6001B Gas Turbine.* 2013. http://site.ge-energy.com/prod_serv/products/gas_turbines_cc/en/midrange/ms6001b.htm (accessed 2013).

General Electric Energy. *6B heavy duty gas turbine.* 2013. http://www.ge-energy.com/products_and_services/products/gas_turbines_heavy_duty/6b_heavy_duty_gas_turbine.jsp (accessed 2013).

Green, D., and R. Perry. *Perry's Chemical Engineers Handbook.* 8th. McGraw-Hill Professional., 2007.

Gumz, Wilhelm. *Gas producers and blast furnaces: theory and methods of calculation.* Michigan: Wiley, 1950.

Gupta, A., & Cichonski, W. "Ultrahigh temperature steam gasification of biomass and solid waste." (Environmental Engineering Science) 24, no. 8 (2007).

Hammond, J., J. Lee, Shayaan Nadeem M., and S. Weiss. *Alaskan natural gas to liquids (GTL) using microchannel reactors.* Department of Chemical and Biomolecular Engineering, Senior Design Report, Philadelphia, PA: University of Pennsylvania, 2009.

Hanaoka, T., Y. Liu, K. Matsunaga, S. Hirata, and K. Sakanishi. "Becn-scale production of hydrocarbon liquid fuel from woody biomass via gasification." (Journal of the Japan Institute of Energy) 86 (2007).

Higman, C., and M. Van Der Burgt. *Gasification.* Elsevier Sciences, 2003.

Hilbert, T., G. Chitnis, B. Umansky, P. Kamienski, V. Patel, and A. Subramanian. "Advances in catalysts enable cracking gasoils at moderate pressures." *Hydrocarbon processing*, 2008: 47 - 56.

Hobbs, M.L. *Modeling Countercurrent Fixed-Bed Coal Gasification.* PhD. Dissertation, Provo, UT: Brigham Young University, 1990.

International Air Transport Association. *Fact sheets : alternative fuels.* 12 2012. http://www.iata.org/pressroom/facts_figures/fact_sheets/pages/alt-fuels.aspx (accessed 02 2013).

International Air Transportation Association (IATA). *Press Room, Airlines International, December 2009, Environment One Voice.* December 2009. http://www.iata.org/pressroom/airlines-international/december-2009/Pages/06.aspx (accessed September 2012).

Kallassy, M., B. Efremenko, and M. Champel. "Waste processing: the status of mechanical and biological treatment." *ISWA Beacon: the global challenge: optimising the cycle of biuological treatment of biowaste.* Perugia, Italy: International Solid Waste Association , 2008.

Kalnes, T., T. Marker, D. Shonnard, and K. Koers. "Green diesel production by hydrorefining renewable feestocks." *Biofuels Technology*, no. 4 (2008): 7 - 11.

Kinoshita, Y., Lee, C.-W., Itaya, Y., & Mori, S. "Production of gaseous fuel in circulating fluidized bed gasification process employing Refused-Derived Fuels. ." (Environmental Engineering Science) 21 (2004).

Klein, A. "Gasification: An Alternative Process for Energy Recovery and Disposal of Municipal Solid Wastes ." n.d.

Kreutz, T., R. Williams, S. Consonni, and P. Chiesa. "Co-production of hydrogen, electricity and CO2 from coal with commercially ready technology ; part B: Economic analysis." *International Journal of Hydrogen Energy* (Elsevier) 30 (2005): 769 - 784.

Larson, E., and H. Jin. "Biomass conversion to Fischer-Tropsch liquids: preliminary energy balances." *Proceedings of the 4th biomass conference of the Americas.* Elsevier Science Ltd., 1999.

Larson, E., and R. Tingjin. "Synthetic fuel production by indirect coal liquefaction." *Energy for sustainable development* 7, no. 4 (2003): 79 - 102.

Larson, E.D., H. Jin, and F.E. Celik. "Large-scale gasification-based coproduction of fuels and electricity from switchgrass." *Biofuels, Bioprod. Bioref*, no. 3 (2009): 174 - 194.

Leviness, S., A. Tonkovitch, K. Jarosj, S. Fitzgerald, B. Yang, and S. McDaniel. "Media / White papers." *Oxford Catalyst Group.* 2011. http://www.oxfordcatalysts.com/press/wp/wp110224_microchannel_FT_white_paper_24Feb11.pdf (accessed 02 2013).

Li, S. "Promoted Iron-based catalysts for the Fischer-Tropsch synthesis: design, synthesis, site densities and catalytic properties." *Journal of Catalysis* 206 (2002): 202-217.

London Metal Exchange. *LME Cobalt.* March 01, 2013. http://www.lme.com/metals/minor-metals/cobalt/#tab2 (accessed March 02, 2013).

Loutfi, H., and T. Harriz. "Mill Use of Petcoke as an Alternative Lime Kiln Fuel to Reduce Energy Costs." *TAPPI Forum on Energy.* Appleton, 2006.

Lv, P. "Hydrogen-rich gas production from biomass air and oxygen/steam gasification in a downdraft gasifier." (Renewable Energy) 32, no. 13 (2007).

Meyers, R. "UOP unicracking process for hydrocracking." In *Handbook of petroleum refining processes*, by Robert Meyers. McGraw-Hill Professional, 2004.

Miller, S., A. Dahlberg, K. Krishna, and R. Krug. Process for producing a highly paraffinic diesel fuel having a high iso-paraffinic to normal-paraffinic mole ratio. US Patent 6204426 B1. 03 20, 2001.

Milne, T. A., Abatzaglou, N., & Evans, R. *Biomass gasifier "tars": their nature, formation and conversion. .* Springfield, VA: NREL, 1998.

Monteiro Nunes, S., Paterson, N., Dugwell, D., & Kandiyioti, R. "Tar formation and destruction in a simulated downdraft, fixed-bed gasifier: reactor design and initial results." (Energy & Fuels) 21 (2007).

Moran, M., and H. Shapiro. *Fundamentals of engineering thermodynamics.* New York: Wiley, 1995.

Mountouris, A. "Solid waste plasma gasification: Equilibrium model development and exergy analysis." (Energy Conversion and Management) 47 (2006).

National Renewable Energy Laboratory. *Survey and Down-Selection of Acid Gas Removal Systems for the Thermochemical Conversion of Biomass to Ethanol with a Detailed Analysis of an MDEA System.* Task 1: Acid Gas Removal Technology Survey and Screening for Thermochemical Ethanol Synthesis, NREL, 2009.

NETL. *ETL Life Cycle Inventory Data – Unit Process: Airplane Combustion of Blended F-T/Conventional Jet Fuel, Operation.* U.S. Department of Energy, National Energy Technology Laboratory, 2010.

Nexant, Inc. *Technical expert's report on the Velocys technology.* Due Diligence, White Plains, NY: Nexant, 2008.

Ng, K.S., and J. Sadhukhan. "Techno-economic performance analysis of bio-oil based Fischer-Tropsch and CHP synthesis platform." *Biomass and Bioenergy* 35, no. 7 (2011): 3218 - 3234.

Parikh, J., S. Channiwala, and G. Ghosal. "A correlation for calculating HHV from proximate analysis of solid fuel." *Fuel* 84 (2005): 487-494.

Perry, R., and C. Chilton. *Chemical Engineer's Handbook.* McGraw-Hill Book Company, 1973.

Platts. *Platts Jet Fuel.* February 22, 2013. http://www.platts.com/JetFuel (accessed March 02, 2013).

Ponzio, A., Kalisz, S., & Blaziak, W. "Effect of operating conditions on tar and gas composition in high temperatureair/steam gasification (HTAG) of plastic containing waste." (Fuel Processing Technology) 87 (2006).

Rabou, L. "Tar in biomass producer gas, the Energy research Center of The Netherlands experience: an enduring challenge. ." (Energy Fuel) 23 (2009).

Rutberg, P., Bratsev, A., Kuznetsov, V., Popov, V., Ufimtsev, A., & Shtengel, S. "On efficiency of plasma gasification of wood residues." (Biomass and Bioenergy) 35 (2011).

Sarofim, A., G. Williams, J. Howard, and J. Rogers. *Design and control of incinerators - Vol 1.* Grant No EC-00330-03, National Technical Information Service - US Department of Commerce, 1973.

Saynor, B., A. Bauen, and M. Leach. *The Potential for Renewable Energy Sources in aviation.* London: Imperial College Centre for Energy Policy and Technology, 2003.

Schultz, H. "Short history and present trends of Fischer-Tropsch synthesis." *APPLIED CATALYSIS* 186 (1999): 3-12.

Shadle, L., D. Berry, and M. Syamlal. "Chemical & Biomolecular Engineering, NC State University." *North Carolina State University.* 01 16, 2010. http://www.che.ncsu.edu/ILEET/CHE596web_Fall2011/resources/coal/Kirk-Othmer_Coal-Gasification.pdf (accessed December 14, 2012).

Shah, P., G. Sturtevant, J. Gregor, M. Humback, and F. Padrta. *Fischer-Tropsch wax characterization and upgrading: final report.* Technical report, UOP, Inc., DOE, 1988.

Shell. "Quick Guide to Biofuels." *www.shell.com.* November 2007. http://www-static.shell.com/static/aboutshell/downloads/what_we_do/quick_guide_to_biofuels_nov2007.pdf (accessed September 2012).

Silla, H. "Chemical process engineering: design and economics." Chap. 2 in *Chemical process engineering: design and economics.*, by Harry Silla, 54. New York, NY: Dekker, 2003.

Speight, J., and B. Ozum. *Petroleum Refining Process.* New York, NY: Marcel Dekker, 2002.

Steynberg, A., and M. Dry. *Fischer-Tropsch Technology.* Elsevier, 2004.

Stipanovitch, A. "General chemistry II, section 01, Class notes, lecture 26 ." *Department of Chemistry of .* 03 29, 2006. http://www.esf.edu/chemistry/stipanovic/fch152/pdfs/fch152%20-%20l26-pdf.pdf (accessed 02 17, 2013).

Swanson, R.M. *Techno-economic analysis of biomass-to-liquids production based on gasification.* Master thesis, Ames: Iowa State University, 2003.

Swart, R. *Gas cleaning downstream biomass gasification.* Project report preapred in commision of the Dutch Agency for Innovation and Sustainability., International Energy Agency, 2009.

The World Bank. *Energy from Biomass - a review of combustion and gasification technologies.* Technical paper #422, Washington, DC: The World Bank, 1999.

Tijm, P. "Shell Middle Distillates Synhtesis: the process, the plant, the products." *Division of Energy & Fuels of the Argonne National Laboratory.* 08 1994.

http://web.anl.gov/PCS/acsfuel/preprint%20archive/Files/39_4_WASHINGTON%20DC_08-94_1146.pdf (accessed 02 2013).

Tijmensen, M., A. Faaij, C. Hamelinck, and M. Hardeveld. "Exploration of the possibilities for production of Fischer-Tropsch liquids and power via biomass gasification." (Biomass and Bioenergy) 23 (2002).

U.S. Department of Labor. *Bureau of Labor Statistics, Consumer Price Index.* 2013. http://www.bls.gov/cpi/ (accessed 2013).

US EIA. *Petroleum & Other Liquids Spot Price.* February 27, 2013. http://www.eia.gov/dnav/pet/pet_pri_spt_s1_a.htm (accessed March 06, 2013).

—. *Petroleum & Other Liquids, US No2 Diesel Wholesale/Resale price by all sellers.* March 01, 2013. http://www.eia.gov/dnav/pet/hist/LeafHandler.ashx?n=pet&s=ema_epd2d_pwa_nus_dpg&f=a (accessed March 06, 2013).

US EPA. *Municipal Solid Waste in the United States - Facts and Figures 2009.* Facts and Figures, Washington, DC: United States Environmental Protection Agency, Office of Solid Waste, 2010.

—. "Wastes - Non-Hazardous Waste - Municipal Solid Waste." *2010 MSW Characterization Reports.* November 2011. http://www.epa.gov/osw/nonhaz/municipal/pubs/msw_2010_rev_factsheet.pdf (accessed November 12, 2012).

Val'dberg, A., V. Lazarev, and T. Kuzina. "Flue gas cleaning systems for waste incineration plant." *Chemical and Petroleum Engineering*, 2003: 553 - 556.

Van der Laan, Gerard Pieter. *Kinetics, Selectivity, and Scale-Up of the Fischer-Tropsch synthesis.* PhD thesis, University of Groningen, 1999.

Van Oost, G., Hrabovsky, M., Kopecky, V., Konrad, M., Hlina, M., & Kavka, T. "Pyrolysis/gasification of biomass for synthetic fuel production using a hybrid gas-water stabilized plasma torch." (Vacuum) 83, no. 1 (2008).

Van Ree, R., A. Oudhuis, A. Faaij, and A. Curvers. "Modeling of a biomass-integrated-gasifier/combined cycle (BIG/CC) system with the flowsheet simulation program Aspen." Jourle II program of the European Commission DG-XII, 1995.

Van Steen, E., & Claeys, M. "Fischer-Tropsch catalysts for the biomass-to-liquid process." (Chemical Engineering Technology) 31, no. 5 (2008).

Van Swaaij, W. "Gasification - the process and the technology." *Resources and conservation*, 1981: 337 - 349.

Vassilev, S., D. Baxter, L. Andersen, and C. Vassileva. "An overview of the chemical composition of biomass." *Fuel* 89, no. 5 (2010): 913 - 933.

Walas, S. *Chemical Process Equipment Selection and Design.* Boston: Butterworth-Heinemann, 1990.

Wang, Y. Fischer-Tropsch synthesis using microchannel technology and novel catalyst and microchannel reactor. USA Patent 7,084,180 B2. 08 01, 2006.

West Virginia University. "College of Engineering and Mineral Resources." 2013. http://www.che.cemr.wvu.edu/publications/projects/styrene/styrene-b.pdf (accessed 2013).

Westinghouse Plasma Corporation. *Gasifiers models.* 2012. http://www.westinghouse-plasma.com/wpc_gasifers_models/ (accessed February 14, 2013).

Willis, K., S. Osada, and K. Willerton. "Plasma gasification: lessons learned at ecovalley WTE facility." *Proceedings of the 18th Annual North American Waste-to-Energy Conference.* Orlando, FL: Columbia Unversity, NY, 2010.

Wolfesberger, U., Aigner, I., & Hofbauer, H. "Tar content and composition in producer gas of fluidized bed gasification of wood—Influence of temperature and pressure." (Environmental Progress & Sustainable Energy) 28, no. 3 (2009).

WorleyParsons Group, Inc. *Nevada Power IGCC Market Status and Feasibility Study - Performance and Estimate Report.* Nevada Power Purchase Order 0001012232, Nevada Division of Environment Protection, 2006.

Yang, C., and J. Ogden. *H2 production via natural gas reforming.* Advanced Energy Pathways project, Public Interest Energy Research Program of the California Energy Commission, Davis, CA: University of California, 2007.

Yin, C. "Prediction of higher heating values of biomass from proximate and ultimate analyses." *Fuel* 90 (2011): 1128 - 1132.

APPENDIX A

CO regression formula

The following formula is the result of the regression analysis performed in Chapter 3. It is used to predict the carbon monoxide mass concentration in the syngas at the outlet of the plasma gasification reactor. It is expressed in percentage.

$(CO)^{1.18}$ =

-26.84790	* Carbon
-555.24935	* Hydrogen
-22.57154	* Oxygen
+6273.61895	* Nitrogen
-3429.48444	* Sulfur
+5.47405E+005	* Chlorine
+24.83377	* Inert
+4.12498	* Moisture
+3.08524	* Carbon * Hydrogen
+1.06438	* Carbon * Oxygen
-63.16992	* Carbon * Nitrogen
+31.05489	* Carbon * Sulfur
-5491.70211	* Carbon * Chlorine
+0.37528	* Carbon * Inert
+0.55157	* Carbon * Moisture
-7.07228E-003	* Carbon * VM
+0.90213	* Carbon * LHV
+5.99359E-004	* Carbon * Coke
+8.91604E-004	* Carbon * Oxidant
+0.011559	* Carbon * Plasma
+7.73202	* Hydrogen * Oxygen
-77.55118	* Hydrogen * Nitrogen
-18.96382	* Hydrogen * Sulfur
-5536.97215	* Hydrogen * Chlorine
+8.48231	* Hydrogen * Inert
+7.82321	* Hydrogen * Moisture
-0.20195	* Hydrogen * VM
+6.77155	* Hydrogen * LHV
+6.95162E-003	* Hydrogen * Coke
-4.10695E-003	* Hydrogen * Oxidant
+59.21499	* Hydrogen * Plasma
-50.33693	* Oxygen * Nitrogen

+43.70564	* Oxygen * Sulfur
-5462.79127	* Oxygen * Chlorine
-0.75544	* Oxygen * Inert
-0.35584	* Oxygen * Moisture
+0.13598	* Oxygen * VM
-2.38590	* Oxygen * LHV
+0.043866	* Oxygen * Coke
-1.37937E-003	* Oxygen * Oxidant
+0.45755	* Oxygen * Plasma
-273.25346	* Nitrogen * Sulfur
-5918.35916	* Nitrogen * Chlorine
-50.59467	* Nitrogen * Inert
-71.18575	* Nitrogen * Moisture
-1.14365	* Nitrogen * VM
-60.56945	* Nitrogen * LHV
-5.54462	* Nitrogen * Coke
+0.013179	* Nitrogen * Oxidant
-8.09657	* Nitrogen * Plasma
-4742.11348	* Sulfur * Chlorine
+39.39258	* Sulfur * Inert
+38.39714	* Sulfur * Moisture
-1.25655	* Sulfur * VM
-8.01248	* Sulfur * LHV
+21.08548	* Sulfur * Coke
-0.027411	* Sulfur * Oxidant
-3802.46827	* Sulfur * Plasma
-5561.04855	* Chlorine * Inert
-5482.72057	* Chlorine * Moisture
-2775.07120	* Chlorine * VM
+4.16477	* Chlorine * Coke
-41.15552	* Chlorine * Oxidant
-57.59506	* Chlorine * Plasma
-0.12174	* Inert * Moisture
-0.058889	* Inert * VM
-1.57500	* Inert * LHV
-7.78153E-003	* Inert * Coke
-1.95875E-003	* Inert * Oxidant
+0.33536	* Inert * Plasma
-0.093330	* Moisture * VM
-0.75337	* Moisture * LHV
+8.06402E-003	* Moisture * Coke
-4.77310E-004	* Moisture * Oxidant
+0.054705	* Moisture * Plasma
+1.25033E-004	* Carbon * Hydrogen * Oxidant
-0.57120	* Carbon * Hydrogen * Plasma
-6.26663E-004	* Carbon * Oxygen * Coke

+0.76917	* Carbon * Nitrogen * LHV
+0.055853	* Carbon * Nitrogen * Coke
-2.63086E-004	* Carbon * Nitrogen * Oxidant
-0.21252	* Carbon * Sulfur * Coke
+5.65377E-004	* Carbon * Sulfur * Oxidant
+38.64832	* Carbon * Sulfur * Plasma
+27.99921	* Carbon * Chlorine * VM
-0.043857	* Carbon * Chlorine * Coke
+0.41238	* Carbon * Chlorine * Oxidant
+2.99606E-004	* Carbon * Inert * Coke
-0.026429	* Carbon * Inert * Plasma
-3.48118E-005	* Carbon * Moisture * Oxidant
-9.98844E-004	* Hydrogen * Oxygen * Coke
-0.71770	* Hydrogen * Oxygen * Plasma
+1.56772	* Hydrogen * Nitrogen * LHV
+0.058694	* Hydrogen * Nitrogen * Coke
+0.76653	* Hydrogen * Sulfur * VM
+2.53069	* Hydrogen * Sulfur * LHV
-0.22480	* Hydrogen * Sulfur * Coke
+37.98723	* Hydrogen * Sulfur * Plasma
+27.47716	* Hydrogen * Chlorine * VM
+0.41548	* Hydrogen * Chlorine * Oxidant
-0.23152	* Hydrogen * Inert * LHV
+1.43675E-004	* Hydrogen * Inert * Oxidant
-0.75070	* Hydrogen * Inert * Plasma
-0.14764	* Hydrogen * Moisture * LHV
-0.64535	* Hydrogen * Moisture * Plasma
+0.054954	* Oxygen * Nitrogen * Coke
-3.02855E-004	* Oxygen * Nitrogen * Oxidant
-0.21492	* Oxygen * Sulfur * Coke
+38.10042	* Oxygen * Sulfur * Plasma
+27.38132	* Oxygen * Chlorine * VM
-0.045630	* Oxygen * Chlorine * Coke
+0.41314	* Oxygen * Chlorine * Oxidant
+0.12035	* Oxygen * Inert * LHV
-7.20464E-004	* Oxygen * Inert * Coke
+0.056487	* Oxygen * Moisture * LHV
-8.09242E-004	* Oxygen * Moisture * Coke
+6.08779E-005	* Oxygen * Moisture * Oxidant
+4.13933	* Nitrogen * Sulfur * VM
-0.15666	* Nitrogen * Sulfur * Coke
+49.07190	* Nitrogen * Sulfur * Plasma
+33.21141	* Nitrogen * Chlorine * VM
+0.42526	* Nitrogen * Chlorine * Oxidant
-0.13894	* Nitrogen * Inert * VM
+0.059625	* Nitrogen * Inert * Coke

+1.11870	* Nitrogen * Moisture * LHV
+0.055461	* Nitrogen * Moisture * Coke
+0.45853	* Sulfur * Chlorine * Oxidant
-0.20856	* Sulfur * Inert * Coke
+37.98928	* Sulfur * Inert * Plasma
-0.21095	* Sulfur * Moisture * Coke
+38.13969	* Sulfur * Moisture * Plasma
+28.55069	* Chlorine * Inert * VM
-0.044788	* Chlorine * Inert * Coke
+0.41356	* Chlorine * Inert * Oxidant
+6.76813	* Chlorine * Inert * Plasma
+28.15556	* Chlorine * Moisture * VM
-0.043942	* Chlorine * Moisture * Coke
+0.41115	* Chlorine * Moisture * Oxidant
+5.44169E-005	* Inert * Moisture * Oxidant

APPENDIX B
Block Flow Diagram

This block flow diagram corresponds to the base case scenario referred in section 4.8.

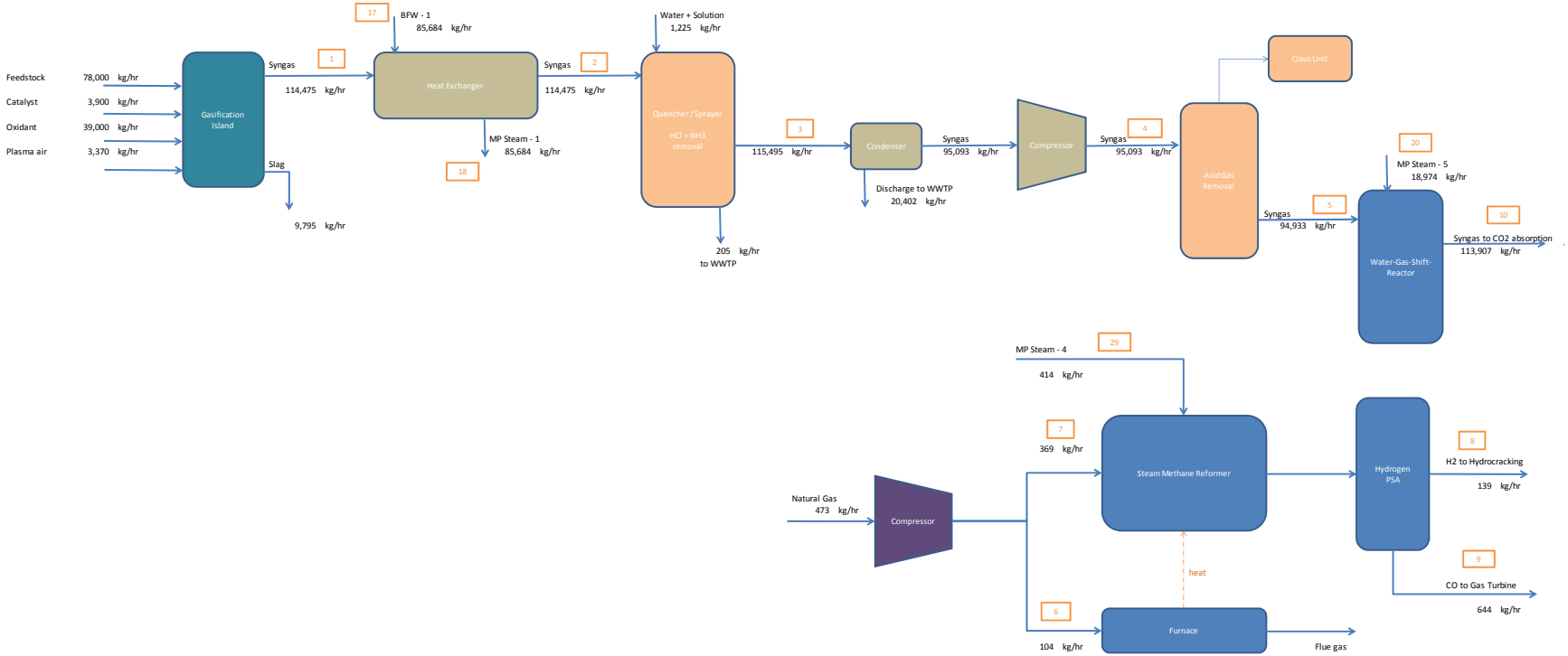

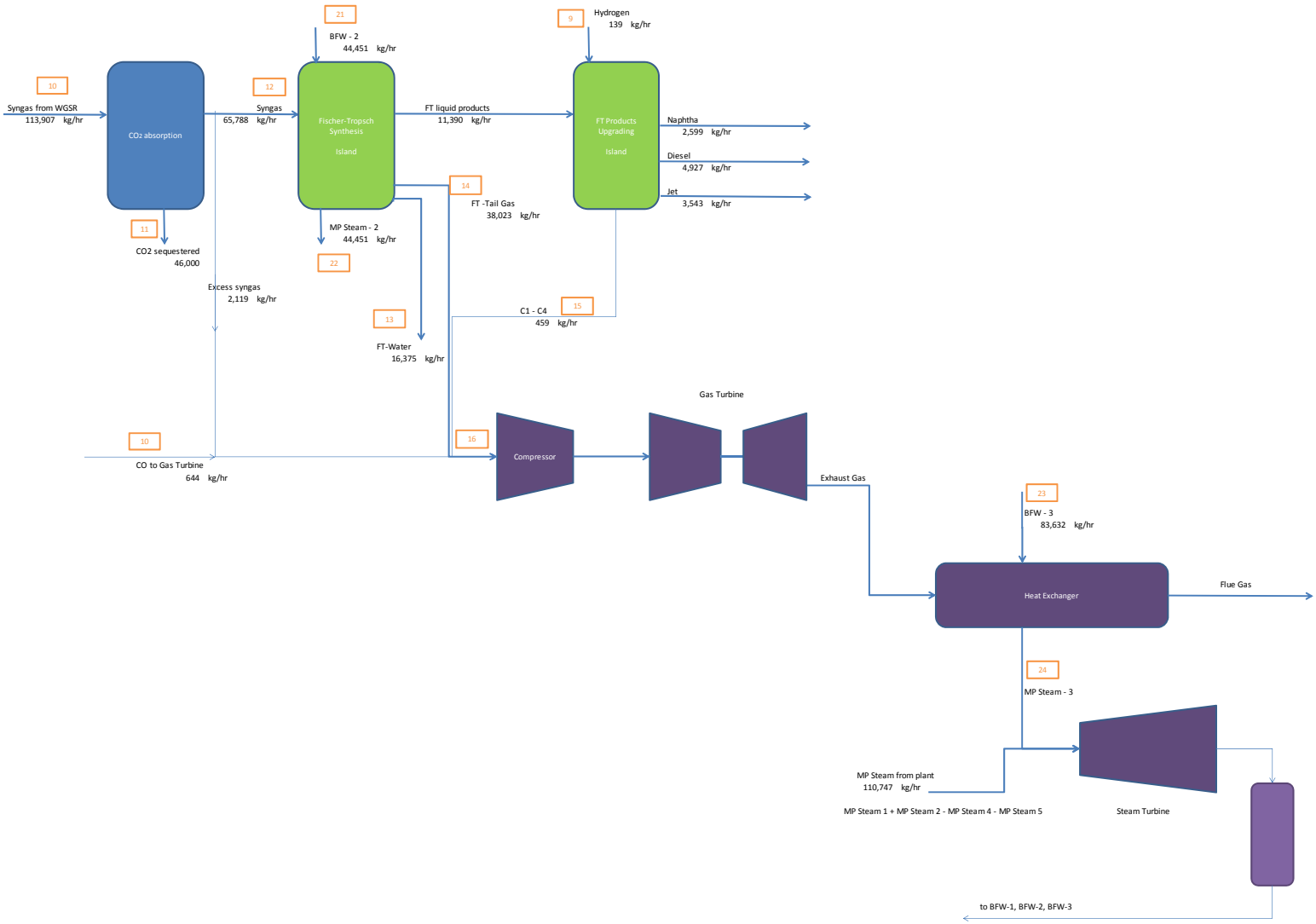
21
BFW - 2
44,451 kg/hr
9
Hydrogen
139 kg/hr
10
Syngas from WGSR
113,907 kg/hr
CO2 absorption
12
Syngas
65,788 kg/hr
Fischer-Tropsch Synthesis Island
FT liquid products
11,390 kg/hr
FT Products Upgrading Island
Naphtha
2,599 kg/hr
Diesel
4,927 kg/hr
Jet
3,543 kg/hr
14
FT -Tail Gas
38,023 kg/hr
11
CO2 sequestered
46,000
MP Steam - 2
44,451 kg/hr
22
Excess syngas
2,119 kg/hr
15
C1 - C4
459 kg/hr
13
FT-Water
16,375 kg/hr
Gas Turbine
10
CO to Gas Turbine
644 kg/hr
16
Compressor
Exhaust Gas
23
BFW - 3
83,632 kg/hr
Heat Exchanger
Flue Gas
24
MP Steam - 3
MP Steam from plant
110,747 kg/hr
MP Steam 1 + MP Steam 2 - MP Steam 4 - MP Steam 5
Steam Turbine
to BFW-1, BFW-2, BFW-3

Material balance

This block flow diagram corresponds to the base case scenario referred in section 4.8.

flow rate (kmol/hr)	1	2	3	4	5	6	7	8	9	10	11	12	13	14	15	16
CO	600.88	600.88	2,343.42	2,343.42	2,343.42	-	-	-	22.98	1,290.26	-	1,250.00	-	375.00	-	438.24
CO2	113.14	113.14	441.23	441.23	441.23	-	-	-	-	1,494.39	1,045.19	435.18	-	435.18	-	449.19
H2	434.20	434.20	1,693.40	1,693.40	1,693.40	-	-	68.95	-	2,746.56	-	2,660.85	-	823.36	-	909.06
N2	52.23	52.23	203.70	203.70	203.70	-	-	-	-	203.70	-	197.34	-	197.34	-	203.70
H2O	284.18	284.18	1,167.42	35.02	35.02	-	-	-	-	35.02	-	33.93	908.93	-	-	-
H2S	1.09	1.09	4.23	4.23	0.00	-	-	-	-	0.00	-	0.00	-	-	-	-
HCl	0.32	0.32	-	-	-	-	-	-	-	-	-	-	-	-	-	-
COS	0.06	0.06	0.25	0.25	0.00	-	-	-	-	-	-	-	-	-	-	-
NH3	0.01	0.01	-	-	-	-	-	-	-	-	-	-	-	-	-	-
HCN	0.00	0.00	0.01	-	-	-	-	-	-	-	-	-	-	-	-	-
CH4	1.95	1.95	7.59	7.59	7.59	6.49	22.98	-	-	7.59	-	7.36	-	16.11	0.01	16.35
C2H4	-	-	-	-	-	-	-	-	-	-	-	-	-	-	-	-
C2+	-	-	-	-	-	-	-	-	-	-	-	-	-	7.88	0.01	7.88
C3+	-	-	-	-	-	-	-	-	-	-	-	-	-	7.09	0.10	7.19
C4+	-	-	-	-	-	-	-	-	-	-	-	-	-	6.38	7.82	14.20
C5 - 300 °F	-	-	-	-	-	-	-	-	-	-	-	-	-	-	-	
550 °F - EP	-	-	-	-	-	-	-	-	-	-	-	-	-	-	-	
Total	1,488.05	1,488.05	5,861.25	4,728.85	4,724.36	6.49	22.98	68.95	22.98	5,777.52	1,045.19	4,584.66	908.93	1,868.32	7.94	2,045.82
kg/kmol	19.73	19.73	19.70	20.11	20.09	16.04	28.05	2.02	28.01	19.72	44.01	14.35	18.02	20.35	57.87	20.15

flow rate (kmol/hr)	17	18	19	20	21	22	23	24
H2O	4,755.94	4,755.94	22.98	1,053.16	2,467.25	2,467.25	4,642.02	4,642.02
Total	4,755.94	4,755.94	22.98	1,053.16	2,467.25	2,467.25	4,642.02	4,642.02
kg/kmol	18.02	18.02	18.02	18.02	18.02	18.02	18.02	18.02
Phase	Liquid	Gas	Gas	Gas	Liquid	Gas	Liquid	Gas

APPENDIX C

This appendix details the calculations to determine the following Fischer-Tropsch system's characteristics of the base case scenario referred in section 4.8:

1. Fischer-Tropsch paraffinic wax production and composition,
2. Quantity of water resulting from the FT process.
3. Carbon, Hydrogen and Oxygen mass balance of the Fischer-Tropsch system.

AFS distribution for FT paraffinic wax production

0.90

n			Wn	MW (kg/kmol)	Chemical conversion
1	-2	0.010	1.00%	16.04	1 CO + 3 H2 ⟶ C 1 H 4 + 1 H2O
2	-2.0457575	0.009	1.80%	30.07	2 CO + 5 H1 ⟶ C 2 H 6 + 2 H2O
3	-2.091515	0.008	2.43%	44.10	3 CO + 7 H0 ⟶ C 3 H 8 + 3 H2O
4	-2.1372725	0.007	2.92%	58.12	4 CO + 9 H1 ⟶ C 4 H 10 + 4 H2O
5	-2.18303	0.007	3.28%	72.15	5 CO + 11 H2 ⟶ C 5 H 12 + 5 H2O
6	-2.2287875	0.006	3.54%	86.18	6 CO + 13 H3 ⟶ C 6 H 14 + 6 H2O
7	-2.2745449	0.005	3.72%	100.21	7 CO + 15 H4 ⟶ C 7 H 16 + 7 H2O
8	-2.3203024	0.005	3.83%	114.23	8 CO + 17 H5 ⟶ C 8 H 18 + 8 H2O
9	-2.3660599	0.004	3.87%	128.26	9 CO + 19 H6 ⟶ C 9 H 20 + 9 H2O
10	-2.4118174	0.004	3.87%	142.29	10 CO + 21 H7 ⟶ C 10 H 22 + 10 H2O
11	-2.4575749	0.003	3.84%	156.31	11 CO + 23 H8 ⟶ C 11 H 24 + 11 H2O
12	-2.5033324	0.003	3.77%	170.34	12 CO + 25 H9 ⟶ C 12 H 26 + 12 H2O
13	-2.5490899	0.003	3.67%	184.37	13 CO + 27 H10 ⟶ C 13 H 28 + 13 H2O
14	-2.5948474	0.003	3.56%	198.39	14 CO + 29 H11 ⟶ C 14 H 30 + 14 H2O
15	-2.6406049	0.002	3.43%	212.42	15 CO + 31 H12 ⟶ C 15 H 32 + 15 H2O
16	-2.6863624	0.002	3.29%	226.45	16 CO + 33 H13 ⟶ C 16 H 34 + 16 H2O
17	-2.7321198	0.002	3.15%	240.48	17 CO + 35 H14 ⟶ C 17 H 36 + 17 H2O
18	-2.7778773	0.002	3.00%	254.50	18 CO + 37 H15 ⟶ C 18 H 38 + 18 H2O
19	-2.8236348	0.002	2.85%	268.53	19 CO + 39 H16 ⟶ C 19 H 40 + 19 H2O
20	-2.8693923	0.001	2.70%	282.56	20 CO + 41 H17 ⟶ C 20 H 42 + 20 H2O
21	-2.9151498	0.001	2.55%	296.58	21 CO + 43 H18 ⟶ C 21 H 44 + 21 H2O
22	-2.9609073	0.001	2.41%	310.61	22 CO + 45 H19 ⟶ C 22 H 46 + 22 H2O
23	-3.0066648	0.001	2.26%	324.64	23 CO + 47 H20 ⟶ C 23 H 48 + 23 H2O
24	-3.0524223	0.001	2.13%	338.66	24 CO + 49 H21 ⟶ C 24 H 50 + 24 H2O
25	-3.0981798	0.001	1.99%	352.69	25 CO + 51 H22 ⟶ C 25 H 52 + 25 H2O
26	-3.1439373	0.001	1.87%	366.72	26 CO + 53 H23 ⟶ C 26 H 54 + 26 H2O
27	-3.1896948	0.001	1.74%	380.75	27 CO + 55 H24 ⟶ C 27 H 56 + 27 H2O
28	-3.2354522	0.001	1.63%	394.77	28 CO + 57 H25 ⟶ C 28 H 58 + 28 H2O
29	-3.2812097	0.001	1.52%	408.80	29 CO + 59 H26 ⟶ C 29 H 60 + 29 H2O
30	-3.3269672	0.000	1.41%	422.83	30 CO + 61 H27 ⟶ C 30 H 62 + 30 H2O
31	-3.3727247	0.000	1.31%	436.85	31 CO + 63 H28 ⟶ C 31 H 64 + 31 H2O
32	-3.4184822	0.000	1.22%	450.88	32 CO + 65 H29 ⟶ C 32 H 66 + 32 H2O
33	-3.4642397	0.000	1.13%	464.91	33 CO + 67 H30 ⟶ C 33 H 68 + 33 H2O
34	-3.5099972	0.000	1.05%	478.93	34 CO + 69 H31 ⟶ C 34 H 70 + 34 H2O
35	-3.5557547	0.000	0.97%	492.96	35 CO + 71 H32 ⟶ C 35 H 72 + 35 H2O
36	-3.6015122	0.000	0.90%	506.99	36 CO + 73 H33 ⟶ C 36 H 74 + 36 H2O
37	-3.6472697	0.000	0.83%	521.02	37 CO + 75 H34 ⟶ C 37 H 76 + 37 H2O
38	-3.6930272	0.000	0.77%	535.04	38 CO + 77 H35 ⟶ C 38 H 78 + 38 H2O
39	-3.7387846	0.000	0.71%	549.07	39 CO + 79 H36 ⟶ C 39 H 80 + 39 H2O
40	-3.7845421	0.000	0.66%	563.10	40 CO + 81 H37 ⟶ C 40 H 82 + 40 H2O
41	-3.8302996	0.000	0.61%	577.12	41 CO + 83 H38 ⟶ C 41 H 84 + 41 H2O
42	-3.8760571	0.000	0.56%	591.15	42 CO + 85 H39 ⟶ C 42 H 86 + 42 H2O
43	-3.9218146	0.000	0.51%	605.18	43 CO + 87 H40 ⟶ C 43 H 88 + 43 H2O
44	-3.9675721	0.000	0.47%	619.20	44 CO + 89 H41 ⟶ C 44 H 90 + 44 H2O
45	-4.0133296	0.000	0.44%	633.23	45 CO + 91 H42 ⟶ C 45 H 92 + 45 H2O
46	-4.0590871	0.000	0.40%	647.26	46 CO + 93 H43 ⟶ C 46 H 94 + 46 H2O
47	-4.1048446	0.000	0.37%	661.29	47 CO + 95 H44 ⟶ C 47 H 96 + 47 H2O
48	-4.1506021	0.000	0.34%	675.31	48 CO + 97 H45 ⟶ C 48 H 98 + 48 H2O
49	-4.1963595	0.000	0.31%	689.34	49 CO + 99 H46 ⟶ C 49 H 100 + 49 H2O
50	-4.242117	0.000	0.29%	703.37	50 CO + 101 H47 ⟶ C 50 H 102 + 50 H2O

AFS distribution for FT paraffinic wax production

0.90

n			Wn	MW (kg/kmol)	Chemical conversion
51	-4.2878745	0.000	0.26%	717.39	51 CO + 103 H48 → C 51 H 104 + 51 H2O
52	-4.333632	0.000	0.24%	731.42	52 CO + 105 H49 → C 52 H 106 + 52 H2O
53	-4.3793895	0.000	0.22%	745.45	53 CO + 107 H50 → C 53 H 108 + 53 H2O
54	-4.425147	0.000	0.20%	759.47	54 CO + 109 H51 → C 54 H 110 + 54 H2O
55	-4.4709045	0.000	0.19%	773.50	55 CO + 111 H52 → C 55 H 112 + 55 H2O
56	-4.516662	0.000	0.17%	787.53	56 CO + 113 H53 → C 56 H 114 + 56 H2O
57	-4.5624195	0.000	0.16%	801.56	57 CO + 115 H54 → C 57 H 116 + 57 H2O
58	-4.608177	0.000	0.14%	815.58	58 CO + 117 H55 → C 58 H 118 + 58 H2O
59	-4.6539345	0.000	0.13%	829.61	59 CO + 119 H56 → C 59 H 120 + 59 H2O
60	-4.6996919	0.000	0.12%	843.64	60 CO + 121 H57 → C 60 H 122 + 60 H2O
61	-4.7454494	0.000	0.11%	857.66	61 CO + 123 H58 → C 61 H 124 + 61 H2O
62	-4.7912069	0.000	0.10%	871.69	62 CO + 125 H59 → C 62 H 126 + 62 H2O
63	-4.8369644	0.000	0.09%	885.72	63 CO + 127 H60 → C 63 H 128 + 63 H2O
64	-4.8827219	0.000	0.08%	899.74	64 CO + 129 H61 → C 64 H 130 + 64 H2O
65	-4.9284794	0.000	0.08%	913.77	65 CO + 131 H62 → C 65 H 132 + 65 H2O
66	-4.9742369	0.000	0.07%	927.80	66 CO + 133 H63 → C 66 H 134 + 66 H2O
67	-5.0199944	0.000	0.06%	941.83	67 CO + 135 H64 → C 67 H 136 + 67 H2O
68	-5.0657519	0.000	0.06%	955.85	68 CO + 137 H65 → C 68 H 138 + 68 H2O
69	-5.1115094	0.000	0.05%	969.88	69 CO + 139 H66 → C 69 H 140 + 69 H2O
70	-5.1572668	0.000	0.05%	983.91	70 CO + 141 H67 → C 70 H 142 + 70 H2O
71	-5.2030243	0.000	0.04%	997.93	71 CO + 143 H68 → C 71 H 144 + 71 H2O
72	-5.2487818	0.000	0.04%	1,011.96	72 CO + 145 H69 → C 72 H 146 + 72 H2O
73	-5.2945393	0.000	0.04%	1,025.99	73 CO + 147 H70 → C 73 H 148 + 73 H2O
74	-5.3402968	0.000	0.03%	1,040.01	74 CO + 149 H71 → C 74 H 150 + 74 H2O
75	-5.3860543	0.000	0.03%	1,054.04	75 CO + 151 H72 → C 75 H 152 + 75 H2O
76	-5.4318118	0.000	0.03%	1,068.07	76 CO + 153 H73 → C 76 H 154 + 76 H2O
77	-5.4775693	0.000	0.03%	1,082.10	77 CO + 155 H74 → C 77 H 156 + 77 H2O
78	-5.5233268	0.000	0.02%	1,096.12	78 CO + 157 H75 → C 78 H 158 + 78 H2O
79	-5.5690843	0.000	0.02%	1,110.15	79 CO + 159 H76 → C 79 H 160 + 79 H2O
80	-5.6148418	0.000	0.02%	1,124.18	80 CO + 161 H77 → C 80 H 162 + 80 H2O
81	-5.6605992	0.000	0.02%	1,138.20	81 CO + 163 H78 → C 81 H 164 + 81 H2O
82	-5.7063567	0.000	0.02%	1,152.23	82 CO + 165 H79 → C 82 H 166 + 82 H2O
83	-5.7521142	0.000	0.01%	1,166.26	83 CO + 167 H80 → C 83 H 168 + 83 H2O
84	-5.7978717	0.000	0.01%	1,180.28	84 CO + 169 H81 → C 84 H 170 + 84 H2O
85	-5.8436292	0.000	0.01%	1,194.31	85 CO + 171 H82 → C 85 H 172 + 85 H2O
86	-5.8893867	0.000	0.01%	1,208.34	86 CO + 173 H83 → C 86 H 174 + 86 H2O
87	-5.9351442	0.000	0.01%	1,222.37	87 CO + 175 H84 → C 87 H 176 + 87 H2O
88	-5.9809017	0.000	0.01%	1,236.39	88 CO + 177 H85 → C 88 H 178 + 88 H2O
89	-6.0266592	0.000	0.01%	1,250.42	89 CO + 179 H86 → C 89 H 180 + 89 H2O
90	-6.0724167	0.000	0.01%	1,264.45	90 CO + 181 H87 → C 90 H 182 + 90 H2O
91	-6.1181742	0.000	0.01%	1,278.47	91 CO + 183 H88 → C 91 H 184 + 91 H2O
92	-6.1639316	0.000	0.01%	1,292.50	92 CO + 185 H89 → C 92 H 186 + 92 H2O
93	-6.2096891	0.000	0.01%	1,306.53	93 CO + 187 H90 → C 93 H 188 + 93 H2O
94	-6.2554466	0.000	0.01%	1,320.55	94 CO + 189 H91 → C 94 H 190 + 94 H2O
95	-6.3012041	0.000	0.00%	1,334.58	95 CO + 191 H92 → C 95 H 192 + 95 H2O
96	-6.3469616	0.000	0.00%	1,348.61	96 CO + 193 H93 → C 96 H 194 + 96 H2O
97	-6.3927191	0.000	0.00%	1,362.64	97 CO + 195 H94 → C 97 H 196 + 97 H2O
98	-6.4384766	0.000	0.00%	1,376.66	98 CO + 197 H95 → C 98 H 198 + 98 H2O
99	-6.4842341	0.000	0.00%	1,390.69	99 CO + 199 H96 → C 99 H 200 + 99 H2O
100	-6.5299916	0.000	0.00%	1,404.72	100 CO + 201 H97 → C 100 H 202 + 100 H2O

AFS distribution for FT paraffinic wax production

n	0.90		Wn		
				MW (kg/kmol)	Chemical conversion
101	-6.5757491	0.000	0.00%	1,418.74	101 CO + 203 H98 → C 101 H 204 + 101 H2O
102	-6.6215065	0.000	0.00%	1,432.77	102 CO + 205 H99 → C 102 H 206 + 102 H2O
103	-6.667264	0.000	0.00%	1,446.80	103 CO + 207 H100 → C 103 H 208 + 103 H2O
104	-6.7130215	0.000	0.00%	1,460.82	104 CO + 209 H101 → C 104 H 210 + 104 H2O
105	-6.758779	0.000	0.00%	1,474.85	105 CO + 211 H102 → C 105 H 212 + 105 H2O
106	-6.8045365	0.000	0.00%	1,488.88	106 CO + 213 H103 → C 106 H 214 + 106 H2O
107	-6.850294	0.000	0.00%	1,502.91	107 CO + 215 H104 → C 107 H 216 + 107 H2O
108	-6.8960515	0.000	0.00%	1,516.93	108 CO + 217 H105 → C 108 H 218 + 108 H2O
109	-6.941809	0.000	0.00%	1,530.96	109 CO + 219 H106 → C 109 H 220 + 109 H2O
110	-6.9875665	0.000	0.00%	1,544.99	110 CO + 221 H107 → C 110 H 222 + 110 H2O
111	-7.033324	0.000	0.00%	1,559.01	111 CO + 223 H108 → C 111 H 224 + 111 H2O
112	-7.0790815	0.000	0.00%	1,573.04	112 CO + 225 H109 → C 112 H 226 + 112 H2O
113	-7.1248389	0.000	0.00%	1,587.07	113 CO + 227 H110 → C 113 H 228 + 113 H2O
114	-7.1705964	0.000	0.00%	1,601.09	114 CO + 229 H111 → C 114 H 230 + 114 H2O
115	-7.2163539	0.000	0.00%	1,615.12	115 CO + 231 H112 → C 115 H 232 + 115 H2O
116	-7.2621114	0.000	0.00%	1,629.15	116 CO + 233 H113 → C 116 H 234 + 116 H2O
117	-7.3078689	0.000	0.00%	1,643.18	117 CO + 235 H114 → C 117 H 236 + 117 H2O
118	-7.3536264	0.000	0.00%	1,657.20	118 CO + 237 H115 → C 118 H 238 + 118 H2O
119	-7.3993839	0.000	0.00%	1,671.23	119 CO + 239 H116 → C 119 H 240 + 119 H2O
120	-7.4451414	0.000	0.00%	1,685.26	120 CO + 241 H117 → C 120 H 242 + 120 H2O
121	-7.4908989	0.000	0.00%	1,699.28	121 CO + 243 H118 → C 121 H 244 + 121 H2O
122	-7.5366564	0.000	0.00%	1,713.31	122 CO + 245 H119 → C 122 H 246 + 122 H2O
123	-7.5824138	0.000	0.00%	1,727.34	123 CO + 247 H120 → C 123 H 248 + 123 H2O
124	-7.6281713	0.000	0.00%	1,741.36	124 CO + 249 H121 → C 124 H 250 + 124 H2O
125	-7.6739288	0.000	0.00%	1,755.39	125 CO + 251 H122 → C 125 H 252 + 125 H2O
126	-7.7196863	0.000	0.00%	1,769.42	126 CO + 253 H123 → C 126 H 254 + 126 H2O
127	-7.7654438	0.000	0.00%	1,783.45	127 CO + 255 H124 → C 127 H 256 + 127 H2O
128	-7.8112013	0.000	0.00%	1,797.47	128 CO + 257 H125 → C 128 H 258 + 128 H2O
129	-7.8569588	0.000	0.00%	1,811.50	129 CO + 259 H126 → C 129 H 260 + 129 H2O
130	-7.9027163	0.000	0.00%	1,825.53	130 CO + 261 H127 → C 130 H 262 + 130 H2O
131	-7.9484738	0.000	0.00%	1,839.55	131 CO + 263 H128 → C 131 H 264 + 131 H2O
132	-7.9942313	0.000	0.00%	1,853.58	132 CO + 265 H129 → C 132 H 266 + 132 H2O
133	-8.0399888	0.000	0.00%	1,867.61	133 CO + 267 H130 → C 133 H 268 + 133 H2O
134	-8.0857462	0.000	0.00%	1,881.63	134 CO + 269 H131 → C 134 H 270 + 134 H2O
135	-8.1315037	0.000	0.00%	1,895.66	135 CO + 271 H132 → C 135 H 272 + 135 H2O
136	-8.1772612	0.000	0.00%	1,909.69	136 CO + 273 H133 → C 136 H 274 + 136 H2O
137	-8.2230187	0.000	0.00%	1,923.72	137 CO + 275 H134 → C 137 H 276 + 137 H2O
138	-8.2687762	0.000	0.00%	1,937.74	138 CO + 277 H135 → C 138 H 278 + 138 H2O
139	-8.3145337	0.000	0.00%	1,951.77	139 CO + 279 H136 → C 139 H 280 + 139 H2O
140	-8.3602912	0.000	0.00%	1,965.80	140 CO + 281 H137 → C 140 H 282 + 140 H2O
141	-8.4060487	0.000	0.00%	1,979.82	141 CO + 283 H138 → C 141 H 284 + 141 H2O
142	-8.4518062	0.000	0.00%	1,993.85	142 CO + 285 H139 → C 142 H 286 + 142 H2O
143	-8.4975637	0.000	0.00%	2,007.88	143 CO + 287 H140 → C 143 H 288 + 143 H2O
144	-8.5433212	0.000	0.00%	2,021.90	144 CO + 289 H141 → C 144 H 290 + 144 H2O
145	-8.5890786	0.000	0.00%	2,035.93	145 CO + 291 H142 → C 145 H 292 + 145 H2O
146	-8.6348361	0.000	0.00%	2,049.96	146 CO + 293 H143 → C 146 H 294 + 146 H2O
147	-8.6805936	0.000	0.00%	2,063.99	147 CO + 295 H144 → C 147 H 296 + 147 H2O
148	-8.7263511	0.000	0.00%	2,078.01	148 CO + 297 H145 → C 148 H 298 + 148 H2O
149	-8.7721086	0.000	0.00%	2,092.04	149 CO + 299 H146 → C 149 H 300 + 149 H2O
150	-8.8178661	0.000	0.00%	2,106.07	150 CO + 301 H147 → C 150 H 302 + 150 H2O
151	-8.8636236	0.000	0.00%	2,120.09	151 CO + 303 H148 → C 151 H 304 + 151 H2O

Detailed calculation for FT products and FT-water produced

n	Amount of C that reacts for this equation (kg/hr)	Amount of CO that reacts for this equation (kg/hr)	Amount H2 required (kg/hr)	FT-X (kg/hr)	FT water (kg/hr)
1	108.48	252.99	54.62	144.90	162.72
2	195.27	455.38	81.94	244.43	292.89
3	263.61	614.77	103.24	322.60	395.41
4	316.33	737.72	119.46	382.70	474.49
5	355.87	829.94	131.41	427.55	533.80
6	384.34	896.33	139.77	459.60	576.50
7	403.56	941.15	145.15	480.97	605.33
8	415.09	968.04	148.05	493.47	622.62
9	420.28	980.14	148.92	498.66	630.41
10	420.28	980.14	148.14	497.88	630.41
11	416.08	970.34	146.02	492.26	624.10
12	408.51	952.69	142.85	482.79	612.76
13	398.30	928.88	138.85	470.29	597.44
14	386.04	900.30	134.22	455.47	579.05
15	372.26	868.14	129.13	438.90	558.37
16	357.37	833.42	123.71	421.10	536.04
17	341.73	796.95	118.09	402.46	512.59
18	325.65	759.45	112.35	383.34	488.47
19	309.37	721.48	106.58	364.03	464.04
20	293.08	683.51	100.85	344.74	439.62
21	276.96	645.91	95.19	325.67	415.44
22	261.14	609.00	89.65	306.96	391.70
23	245.71	573.02	84.28	288.74	368.55
24	230.75	538.14	79.08	271.10	346.12
25	216.33	504.50	74.07	254.09	324.49
26	202.48	472.22	69.28	237.78	303.72
27	189.24	441.34	64.70	222.19	283.86
28	176.63	411.92	60.35	207.33	264.94
29	164.64	383.97	56.22	193.23	246.96
30	153.29	357.49	52.32	179.87	229.93
31	142.56	332.46	48.63	167.26	213.83
32	132.44	308.87	45.15	155.37	198.66
33	122.92	286.67	41.89	144.18	184.38
34	113.98	265.82	38.83	133.68	170.97
35	105.60	246.27	35.96	123.83	158.40
36	97.76	227.98	33.27	114.62	146.63
37	90.42	210.88	30.77	106.01	135.63
38	83.58	194.92	28.43	97.98	125.37
39	77.20	180.05	26.25	90.49	115.80
40	71.26	166.20	24.22	83.52	106.89
41	65.74	153.32	22.34	77.05	98.61
42	60.61	141.35	20.59	71.03	90.91
43	55.85	130.24	18.97	65.44	83.77
44	51.43	119.95	17.46	60.26	77.15
45	47.34	110.40	16.07	55.46	71.01
46	43.55	101.57	14.78	51.02	65.33
47	40.05	93.40	13.59	46.92	60.07
48	36.81	85.85	12.49	43.12	55.22
49	33.82	78.88	11.47	39.61	50.73
50	31.06	72.44	10.53	36.38	46.59

Detailed calculation for FT products and FT-water produced

n	Amount of C that reacts for this equation (kg/hr)	Amount of CO that reacts for this equation (kg/hr)	Amount H2 required (kg/hr)	FT-X (kg/hr)	FT water (kg/hr)
51	28.51	66.50	9.67	33.39	42.77
52	26.17	61.02	8.87	30.64	39.25
53	24.00	55.97	8.13	28.11	36.00
54	22.01	51.33	7.46	25.77	33.01
55	20.17	47.05	6.83	23.62	30.26
56	18.49	43.12	6.26	21.65	27.73
57	16.94	39.50	5.74	19.83	25.40
58	15.51	36.17	5.25	18.16	23.26
59	14.20	33.11	4.81	16.62	21.30
60	13.00	30.31	4.40	15.21	19.49
61	11.89	27.73	4.02	13.92	17.84
62	10.88	25.37	3.68	12.73	16.32
63	9.95	23.20	3.37	11.64	14.92
64	9.10	21.21	3.08	10.65	13.64
65	8.31	19.39	2.81	9.73	12.47
66	7.60	17.72	2.57	8.89	11.40
67	6.94	16.19	2.35	8.12	10.41
68	6.34	14.79	2.14	7.42	9.51
69	5.79	13.50	1.96	6.78	8.69
70	5.29	12.33	1.79	6.19	7.93
71	4.83	11.25	1.63	5.65	7.24
72	4.40	10.27	1.49	5.15	6.61
73	4.02	9.37	1.36	4.70	6.03
74	3.67	8.55	1.24	4.29	5.50
75	3.34	7.80	1.13	3.91	5.02
76	3.05	7.11	1.03	3.57	4.58
77	2.78	6.49	0.94	3.25	4.17
78	2.54	5.91	0.86	2.97	3.80
79	2.31	5.39	0.78	2.70	3.47
80	2.11	4.91	0.71	2.46	3.16
81	1.92	4.48	0.65	2.25	2.88
82	1.75	4.08	0.59	2.05	2.62
83	1.59	3.72	0.54	1.86	2.39
84	1.45	3.38	0.49	1.70	2.18
85	1.32	3.08	0.45	1.55	1.98
86	1.20	2.81	0.41	1.41	1.81
87	1.10	2.56	0.37	1.28	1.64
88	1.00	2.33	0.34	1.17	1.50
89	0.91	2.12	0.31	1.06	1.36
90	0.83	1.93	0.28	0.97	1.24
91	0.75	1.75	0.25	0.88	1.13
92	0.68	1.60	0.23	0.80	1.03
93	0.62	1.45	0.21	0.73	0.93
94	0.57	1.32	0.19	0.66	0.85
95	0.52	1.20	0.17	0.60	0.77
96	0.47	1.09	0.16	0.55	0.70
97	0.43	0.99	0.14	0.50	0.64
98	0.39	0.90	0.13	0.45	0.58
99	0.35	0.82	0.12	0.41	0.53
100	0.32	0.75	0.11	0.37	0.48

Detailed calculation for FT products and FT-water produced

n	Amount of C that reacts for this equation (kg/hr)	Amount of CO that reacts for this equation (kg/hr)	Amount H2 required (kg/hr)	FT-X (kg/hr)	FT water (kg/hr)
101	0.29	0.68	0.10	0.34	0.44
102	0.26	0.62	0.09	0.31	0.40
103	0.24	0.56	0.08	0.28	0.36
104	0.22	0.51	0.07	0.26	0.33
105	0.20	0.46	0.07	0.23	0.30
106	0.18	0.42	0.06	0.21	0.27
107	0.16	0.38	0.06	0.19	0.25
108	0.15	0.35	0.05	0.17	0.22
109	0.14	0.32	0.05	0.16	0.20
110	0.12	0.29	0.04	0.14	0.18
111	0.11	0.26	0.04	0.13	0.17
112	0.10	0.24	0.03	0.12	0.15
113	0.09	0.21	0.03	0.11	0.14
114	0.08	0.19	0.03	0.10	0.13
115	0.08	0.18	0.03	0.09	0.11
116	0.07	0.16	0.02	0.08	0.10
117	0.06	0.15	0.02	0.07	0.09
118	0.06	0.13	0.02	0.07	0.09
119	0.05	0.12	0.02	0.06	0.08
120	0.05	0.11	0.02	0.05	0.07
121	0.04	0.10	0.01	0.05	0.06
122	0.04	0.09	0.01	0.04	0.06
123	0.03	0.08	0.01	0.04	0.05
124	0.03	0.07	0.01	0.04	0.05
125	0.03	0.07	0.01	0.03	0.04
126	0.03	0.06	0.01	0.03	0.04
127	0.02	0.06	0.01	0.03	0.04
128	0.02	0.05	0.01	0.03	0.03
129	0.02	0.05	0.01	0.02	0.03
130	0.02	0.04	0.01	0.02	0.03
131	0.02	0.04	0.01	0.02	0.02
132	0.01	0.03	0.00	0.02	0.02
133	0.01	0.03	0.00	0.02	0.02
134	0.01	0.03	0.00	0.01	0.02
135	0.01	0.03	0.00	0.01	0.02
136	0.01	0.02	0.00	0.01	0.01
137	0.01	0.02	0.00	0.01	0.01
138	0.01	0.02	0.00	0.01	0.01
139	0.01	0.02	0.00	0.01	0.01
140	0.01	0.02	0.00	0.01	0.01
141	0.01	0.01	0.00	0.01	0.01
142	0.01	0.01	0.00	0.01	0.01
143	0.00	0.01	0.00	0.01	0.01
144	0.00	0.01	0.00	0.01	0.01
145	0.00	0.01	0.00	0.00	0.01
146	0.00	0.01	0.00	0.00	0.01
147	0.00	0.01	0.00	0.00	0.00
148	0.00	0.01	0.00	0.00	0.00
149	0.00	0.01	0.00	0.00	0.00
150	0.00	0.01	0.00	0.00	0.00
151	0.00	0.01	0.00	0.00	0.00
		Total CO that reacts	Total H2 that reacts	Total FT-X	Total FT Water
		25,299.01	3,823.71	12,851.01	16,271.89
		CO that reacts for C1-C4	H2 that reacts for C1-C4	FT-X : C1-C4	
		2,060.86	359.27	1,094.63	
		CO that reacts for C5+	H2 that reacts for C5+	FT-X : C5+	
		23,238.15	3,464.44	11,756.37	

Carbon - Hydrogen - Oxygen mass balance

n	C_in	H2_in	O_in	C_out	H2_out	O_out	Diff
1	108.48	54.62	144.509	108.48	54.62	144.51	-
2	195.27	81.94	260.117	195.27	81.94	260.12	-
3	263.61	103.24	351.158	263.61	103.24	351.16	-
4	316.33	119.46	421.389	316.33	119.46	421.39	-
5	355.87	131.41	474.063	355.87	131.41	474.06	-
6	384.34	139.77	511.988	384.34	139.77	511.99	-
7	403.56	145.15	537.587	403.56	145.15	537.59	-
8	415.09	148.05	552.947	415.09	148.05	552.95	-
9	420.28	148.92	559.859	420.28	148.92	559.86	-
10	420.28	148.14	559.859	420.28	148.14	559.86	-
11	416.08	146.02	554.26	416.08	146.02	554.26	-
12	408.51	142.85	544.183	408.51	142.85	544.18	-
13	398.30	138.85	530.578	398.30	138.85	530.58	-
14	386.04	134.22	514.253	386.04	134.22	514.25	-
15	372.26	129.13	495.886	372.26	129.13	495.89	-
16	357.37	123.71	476.051	357.37	123.71	476.05	-
17	341.73	118.09	455.224	341.73	118.09	455.22	-
18	325.65	112.35	433.801	325.65	112.35	433.80	-
19	309.37	106.58	412.111	309.37	106.58	412.11	-
20	293.08	100.85	390.421	293.08	100.85	390.42	-
21	276.96	95.19	368.948	276.96	95.19	368.95	-
22	261.14	89.65	347.865	261.14	89.65	347.87	-
23	245.71	84.28	327.31	245.71	84.28	327.31	-
24	230.75	79.08	307.386	230.75	79.08	307.39	-
25	216.33	74.07	288.175	216.33	74.07	288.17	-
26	202.48	69.28	269.732	202.48	69.28	269.73	-
27	189.24	64.70	252.095	189.24	64.70	252.10	-
28	176.63	60.35	235.289	176.63	60.35	235.29	-
29	164.64	56.22	219.323	164.64	56.22	219.32	-
30	153.29	52.32	204.197	153.29	52.32	204.20	-
31	142.56	48.63	189.903	142.56	48.63	189.90	-
32	132.44	45.15	176.426	132.44	45.15	176.43	-
33	122.92	41.89	163.746	122.92	41.89	163.75	-
34	113.98	38.83	151.837	113.98	38.83	151.84	-
35	105.60	35.96	140.672	105.60	35.96	140.67	-
36	97.76	33.27	130.223	97.76	33.27	130.22	-
37	90.42	30.77	120.456	90.42	30.77	120.46	-
38	83.58	28.43	111.34	83.58	28.43	111.34	-
39	77.20	26.25	102.843	77.20	26.25	102.84	-
40	71.26	24.22	94.9322	71.26	24.22	94.93	-
41	65.74	22.34	87.575	65.74	22.34	87.57	-
42	60.61	20.59	80.7398	60.61	20.59	80.74	-
43	55.85	18.97	74.396	55.85	18.97	74.40	-
44	51.43	17.46	68.5135	51.43	17.46	68.51	-
45	47.34	16.07	63.0636	47.34	16.07	63.06	-
46	43.55	14.78	58.0185	43.55	14.78	58.02	-
47	40.05	13.59	53.3518	40.05	13.59	53.35	-
48	36.81	12.49	49.0382	36.81	12.49	49.04	-
49	33.82	11.47	45.0539	33.82	11.47	45.05	-
50	31.06	10.53	41.376	31.06	10.53	41.38	-

Carbon - Hydrogen - Oxygen mass balance

n	C_in	H2_in	O_in	C_out	H2_out	O_out	Diff
51	28.51	9.67	37.9832	28.51	9.67	37.98	-
52	26.17	8.87	34.8552	26.17	8.87	34.86	-
53	24.00	8.13	31.9729	24.00	8.13	31.97	-
54	22.01	7.46	29.3186	22.01	7.46	29.32	-
55	20.17	6.83	26.8753	20.17	6.83	26.88	-
56	18.49	6.26	24.6276	18.49	6.26	24.63	-
57	16.94	5.74	22.5606	16.94	5.74	22.56	-
58	15.51	5.25	20.6608	15.51	5.25	20.66	-
59	14.20	4.81	18.9153	14.20	4.81	18.92	-
60	13.00	4.40	17.3123	13.00	4.40	17.31	-
61	11.89	4.02	15.8408	11.89	4.02	15.84	-
62	10.88	3.68	14.4904	10.88	3.68	14.49	-
63	9.95	3.37	13.2517	9.95	3.37	13.25	-
64	9.10	3.08	12.1158	9.10	3.08	12.12	-
65	8.31	2.81	11.0746	8.31	2.81	11.07	-
66	7.60	2.57	10.1205	7.60	2.57	10.12	-
67	6.94	2.35	9.24647	6.94	2.35	9.25	-
68	6.34	2.14	8.44603	6.34	2.14	8.45	-
69	5.79	1.96	7.71322	5.79	1.96	7.71	-
70	5.29	1.79	7.0425	5.29	1.79	7.04	-
71	4.83	1.63	6.4288	4.83	1.63	6.43	-
72	4.40	1.49	5.86741	4.40	1.49	5.87	-
73	4.02	1.36	5.35401	4.02	1.36	5.35	-
74	3.67	1.24	4.88462	3.67	1.24	4.88	-
75	3.34	1.13	4.45556	3.34	1.13	4.46	-
76	3.05	1.03	4.06347	3.05	1.03	4.06	-
77	2.78	0.94	3.70525	2.78	0.94	3.71	-
78	2.54	0.86	3.37803	2.54	0.86	3.38	-
79	2.31	0.78	3.0792	2.31	0.78	3.08	-
80	2.11	0.71	2.80636	2.11	0.71	2.81	-
81	1.92	0.65	2.5573	1.92	0.65	2.56	-
82	1.75	0.59	2.32998	1.75	0.59	2.33	-
83	1.59	0.54	2.12256	1.59	0.54	2.12	-
84	1.45	0.49	1.93332	1.45	0.49	1.93	-
85	1.32	0.45	1.7607	1.32	0.45	1.76	-
86	1.20	0.41	1.60327	1.20	0.41	1.60	-
87	1.10	0.37	1.45972	1.10	0.37	1.46	-
88	1.00	0.34	1.32885	1.00	0.34	1.33	-
89	0.91	0.31	1.20956	0.91	0.31	1.21	-
90	0.83	0.28	1.10083	0.83	0.28	1.10	-
91	0.75	0.25	1.00176	0.75	0.25	1.00	-
92	0.68	0.23	0.91149	0.68	0.23	0.91	-
93	0.62	0.21	0.82926	0.62	0.21	0.83	-
94	0.57	0.19	0.75436	0.57	0.19	0.75	-
95	0.52	0.17	0.68614	0.52	0.17	0.69	-
96	0.47	0.16	0.62403	0.47	0.16	0.62	-
97	0.43	0.14	0.56748	0.43	0.14	0.57	-
98	0.39	0.13	0.51599	0.39	0.13	0.52	-
99	0.35	0.12	0.46913	0.35	0.12	0.47	-
100	0.32	0.11	0.42649	0.32	0.11	0.43	-

Carbon - Hydrogen - Oxygen mass balance

n	C_in	H2_in	O_in	C_out	H2_out	O_out	Diff
101	0.29	0.10	0.38768	0.29	0.10	0.39	-
102	0.26	0.09	0.35236	0.26	0.09	0.35	-
103	0.24	0.08	0.32024	0.24	0.08	0.32	-
104	0.22	0.07	0.29101	0.22	0.07	0.29	-
105	0.20	0.07	0.26443	0.20	0.07	0.26	-
106	0.18	0.06	0.24025	0.18	0.06	0.24	-
107	0.16	0.06	0.21827	0.16	0.06	0.22	-
108	0.15	0.05	0.19828	0.15	0.05	0.20	-
109	0.14	0.05	0.1801	0.14	0.05	0.18	-
110	0.12	0.04	0.16358	0.12	0.04	0.16	-
111	0.11	0.04	0.14856	0.11	0.04	0.15	-
112	0.10	0.03	0.13491	0.10	0.03	0.13	-
113	0.09	0.03	0.1225	0.09	0.03	0.12	-
114	0.08	0.03	0.11123	0.08	0.03	0.11	-
115	0.08	0.03	0.10098	0.08	0.03	0.10	-
116	0.07	0.02	0.09167	0.07	0.02	0.09	-
117	0.06	0.02	0.08322	0.06	0.02	0.08	-
118	0.06	0.02	0.07554	0.06	0.02	0.08	-
119	0.05	0.02	0.06856	0.05	0.02	0.07	-
120	0.05	0.02	0.06222	0.05	0.02	0.06	-
121	0.04	0.01	0.05647	0.04	0.01	0.06	-
122	0.04	0.01	0.05124	0.04	0.01	0.05	-
123	0.03	0.01	0.04649	0.03	0.01	0.05	-
124	0.03	0.01	0.04218	0.03	0.01	0.04	-
125	0.03	0.01	0.03827	0.03	0.01	0.04	-
126	0.03	0.01	0.03472	0.03	0.01	0.03	-
127	0.02	0.01	0.0315	0.02	0.01	0.03	-
128	0.02	0.01	0.02857	0.02	0.01	0.03	-
129	0.02	0.01	0.02591	0.02	0.01	0.03	-
130	0.02	0.01	0.0235	0.02	0.01	0.02	-
131	0.02	0.01	0.02132	0.02	0.01	0.02	-
132	0.01	0.00	0.01933	0.01	0.00	0.02	-
133	0.01	0.00	0.01753	0.01	0.00	0.02	-
134	0.01	0.00	0.01589	0.01	0.00	0.02	-
135	0.01	0.00	0.01441	0.01	0.00	0.01	-
136	0.01	0.00	0.01307	0.01	0.00	0.01	-
137	0.01	0.00	0.01185	0.01	0.00	0.01	-
138	0.01	0.00	0.01074	0.01	0.00	0.01	-
139	0.01	0.00	0.00974	0.01	0.00	0.01	-
140	0.01	0.00	0.00883	0.01	0.00	0.01	-
141	0.01	0.00	0.008	0.01	0.00	0.01	-
142	0.01	0.00	0.00725	0.01	0.00	0.01	-
143	0.00	0.00	0.00657	0.00	0.00	0.01	-
144	0.00	0.00	0.00596	0.00	0.00	0.01	-
145	0.00	0.00	0.0054	0.00	0.00	0.01	-
146	0.00	0.00	0.00489	0.00	0.00	0.00	-
147	0.00	0.00	0.00443	0.00	0.00	0.00	-
148	0.00	0.00	0.00402	0.00	0.00	0.00	-
149	0.00	0.00	0.00364	0.00	0.00	0.00	-
150	0.00	0.00	0.0033	0.00	0.00	0.00	-
151	0.00	0.00	0.00299	0.00	0.00	0.00	-

APPENDIX D

This appendix details the calculation to determine the direct cost of the Fischer-Tropsch system

	Volumeric flow of syngas	5,043	kmol/hr			
		112,975,185	Litres at 1 atm / 273 K			
		3,989,681	ft3/hr at 1 atm / 273 K			
	Contact time	0.25	sec			
		6.94E-05	hr			
	Reaction zone volume	277.06	ft3			
		7.85E+09	mm3			
	Plate geometry					
	width	1	m	1000	mm	
	height	1.5	m	1500	mm	
	margin for manifold	5	cm	50	mm	
	channel length (width-wise)			900	mm	
	Active length for channel			1400	mm	
	Reaction plates					
	reactive channel thickness	0.95	mm	0.0374	inches	
	cover plate thickness	1	mm	0.0394	inches	
	reaction channel width	17	mm	0.6693	inches	
	spacer width	3	mm	0.1181	inches	
	reaction channel pitch	20				
	# channel per plate	70				
	cover plate metal volume	1,500,000	mm3/plate	5.30E-02	ft3/plate	
	spacer plate metal volume	407,550	mm3/plate	1.44E-02	ft3/plate	
	Cooling plates					
	coolant channel thickness	1.5	mm	0.0591	inches	
	cover plate thickness	1	mm	0.0394	inches	
	cooling channel width	3	mm	0.1181	inches	
	spacer width	2	mm	0.0787	inches	
	cooling channel pitch	5				
	# channel per plate	280				
	cover plate metal volume	1,500,000	mm3/plate	5.30E-02	ft3/plate	
	spacer plate metal volume	1,116,000	mm3/plate	3.94E-02	ft3/plate	
	combustion volume	1,134,000	mm3/plate	4.00E-02	ft3/plate	

	Plate pairs					
	pair thickness	4.45	mm			
	total reaction volume	1,017,450	mm3/plate	3.59E-02	ft3/plate	
	cooling area	2,142,000	mm2/plate	23.06	ft2/plate	
	metal density (304 SS)	8.01	g/cm3			
	metal mass	36.23	kg			
	Modules					
	module thickness	1	m	3.28	ft	
	plate pairs	225	per module			
	Total reaction volume	228,926,250	mm3/module	8.08E+00	ft3/module	
	cooling area	481,950,000	mm2/module	5,187.67	ft2/module	
	metal mass	8,152.57	kg/module			
		14,535	mm3/channel			
	Assumed void fraction	40%				
	Number of plates required	19,278				
	Number of modules required	**86.00**				
FT Module Price						
http://www.meps.co.uk/Stainless%20Price-N.Amer.htm						
	Price of 304-SS	$ 4,270	$/tonne			
	Price per module	$ 34,811	$/module			
	Factor for bare module cost	5				
	Bare module cost/module	$ 174,057	$/module			
	Total FT equipment cost	$ 14,968,930				
	installation factor	1.4				
	Direct Capital Cost	**$ 20,956,502.11**				

APPENDIX E

Discounted Cash Flow for product value calculation

	-1	0	1	2	3	4	5	6	7	8	9	10
Investment and Salvage Costs	(321,784,312.20)	(218,813,332.3)										
slag production (tpy)			39,180	78,361	78,361	78,361	78,361	78,361	78,361	78,361	78,361	78,361
slag price ($/tonne)		$	1.05	$ 1.07	$ 1.10	$ 1.13	$ 1.15	$ 1.18	$ 1.21	$ 1.24	$ 1.27	$ 1.30
slag revenues ($/yr)		$	41,083.48	$ 84,138.97	$ 86,158.30	$ 88,226.10	$ 90,343.53	$ 92,511.77	$ 94,732.05	$ 97,005.62	$ 99,333.76	$ 101,717.77
Feedstock consumption (tpy)			312,000.00	624,000.00	624,000.00	624,000.00	624,000.00	624,000.00	624,000.00	624,000.00	624,000.00	624,000.00
Feedstock price ($/tonne)		$	-	$ -	$ -	$ -	$ -	$ -	$ -	$ -	$ -	$ -
Feedstock revenues ($/yr)		$	-	$ -	$ -	$ -	$ -	$ -	$ -	$ -	$ -	$ -
CO2 captured (tpy)			184,000	368,000	368,000	368,000	368,000	368,000	368,000	368,000	368,000	368,000
CO2 price price ($/tonne)		$	-	$ -	$ -	$ -	$ -	$ -	$ -	$ -	$ -	$ -
CO2 revenues ($/yr)		$	-	$ -	$ -	$ -	$ -	$ -	$ -	$ -	$ -	$ -
JetFuel annual production (tonnes/yr)			14,172.25	28,344.50	28,344.50	28,344.50	28,344.50	28,344.50	28,344.50	28,344.50	28,344.50	28,344.50
Jetfuel price ($/tonne)		$	785.04	$ 803.88	$ 823.17	$ 842.93	$ 863.16	$ 883.87	$ 905.09	$ 926.81	$ 949.05	$ 971.83
JetFuel annual revenues ($/yr)		$	11,125,738.17	$ 22,785,511.77	$ 23,332,364.05	$ 23,892,340.79	$ 24,465,756.96	$ 25,052,935.13	$ 25,654,205.57	$ 26,269,906.51	$ 26,900,384.26	$ 27,545,993.49
Diesel annual production (tonnes/yr)			19,706.40	39,412.81	39,412.81	39,412.81	39,412.81	39,412.81	39,412.81	39,412.81	39,412.81	39,412.81
Diesel price ($/tonne)		$	736.43	$ 754.11	$ 772.21	$ 790.74	$ 809.72	$ 829.15	$ 849.05	$ 869.43	$ 890.29	$ 911.66
Diesel annual revenues ($/yr)		$	14,512,432.74	$ 29,721,462.26	$ 30,434,777.35	$ 31,165,212.01	$ 31,913,177.10	$ 32,679,093.35	$ 33,463,391.59	$ 34,266,512.99	$ 35,088,909.30	$ 35,931,043.12
Naphtha annual production (tonnes/yr)			10,397.81	20,795.62	20,795.62	20,795.62	20,795.62	20,795.62	20,795.62	20,795.62	20,795.62	20,795.62
Naphtha price ($/tonne)		$	693.06	$ 709.69	$ 726.72	$ 744.16	$ 762.02	$ 780.31	$ 799.04	$ 818.22	$ 837.85	$ 857.96
Naphtha annual revenues ($/yr)		$	7,206,269.07	$ 14,758,439.06	$ 15,112,641.59	$ 15,475,344.99	$ 15,846,753.27	$ 16,227,075.35	$ 16,616,525.16	$ 17,015,321.76	$ 17,423,689.49	$ 17,841,858.03
Electricity annual production (MWh/yr)			325,329	650,659	650,659	650,659	650,659	650,659	650,659	650,659	650,659	650,659
Electricity price ($/MWh)		$	76.55	$ 78.38	$ 80.26	$ 82.19	$ 84.16	$ 86.18	$ 88.25	$ 90.37	$ 92.54	$ 94.76
Electricity annual revenues ($/yr)		$	24,902,673.25	$ 51,000,674.82	$ 52,224,691.02	$ 53,478,083.60	$ 54,761,557.61	$ 56,075,834.99	$ 57,421,655.03	$ 58,799,774.75	$ 60,210,969.34	$ 61,656,032.61
Total Revenues		$	57,788,196.71	$ 118,350,226.87	$ 121,190,632.31	$ 124,099,207.49	############	############	############	############	############	############
O&M annual cost			($3,985,527.92)	($8,130,476.96)	($8,293,086.50)	($8,458,948.23)	($8,628,127.19)	($8,800,689.74)	($8,976,703.53)	($9,156,237.60)	($9,339,362.35)	($9,526,149.60)
Catalyst & Chemicals			($1,255,237.67)	($2,560,684.85)	($2,611,898.54)	($2,664,136.51)	($2,717,419.24)	($2,771,767.63)	($2,827,202.98)	($2,883,747.04)	($2,941,421.98)	($3,000,250.42)
Electricity annual demand			($7,533,459.86)	($15,428,525.78)	($15,798,810.40)	($16,177,981.85)	($16,566,253.42)	($16,963,843.50)	($17,370,975.74)	($17,787,879.16)	($18,214,788.26)	($18,651,943.18)
Natural Gas annual cost			($300,744.25)	($615,924.22)	($630,706.40)	($645,843.36)	($661,343.60)	($677,215.85)	($693,469.03)	($710,112.28)	($727,154.98)	($744,606.70)
Demolition sinking fund			($458,185.06)	($458,185.06)	($458,185.06)	($458,185.06)	($458,185.06)	($458,185.06)	($458,185.06)	($458,185.06)	($458,185.06)	($458,185.06)
Total Expenses			($13,533,154.75)	($27,193,796.87)	($27,792,686.91)	($28,405,095.01)	($29,031,328.51)	($29,671,701.77)	($30,326,536.34)	($30,996,161.14)	($31,680,912.63)	($32,381,134.96)
Operating Income			$44,255,041.96	$91,156,430.00	$93,397,945.41	$95,694,112.48	$98,046,259.96	$100,455,748.82	$102,923,973.07	$105,452,360.49	$108,042,373.52	$110,695,510.06
GDS Recovery rates			0.1429	0.2449	0.1749	0.1249	0.0893	0.0892	0.0893	0.0446		
Depreciation			($76,638,297.02)	($131,341,630.10)	($93,800,127.01)	($66,984,767.66)	($47,892,231.80)	($47,838,601.08)	($47,892,231.80)	($23,919,300.54)		
Interest Payment for 1st YR constr.		$0.00	$0.00	$0.00	$0.00	$0.00	$0.00	$0.00	$0.00	$0.00	$0.00	
Principal Payment for 1st YR constr.		$0.00	$0.00	$0.00	$0.00	$0.00	$0.00	$0.00	$0.00	$0.00	$0.00	
Interest Payment for 2nd YR constr.			$0.00	$0.00	$0.00	$0.00	$0.00	$0.00	$0.00	$0.00	$0.00	$0.00
Principal Payment for 2nd YR constr.			$0.00	$0.00	$0.00	$0.00	$0.00	$0.00	$0.00	$0.00	$0.00	$0.00
Total debt payment		$0.00	$0.00	$0.00	$0.00	$0.00	$0.00	$0.00	$0.00	$0.00	$0.00	$0.00
Taxable Income		$0.00	($32,383,255.06)	($40,185,200.10)	($402,181.60)	$28,709,344.82	$50,154,028.16	$52,617,147.74	$55,031,741.27	$81,533,059.95	$108,042,373.52	$110,695,510.06
Income Tax			$0.00	$0.00	$0.00	($8,612,803.45)	($15,046,208.45)	($15,785,144.32)	($16,509,522.38)	($24,459,917.98)	($32,412,712.06)	($33,208,653.02)
ATCF (A$)	(321,784,312.20)	(218,813,332.30)	44,255,041.96	91,156,430.00	93,397,945.41	87,081,309.03	83,000,051.51	84,670,604.50	86,414,450.69	80,992,442.50	75,629,661.46	77,486,857.04
ATCF (R$)	(321,784,312.20)	(213,684,894.82)	42,204,896.89	84,896,041.08	84,944,936.50	77,343,739.44	71,991,068.93	71,718,791.68	71,480,358.25	65,425,174.03	59,661,283.20	59,693,703.31
NPV (R$)	(516,043,307.49)		(481,163,227.42)	(417,379,575.22)	(359,361,040.62)	(311,336,663.60)	(270,699,581.99)	(233,896,501.81)	(200,550,387.15)	(172,803,726.66)	(149,801,719.28)	(128,879,440.44)

AW (R$)	$0.00	
IRR (R$)	10.0000%	
Product Value	16.24	USD/GJ

	11	12	13	14	15	16	17	18	19	20
Investment and Salvage Costs										
slag production (tpy)	78,361	78,361	78,361	78,361	78,361	78,361	78,361	78,361	78,361	78,361
slag price ($/tonne)	$ 1.33	$ 1.36	$ 1.39	$ 1.43	$ 1.46	$ 1.50	$ 1.53	$ 1.57	$ 1.61	$ 1.65
slag revenues ($/yr)	$ 104,159.00	$ 106,658.81	$ 109,218.62	$ 111,839.87	$ 114,524.03	$ 117,272.60	$ 120,087.15	$ 122,969.24	$ 125,920.50	$ 128,942.59
Feedstock consumption (tpy)	624,000.00	624,000.00	624,000.00	624,000.00	624,000.00	624,000.00	624,000.00	624,000.00	624,000.00	624,000.00
Feedstock price ($/tonne)	$ -	$ -	$ -	$ -	$ -	$ -	$ -	$ -	$ -	$ -
Feedstock revenues ($/yr)	$ -	$ -	$ -	$ -	$ -	$ -	$ -	$ -	$ -	$ -
CO2 captured (tpy)	368,000	368,000	368,000	368,000	368,000	368,000	368,000	368,000	368,000	368,000
CO2 price price ($/tonne)	$ -	$ -	$ -	$ -	$ -	$ -	$ -	$ -	$ -	$ -
CO2 revenues ($/yr)	$ -	$ -	$ -	$ -	$ -	$ -	$ -	$ -	$ -	$ -
JetFuel annual production (tonnes/yr)	28,344.50	28,344.50	28,344.50	28,344.50	28,344.50	28,344.50	28,344.50	28,344.50	28,344.50	28,344.50
Jetfuel price ($/tonne)	$ 995.15	$ 1,019.04	$ 1,043.49	$ 1,068.54	$ 1,094.18	$ 1,120.44	$ 1,147.33	$ 1,174.87	$ 1,203.07	$ 1,231.94
JetFuel annual revenues ($/yr)	$ 28,207,097.33	$ 28,884,067.67	$ 29,577,285.29	$ 30,287,140.14	$ 31,014,031.50	$ 31,758,368.26	$ 32,520,569.09	$ 33,301,062.75	$ 34,100,288.26	$ 34,918,695.18
Diesel annual production (tonnes/yr)	39,412.81	39,412.81	39,412.81	39,412.81	39,412.81	39,412.81	39,412.81	39,412.81	39,412.81	39,412.81
Diesel price ($/tonne)	$ 933.54	$ 955.94	$ 978.89	$ 1,002.38	$ 1,026.44	$ 1,051.07	$ 1,076.30	$ 1,102.13	$ 1,128.58	$ 1,155.67
Diesel annual revenues ($/yr)	$ 36,793,388.16	$ 37,676,429.47	$ 38,580,663.78	$ 39,506,599.71	$ 40,454,758.10	$ 41,425,672.30	$ 42,419,888.43	$ 43,437,965.76	$ 44,480,476.93	$ 45,548,008.38
Naphtha annual production (tonnes/yr)	20,795.62	20,795.62	20,795.62	20,795.62	20,795.62	20,795.62	20,795.62	20,795.62	20,795.62	20,795.62
Naphtha price ($/tonne)	$ 878.55	$ 899.64	$ 921.23	$ 943.34	$ 965.98	$ 989.16	$ 1,012.90	$ 1,037.21	$ 1,062.11	$ 1,087.60
Naphtha annual revenues ($/yr)	$ 18,270,062.63	$ 18,708,544.13	$ 19,157,549.19	$ 19,617,330.37	$ 20,088,146.30	$ 20,570,261.81	$ 21,063,948.09	$ 21,569,482.85	$ 22,087,150.43	$ 22,617,242.04
Electricity annual production (MWh/yr)	650,659	650,659	650,659	650,659	650,659	650,659	650,659	650,659	650,659	650,659
Electricity price ($/MWh)	$ 97.03	$ 99.36	$ 101.75	$ 104.19	$ 106.69	$ 109.25	$ 111.87	$ 114.56	$ 117.31	$ 120.12
Electricity annual revenues ($/yr)	$ 63,135,777.39	$ 64,651,036.05	$ 66,202,660.91	$ 67,791,524.77	$ 69,418,521.37	$ 71,084,565.88	$ 72,790,595.46	$ 74,537,569.75	$ 76,326,471.43	$ 78,158,306.74
Total Revenues	############	############	############	############	############	############	############	############	############	############
O&M annual cost	($9,716,672.59)	($9,911,006.05)	($10,109,226.17)	($10,311,410.69)	($10,517,638.90)	($10,727,991.68)	($10,942,551.51)	($11,161,402.55)	($11,384,630.60)	($11,612,323.21)
Catalyst & Chemicals	($3,060,255.43)	($3,121,460.54)	($3,183,889.75)	($3,247,567.54)	($3,312,518.89)	($3,378,769.27)	($3,446,344.66)	($3,515,271.55)	($3,585,576.98)	($3,657,288.52)
Electricity annual demand	($19,099,589.82)	($19,557,979.97)	($20,027,371.49)	($20,508,028.41)	($21,000,221.09)	($21,504,226.39)	($22,020,327.83)	($22,548,815.70)	($23,089,987.27)	($23,644,146.97)
Natural Gas annual cost	($762,477.26)	($780,776.71)	($799,515.35)	($818,703.72)	($838,352.61)	($858,473.07)	($879,076.43)	($900,174.26)	($921,778.44)	($943,901.13)
Demolition sinking fund	($458,185.06)	($458,185.06)	($458,185.06)	($458,185.06)	($458,185.06)	($458,185.06)	($458,185.06)	($458,185.06)	($458,185.06)	($458,185.06)
Total Expenses	($33,097,180.15)	($33,829,408.32)	($34,578,187.82)	($35,343,895.42)	($36,126,916.55)	($36,927,645.48)	($37,746,485.49)	($38,583,849.11)	($39,440,158.35)	($40,315,844.88)
Operating Income	$113,413,304.34	$116,197,327.80	$119,049,189.98	$121,970,539.44	$124,963,064.74	$128,028,495.37	$131,168,602.74	$134,385,201.24	$137,680,149.20	$141,055,350.06
GDS Recovery rates										
Depreciation										
Interest Payment for 1st YR constr.										
Principal Payment for 1st YR constr.										
Interest Payment for 2nd YR constr.										
Principal Payment for 2nd YR constr.										
Total debt payment										
Taxable Income	$113,413,304.34	$116,197,327.80	$119,049,189.98	$121,970,539.44	$124,963,064.74	$128,028,495.37	$131,168,602.74	$134,385,201.24	$137,680,149.20	$141,055,350.06
Income Tax	($34,023,991.30)	($34,859,198.34)	($35,714,756.99)	($36,591,161.83)	($37,488,919.42)	($38,408,548.61)	($39,350,580.82)	($40,315,560.37)	($41,304,044.76)	($42,316,605.02)
ATCF (A$)	79,389,313.04	81,338,129.46	83,334,432.98	85,379,377.61	87,474,145.32	89,619,946.76	91,818,021.92	94,069,640.86	96,376,104.44	98,738,745.04
ATCF (R$)	59,725,880.96	59,757,819.81	59,789,523.44	59,820,995.36	59,852,239.02	59,883,257.75	59,914,054.87	59,944,633.58	59,974,997.04	60,005,148.33
NPV (R$)	(109,848,934.15)	(92,539,222.34)	(76,794,772.14)	(62,474,101.46)	(49,448,510.41)	(37,600,927.11)	(26,824,857.70)	(17,023,431.10)	(8,108,529.95)	0.00

AW (R$)
IRR (R$)

Product Value